Development of a full-thickness skin model with stably integrated immunocompetent cells and a prediction model for skin sensitization

Inaugural-Dissertation

zur Erlangung des Doktorgrades
der Mathematisch-Naturwissenschaftlichen
Fakultät
der Heinrich-Heine-Universität Düsseldorf

Vorgelegt von

Patricia Böttcher

Aus Berlin

Köln, 16. März 2025

The thesis was externally conducted at Henkel AG & Co. KGaA, Düsseldorf under the supervision of Prof. Dr. Dr. h. c. Holger Stark from the Institute of Pharmaceutical and Medicinal Chemistry at the Heinrich Heine University Düsseldorf.

Published by permission of the Faculty of Mathematics and Natural Sciences at Heinrich Heine University Düsseldorf

Supervisor:
Prof. Dr. Dr. h. c. Holger Stark
Prof. Dr. Jörg Breitkreutz
Dr. Karsten R. Mewes

Date of the oral examination: September 19, 2025

Acknowledgement

First, I would like to thank my esteemed supervisors Prof. Dr. Dr. h.c. Stark and Prof. Dr. Breitkreutz from the Heinrich Heine University Düsseldorf for their assistance at every stage of the research project and their valuable inputs. Furthermore, I want to express my thanks to Dr. Karsten Mewes for his continuous support during the whole project, his patience and the long hours of brainstorming and problem solving sessions. My gratitude extends to the federal Ministry for Food and Agriculture (BMEL) for funding the project.

Next, I would like to thank Laura Steinmeyer for her help in the laboratory, but also for her moral support when needed. I particularly cherished our hot cocoa breaks – especially energizing during the more stressful days. I am truly grateful that we have met at Henkel and became close friends.

Of course I also want to extend my gratitude to all my other Henkel colleagues who supported me: Nelli, Marion, Jürgen, Claudia, Swenja, Lars, Christoph, Jessica, Gudrun and Uschi.

My PhD was certainly a rocky journey with up and downs. I want to express my appreciation to Oliver, who has demonstrated remarkable patience in tolerating my occasionally bad moods at home when my experiments did not unfold the way I hoped. Oli, thank you so much for pushing me through all the downs, celebrating the ups and always having my back. I am truly grateful to have such a supportive partner by my side.

However, this work would not have been possible without my mother, who supported me my whole life. So my biggest thanks goes to her! Thanks for encouraging me to do what I want, thanks for always having my back, thanks for always having an open ear, thanks for always believing in me and and and – I could go on and on, but my acknowledgement should not be longer than my thesis. Also vielen Dank Mama für deine unermüdliche Unterstützung!

Abstract

In the last decades, there has been a significant shift towards animal-free experiments in scientific research. It has been driven by a range of factors, including ethical concerns, as outlined in the 3R principle published by Russel and Burch in 1959. This publication emphasized the ethical guidelines for animal research: to replace, reduce and refine the use of animals. In alignment with the principles, the movement has been reinforced by regulatory frameworks, e.g., the ban of testing final cosmetic products on animals by the European Commission (Article 18, No 1233/2009). Additionally, the limitation and differences between animal models and human biology highlight the need for alternative methods. As a result, the demand to develop new *in vitro* test methods has increased even further.

The aim of this project is to develop a physiologically relevant immunocompetent skin model with integrated dendritic cells that represent the immune responses within the skin, with specific emphasis on allergic reactions. To generate cells that closely resembles Langerhans cells (LCs), the dendritic cells of the skin, MUTZ-3 cells were differentiated into MUTZ-LCs which are commonly used as LC surrogates. Hereby, various differentiation media were tested to optimize the differentiation protocol, especially the standardization. For that, two undefined medium supplements were tested that are recommended by the Leibniz-Institute DSMZ (German Collection of Microorganisms and Cell Cultures GmbH) to maintain MUTZ-3 cells: 5637-conditioned medium (5637CM) and fetal calf serum (FCS). The differentiation of the cells was morphologically as well as phenotypically analyzed by documenting the structural characteristics and the expression of specific markers, e.g., CD207 and CD1a. The results demonstrated that 5637CM has no positive impact on the MUTZ-LC differentiation, as the expression of pivotal proteins remained unchanged. In addition, when reducing FCS percentage by 75 %, the desired differentiation status was already achieved after 7 instead of 14 days of culture in the majority of cells. As a side project, it was tested whether FCS can be replaced with the commercially available FCS alternative Ultroser G. However, the differentiation with FCS was more successful than with Ultroser G. Furthermore, the immunocompetence of the MUTZ-LCs was studied, as it is a prerequisite for their

intended role in an immunocompetent skin model. The treatment with the sensitizer DNCB resulted in the upregulation of CD83, a marker for activated LCs, as well as the characteristic morphological changes, the detachment of MUTZ-LCs. However, this could not be detected after $NiSO_4$ treatment, another tested sensitizer.

As a subsequent step, the successful integration of MUTZ-LCs into the Phenion® Full-Thickness skin model was achieved. The structural integrity of the skin models was confirmed by optical coherence tomography images and hematoxylin-eosin staining of tissue sections. Furthermore, the precise localization of the MUTZ-LCs was demonstrated through immunofluorescence staining. Finally, the immunocompetence of the skin models with integrated MUTZ-LCs was tested by treating the skin models with the sensitizers DNCB and $NiSO_4$. It could be demonstrated that hydrocortisone, which is originally supplemented to the Phenion® Full-Thickness skin model culture medium, hinders the migration of MUTZ-LCs from the epidermis into the dermis after sensitizer treatment. Further experiments need to be conducted to validate the immunocompetence of the skin model and to establish a new accepted method to assess the sensitization potential of chemicals. Such a model would be an important test method to demonstrate the skin tolerability of cosmetic products.

Zusammenfassung

In den letzten Jahrzehnten hat sich die wissenschaftliche Forschung zunehmend von Tierexperimenten abgewandt und vermehrt alternative Methoden entwickelt. Dieser Wandel wurde durch eine Reihe von Faktoren vorangetrieben, darunter ethische Bedenken, wie sie in dem von Russel und Burch veröffentlichten 3R-Prinzip dargelegt wurden (1959). In dieser Veröffentlichung wurden die ethischen Leitlinien für die Tierforschung definiert: das Ersetzen, Reduzieren und Verfeinern des Einsatzes von Tieren. Im Einklang mit diesen Grundsätzen wurde die Bewegung durch rechtliche Rahmenbedingungen verstärkt, z. B. durch die Europäische Kommission, die Tierversuche für die Testung kosmetischer Endprodukte verboten hat (Artikel 18, Nr. 1233/2009). Darüber hinaus untermauern die Unterschiede von Tiermodellen und der menschlichen Biologie die Notwendigkeit von alternativen Methoden. Aus den genannten Gründen ist die Nachfrage nach neuen *In-vitro*-Testmethoden weiter steigend.

Das Ziel des Projektes ist die Entwicklung eines physiologisch relevanten immunkompetenten Hautmodells mit integrierten Dendritischen Zellen, welches die Immunreaktionen der Haut repräsentiert, mit dem Schwerpunkt auf allergische Reaktionen. Um Zellen zu generieren, die den Dendritischen Zellen der Haut, den Langerhans Zellen (LC), ähneln, wurden MUTZ-3 Zellen zu MUTZ-LCs differenziert. Diese Zellen werden häufig als LC-Surrogate verwendet. Zunächst wurden verschiedene Differenzierungsmedien getestet, um besonders die Standardisierbarkeit des Differenzierungsprotokolls zu verbessern. Dafür wurden zwei undefinierte Mediumzusätze getestet, die von dem Leibniz-Institut DSMZ (Deutsche Sammlung von Mikroorganismen und Zellkulturen GmbH) für die MUTZ-3 Zellkultur empfohlen werden: 5637-konditioniertes Medium (5637CM) und fetales Kälberserum (FCS). Die Differenzierung der Zellen wurde morphologisch sowie phänotypisch analysiert, indem die strukturellen Merkmale und die Expression spezifischer Marker, wie beispielsweise CD207 und CD1a, dokumentiert wurden. Die Ergebnisse zeigten, dass 5637CM keine positive Auswirkung auf die MUTZ-LC Differenzierung hat, da die Expression von Schlüsselproteinen unverändert blieb. Durch die Reduzierung des FCS-Gehalts um 75 % wurde der gewünschte Differenzierungsstatus in den meisten Zellen bereits nach 7 statt 14 Tagen erreicht. Als Nebenprojekt wurde außerdem getestet, ob FCS komplett durch

die kommerziell verfügbare FCS Alternative Ultroser G ersetztet werden kann. Jedoch war die Differenzierung mit FCS erfolgreicher als mit Ultroser G. Des Weiteren wurde die Immunkompetenz der MUTZ-LCs überprüft, da diese Eigenschaft eine Voraussetzung für ihre beabsichtigte Rolle im immunkompetenten Hautmodell ist. Die Behandlung mit dem Sensibilisator DNCB resultierte in die Hochregulierung von CD83, einem Marker für aktivierte LCs, sowie die charakteristischen morphologischen Veränderungen, wie die Ablösung der MUTZ-LCs. Dies konnte jedoch nicht nach der Behandlung mit $NiSO_4$, einem weiteren Sensibilisator, festgestellt werden.

Im nächsten Schritt wurde die erfolgreiche Integration der MUTZ-LCs in das Phenion® Vollhautmodell erreicht. Die strukturelle Integrität des Hautmodells wurde durch Bilder der optischen Kohärenztomographie und Hämatoxylin-Eosin-Färbung von Gewebsschnitten bestätigt. Zudem erfolgte die Lokalisation der MUTZ-LCs mittels Immunfluoreszenzfärbungen. Schließlich wurde die Immunkompetenz der Hautmodelle mit integrierten MUTZ-LCs getestet, indem die Modelle mit den Sensibilisatoren DNCB und $NiSO_4$ behandelt wurden. Es konnte nachgewiesen werden, dass Hydrokortison, das ursprünglich dem Phenion® Vollhautmodell-Kulturmedium hinzugefügt wurde, die Migration der MUTZ-LCs von der Epidermis in die Dermis beeinträchtigt beziehungsweise verhindert. Für eine Validierung der Immunkompetenz des Hautmodells sowie der Etablierung einer akzeptierten *in vitro* Methode zur Prüfung des Sensibilisierungspotenzials von Chemikalien müssen jedoch weitere Experimente durchgeführt werden. Ein solches Modell wäre eine wichtige Testmethode, um die Hautverträglichkeit von kosmetischen Mitteln nachzuweisen.

Table of Contents

Abbreviations

1-Chloro-2,4,dinitrobenzene	DNCB
4′,6-diamidino-2-phenylindole	DAPI
5637-conditioned medium	5637CM
Adverse outcome pathway	AOP
Air-Liquid Interface	ALI
Allergic contact dermatitis	ACD
Allophycocyanin	APC
Bovine serum albumin	BSA
C-X-C motif chemokine ligand	CXCL
C-X-C motif chemokine receptor	CXCR
Carboxyfluorescein succinimidyl ester	CFSE
Cell viability	CV
Cluster of differentiation	CD
Danger-associated molecular patterns	DAMPs
Deoxyribonuclease	DNase
Deoxyribonucleic acid	DNA
Dimethyl sulfoxide	DMSO
Dulbecco´s Modified Eagle Medium	DMEM
Epidermal growth factor	EGF
Enzyme-linked immunosorbent assay	ELISA
Fetal calf serum	FCS
Fluorescein isothiocyanate	FITC
Full-Thickness	FT
German Collection of Microorganisms and Cell Cultures GmbH	DSMZ
Granulocyte-macrophage colony-stimulating factor	GM-CSF
Hematoxylin-eosin	HE
Hydrocortisone	HC
Imidazolidinyl urea	I. Urea
Interleukin	IL
Langerhans cells	LCs
Major histocompatibility complex	MHC

Mean fluorescence intensity	MFI
Nickel sulfate	$NiSO_4$
Pathogen-associated molecular patterns	PAMPS
Phosphate-buffered saline	PBS
Phycoerythrin	PE
Propidium iodide	PI
Ribonucleic acid	RNA
Terminal deoxynucleotidyl transferase-mediated dUTP-X nick end labeling	TUNEL
Test guideline	TG
Thiazolyl blue tetrazolium blue	MTT
Transforming growth factor	TGF
Tumor necrosis factor	TNF
Versus	vs.

List of Figures

List of Tables

1. Introduction

1.1 The native human skin

1.1.1 Structure of the human skin

The skin is the largest as well as most exposed organ of the human body and functions as a barrier to the environment. The three different layers of the skin, epidermis, dermis and hypodermis (Figure 1), can be clearly distinguished based on tissue architecture and physiology. Fat, nerves and bigger blood vessels can be found in the inner layer of the skin, the hypodermis, also called subcutis. The second layer, the dermis, consists of fibroblasts, which are embedded in a dense network of extra cellular matrix proteins and glucosaminoglycans. Keratinocytes, immunocompetent cells, e.g., Langerhans cells (LCs), melanocytes and Merkel cells constitute the epidermis, the barrier to the environment. (Nguyen and Soulika, 2019; Fritsch, 2003)

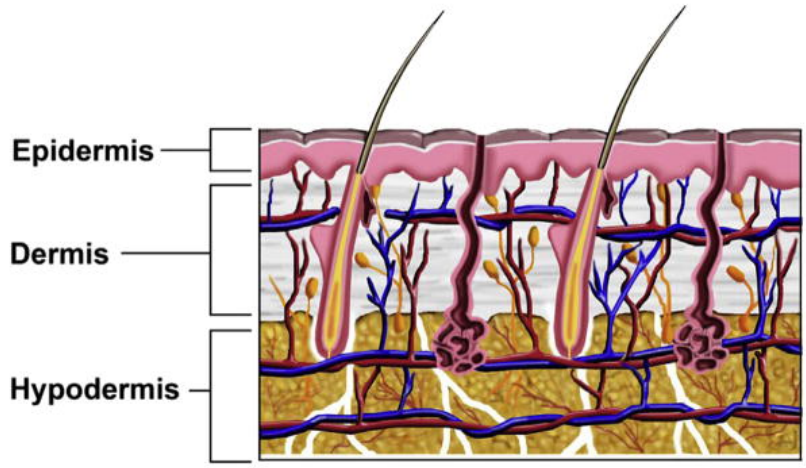

Figure 1: The three layers of the human skin.
The human skin consists of three layers, the epidermis, dermis and hypodermis (also called subcutis). [Gao et al., 2013]

The epidermis can be further divided into four layers, the stratum basale, stratum spinosum, stratum granulosum, and stratum corneum (Figure 2). These layers represent different developmental stages of keratinocytes, which can be distinguished through the

expression of characteristic protein markers, e.g., keratin 5 and 14 in the stratum basale, keratin 1 and 10 in the stratum spinosum, loricrin and profilaggrin in the stratum granulosum as well as filaggrin in the stratum corneum (Lee et al., 2017). The only proliferative cells in the epidermis are the basal cells, the precursors of keratinocytes, which can be found in the single-layered stratum basale (Fuchs and Raghaven, 2002). Arising from the stratum basale, the cells of the outer layers are continuously replaced by new keratinocytes (Watt, 1998). Apart from the basal cells, the stratum basale also contains Merkel cells and melanocytes (Halata et al., 2003; Cichorek et al., 2013). This layer connects the epidermis to the basement membrane. The keratinocytes become flatter in the outer layers, respectively, with later differentiation status (Watt, 1998). Immunocompetent cells, e.g., LCs, are mainly located in the stratum spinosum (Breathnach, 1964), which is formed by eight to ten layers of keratinocytes (Tortora and Nielsen, 2020). The LCs with their long dendritic processes form a dense network to recognize pathogens which had penetrated the epidermis (Nishibu et al., 2006; Kubo et al., 2009). Above the stratum spinosum, three to five rows of keratinocytes form the stratum granulosum. The stratum corneum, the superficial layer, consists of dead and flattened keratinocytes with about 15 to 30 layers. (Tortora and Nielsen, 2020)

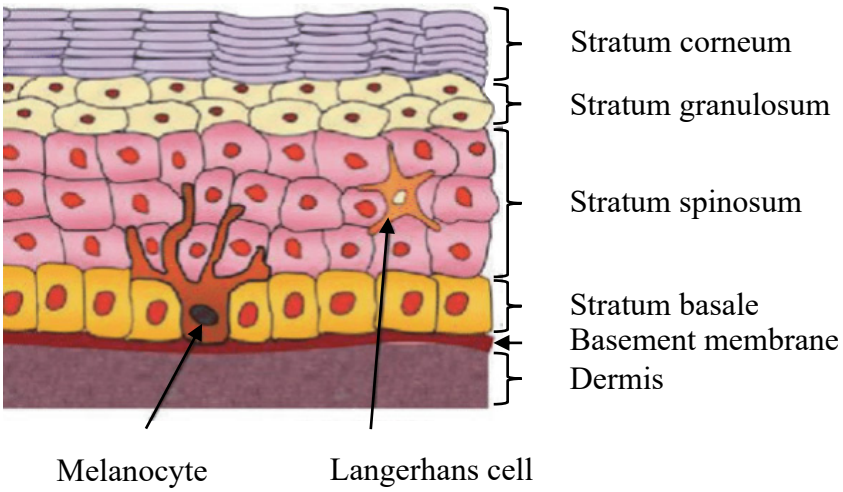

Figure 2: The layers of the epidermis.
The epidermis consists of four layers, stratum corneum, granulosum., spinosum and basale, as well as a basement membrane, which function as a barrier between epidermis and dermis. Apart from the proliferating keratinocytes, Merkel cells as well as melanocytes can be found in the stratum basale. The dendritic cells of the skin, the Langerhans cells, are mainly located in the stratum spinosum. [modified from Visscher and Narendran, 2014]

1.1.2 Langerhans cells – immunocompetent cells of the skin

In 1868, Paul Langerhans discovered the LCs, a subtype of the dendritic cells (Langerhans, 1868). LCs arise from bone marrow precursors. They express the LC-typical Birbeck granules which are cytoplasmic organelles (Birbeck et al., 1961). One characteristic marker to identify LCs is cluster of differentiation (CD) 207, also known as langerin, which plays a role in the formation of the Birbeck granules (Valladeau et al., 2000). Another typical marker for LCs is the surface protein CD1a, which is expressed on the membrane and functions as a lipid antigen presenting molecule (Fithian et al., 1981; Murphy et al., 1981; De Libero and Mori, 2005).

LCs constantly check their environment for danger-associated molecular patterns (DAMPs) and pathogen-associated molecular patterns (PAMPs) by extending and retracting their dendritic processes (Nishibu et al., 2006; Kubo et al., 2009). Once they capture the DAMPs and PAMPs employing endocytosis, micropinocytosis and phagocytosis, the LCs become activated and undergo several morphological as well as physiological changes. After several processing steps of the antigens, LCs present the antigen-peptides on their cell surface (Romani et al., 1989; Kashem et al., 2017). In addition, they start to migrate from the epidermis to the local lymph nodes to activate T cells, resulting in other immune reactions. The respective biological processes are described in chapter 1.3.2 in more detail. In the steady state, the LC population is maintained mostly via self-renewal (Merad et al., 2002; Kanitakis et al., 2011). Upon inflammation, the depleted epidermal LC population is also replaced by bone-marrow origin, the circulating blood monocytes – the corresponding derived LCs are also known as inflammatory dendritic epidermal cells (Ginhoux et al., 2006; Yoshida et al., 2014; Otsuka et al., 2018).

1.2 The Phenion® Full-Thickness skin model

With its brand Phenion®, Henkel AG & Co. KGaA has had experience in tissue engineering and alternative methods for more than 30 years. Phenion® focuses on the production of *in vitro* generated skin model. One of the models is the Phenion® Full-

Thickness (FT) skin model (Figure 3A). This three-dimensional skin equivalent consists of a stratified epidermis and dermis (Figure 3B), based on an IP-protected collagen matrix. The porous matrix is made from bovine collagen which maintains its structure during culture and thus enables the formation of a mechanically stable dermis (Mewes, 2020). Analogous to the native skin, a xenobiotic metabolism exists and extracellular matrix proteins like collagen, elastin as well as fibrillin-1 are synthesized by the dermis (Mewes et al., 2007; Wiegand et al., 2014). In addition, the fibroblasts and keratinocytes are of human origin and are derived from the same cell donor to prevent donor variability and to increase standardization. The air-liquid interface culture of the skin models (Figure 3A) simulates the condition of the native skin, where the air supplies the epidermis with oxygen and nutrients. Moreover, this culture enables the correct epidermal differentiation, including the formation of a selective skin barrier (Mewes, 2020). Therefore, the Phenion® FT skin model reflects the native skin architecture as well as metabolism and is ideally suited for cosmetic and dermatological testing.

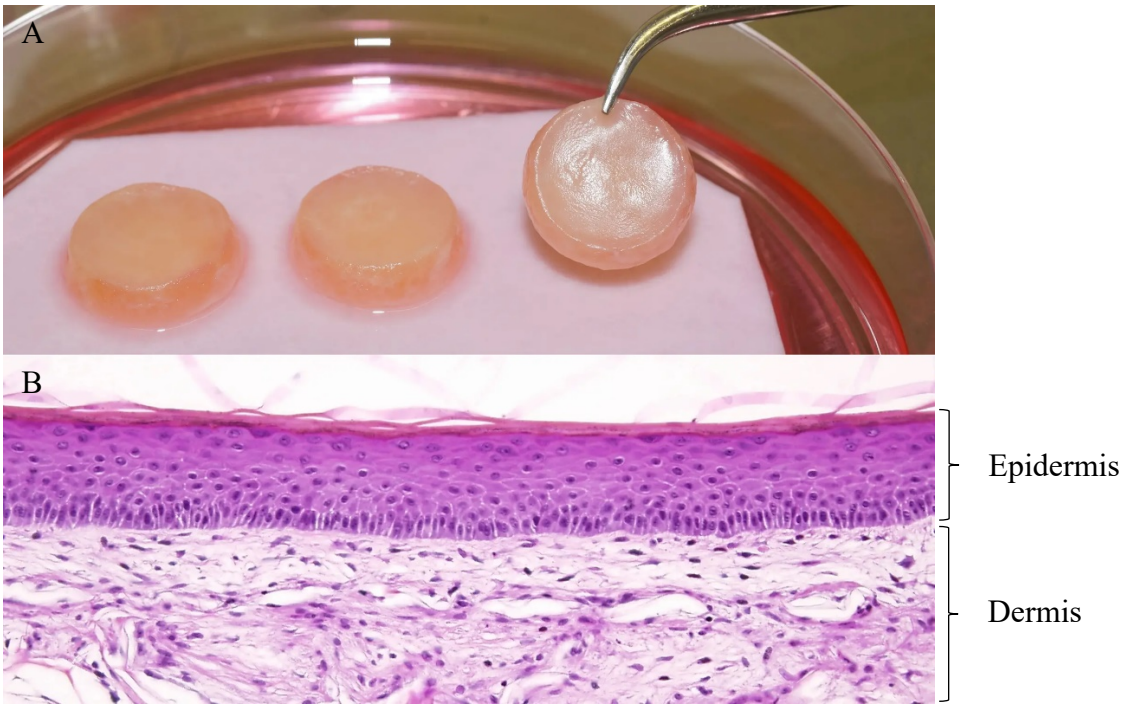

Figure 3: The structure of Phenion® Full-Thickness standard skin models.
The Phenion® Full-Thickness standard skin model has a tissue surface area of 1.5 cm^2, which can be cultured individually (not depicted) or jointly with five other skin models in a petri dish (A). The hematoxylin-eosin staining of the Phenion® Full-Thickness standard skin model shows a differentiated epidermis with a stratified corneum and stratum basale, allowing a clear distinguishment between epidermis and dermis (B). [www.phenion.com]

Different versions of the Phenion® FT skin model are available, e.g., the LONG-LIFE skin model. The Phenion® FT LONG-LIFE skin model enables with up to 50 days a 4-times longer culture time compared to the standard version. In this model, a homeostasis of fibroblasts and keratinocytes is achieved at an early state and maintained during the culture (Mewes, 2020). Thus, it is suited for long-term experiments.

These models are a sophisticated and ethical alternative to animal experiments as they enable the generation of reproducible, human-relevant data und thus support a variety of research areas, e.g., dermatology, pharmacy, toxicology and cosmetic testing.

1.3 Allergic contact dermatitis

Allergic contact dermatitis (ACD) is one of the two types of contact dermatitis, with the other one being the irritant contact dermatitis. The biological reactions of these diseases differ. This study focuses on the skin sensitizing potential of a substance and thus covers the cellular reactions of ACD.

1.3.1 Epidemiology of allergic contact dermatitis

ACD is an acquired delayed type IV hypersensitivity and can occur after the skin comes into contact with an allergen, followed by repeated skin exposure to the allergen which results in an allergic reaction (Peiser et al., 2012). Usually, the patients suffer of a red, swollen, itchy and painful skin area (Kalboussi et al., 2019). In line with the industrialization, and the modern lifestyle, the prevalence of ACD has increased. Nowadays, ACD is a common disease with nearly 20 % of the European population suffering from it (Diepgen et al., 2016). Substances, which can potentially trigger an allergic reaction can be found in jewelry (e.g., nickel), preservatives (e.g., formaldehyde), plants (e.g., poison ivy) cosmetic products (e.g., fragrances, hair dyes), medications (e.g., antibiotic creams) and others (Treadwell, 2020; Uter et al., 2020). According to Chittiboyina et al. (2015), “approximately 4000 low-molecular-weight allergens have been identified”. Hence, one can be surrounded with allergens on a daily basis.

Consequently, ACD occurs frequently in specific employment groups and might result in permanent inability to work, e.g., hairdresser, health care workers, florists, metal workers, cleaners, and painters (Rodriguez et al., 2022). Due to the associated impairments of professional as well as personal quality of life, ACD has a significant impact on healthcare expenditures and industry productivity (Cvetkovski et al., 2005). Therefore, a lot of research has been and will be performed to analyze the molecular mechanisms of ACD in order to prevent the occurrence of this common disease.

1.3.2 Molecular mechanisms - Adverse outcome pathway

The biological reactions of the ACD have been summarized and published by the organization for economic co-operation and development (OECD), the adverse outcome pathway (AOP) "for skin sensitisation initiated by covalent binding to proteins" (OECD No. 168, 2014). The AOP is divided into two phases, the induction (first contact with an allergen) and the elicitation phase (further contact with the same antigen). The induction phase occurs after the initial exposure to a contact allergen, resulting in the sensitization to a substance (Figure 4). This is summarized in four key events: from the haptenization of the chemicals, the inflammatory responses of keratinocytes, the activation of dendritic cells up to the T cell activation. (OECD No. 168, 2014)

Most of the contact allergens have a low molecular weight (below 500 g/mol) and are hydrophobic, as these properties facilitate the penetration into the lipid-rich stratum corneum (Smith Pease et al., 2003). After the contact allergen (hapten) penetrates the epidermis, it binds covalently to the nucleophilic groups of epidermal proteins (Smith Pease et al., 2003). In some cases, the contact allergens (in this case pro-haptens) have to be activated in the epidermis by xenobiotic metabolic processes in order to be sufficiently electrophilic to build the characteristic hapten-protein complexes (Smith Pease et al., 2003). The haptens are also recognized by the keratinocytes of the epidermis, mostly via Toll-like-receptors, which results in the secretion of pro-inflammatory cytokines, e.g., Interleukin-1b (IL-1b), IL-18 and Tumor necrosis factor-α (TNF-α) (Kaplan et al., 2012). These cytokines play a role in the hapten-induced LC activation. LCs recognize and internalize the hapten-protein complexes. After processing the complexes, the LCs display the antigens on the cell surface proteins, the class I and II molecules of the major

histocompatibility complex (MHC) (OECD No. 168, 2014). In addition, the LCs start to mature (get activated). During this maturation (activation) process several cytokines, e.g., IL-8, are secreted and costimulatory proteins, e.g., CD86, are upregulated, which play a role in the activation of the T cells (Toebak et al., 2006). Furthermore, the LCs start to migrate from the epidermis into the dermis and from there to the local lymph node. This migration takes place due to the downregulation of adhesion molecules, e.g., E-cadherin, as well as upregulation of chemokine receptors, e.g., C-X-C motif chemokine receptor 4 (CXCR4), on activated LCs, which facilitate and guide the LC migration (Lin et al. 1998; Sallusto et al. 1998). In addition, TNF-α, secreted by the activated keratinocytes, also stimulates the dermal fibroblasts to secrete, e.g., C-X-C motif chemokine ligand 12 (CXCL12) (Ouwehand et al., 2008). As CXCL12 is the ligand of the up-regulated CXCR4 receptor on LCs, the resulting CXCL12 gradient is one of the key players in the migration of LCs into the dermis and, subsequently, to the local draining lymph nodes (Ouwehand et al., 2008). In the lymph node, the activated (mature) LCs prime the naïve T cells. This results in the expansion of hapten-specific T cells and the formation of memory T cells. (OECD No. 168, 2014)

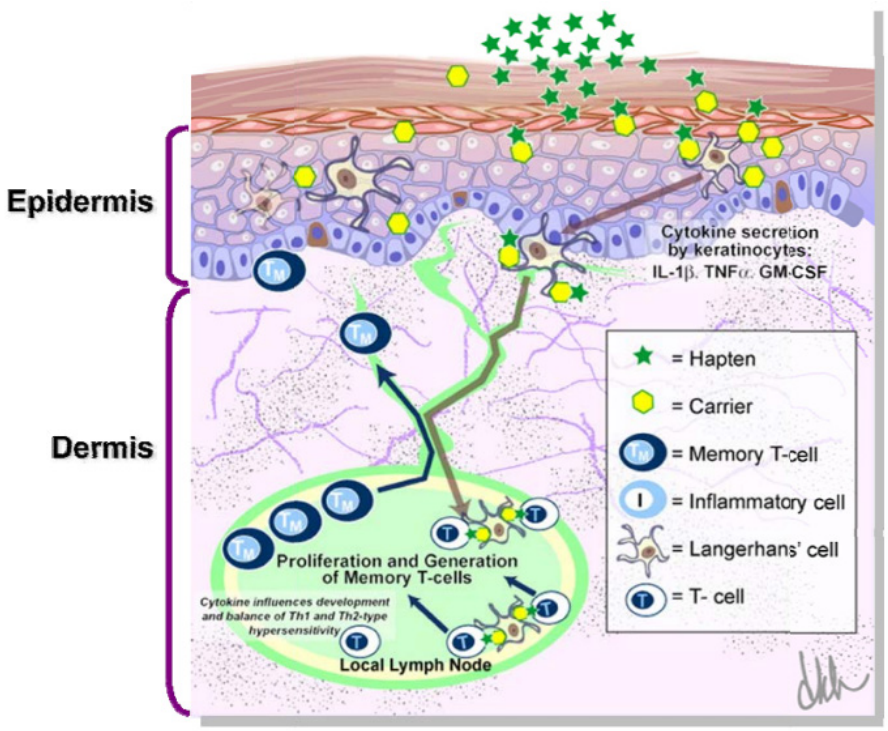

Figure 4: The induction phase of the adverse outcome pathway of skin sensitization.
Depicted are the molecular mechanisms of the first phase of the adverse outcome pathway of skin sensitization – the induction phase. [OECD No. 168, 2014]

The second phase, the elicitation phase, happens upon additional contact with the same allergen, resulting in an adaptive immune response (Figure 5). The haptens penetrate the epidermis, bind to epidermal proteins and are internalized by antigen-presenting cells, which present the antigens to the recruited hapten-specific T cells. The secretion of proinflammatory cytokines results in the clinical manifestation, e.g., inflamed, red and swollen skin areas. (OECD No. 168, 2014)

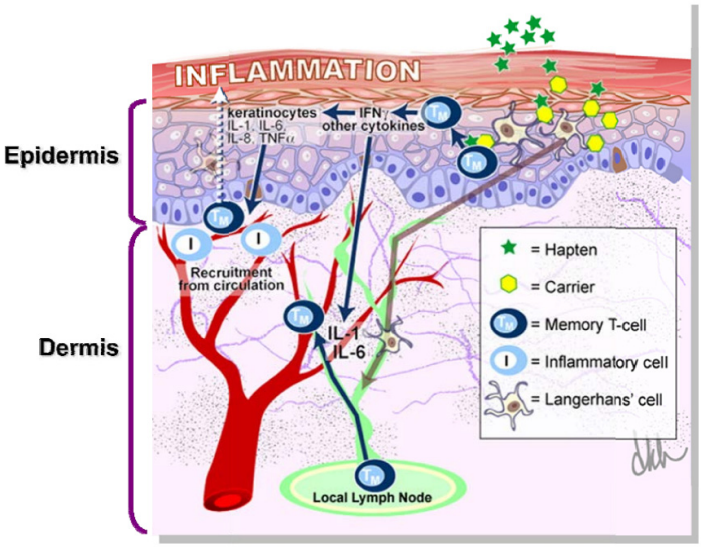

Figure 5: The elicitation phase of the adverse outcome pathway of skin sensitization.
Depicted are the molecular mechanisms of the second phase of the adverse outcome pathway of skin sensitization – the elicitation phase. [OECD No. 168, 2014]

1.4 Methods to assess skin sensitization potential

1.4.1 Animal-based sensitization methods

There are several methods to assess the skin sensitization potential of a chemical. In the past, substances were mainly analyzed for their skin-sensitizing potential with animal experiments, e.g., the Buehler Test, which uses guinea pigs (OECD test guideline (TG) 406, 2022), and the local lymph node assay, which is based on the detection of labeled T cell proliferation in the local lymph nodes after applying a sensitizer to the mouse ear (OECD TG 442A, 2010; OECD TG 442B, 2018).

However, regulatory restrictions, among other factors, have led to a noticeable shift from animal testing to alternative methods. One example is the EU Cosmetics Regulation EC 1223/2009 (2009) which has put a complete marketing ban on cosmetic ingredients and formulations which have been tested on animals. As a result, the demand of alternative *in vitro* methods, or new approach methodologies (NAMs) increased, as the non-toxicity of the products has still to be reported by the manufacturer. Another key driver for the shift to animal-free methods are the ethical concerns. Already in 1959, Russell and Burch published the ethical guidelines of the 3Rs: to replace, reduce, and refine the use of animals in research. In addition, the results of animal tests may not be fully transferable to humans, which is discussed and reviewed critically by Akhtar (2015).

1.4.2 Potential surrogate cell lines for the dendritic cells of the skin

LCs constitute the relevant immunocompetent cells in this project. However, the use of native human LCs for *in vitro* studies has several disadvantages. Fresh LCs, e.g., isolated from human blood, are restrained by limited supply and donor variability, thus, hindering the reproducibility (Santegoets et al., 2008). Commonly used cell lines are the THP-1 cells, the U937 cells and the MUTZ-3 cells (refer to Table 1). Santegoets et al. (2008) analyzed the LC characteristic of these cell lines and concluded that MUTZ-3 cells, when being differentiated with a cytokine cocktail to MUTZ-LCs, resemble the LCs the most. The morphology and phenotype of the MUTZ-3 cells are similar to the ones of human CD34-positive dendritic cells (Masterson et al., 2002).

1.4.3 OECD-accepted alternative methods for skin sensitization

The OECD published several TGs which describe alternative methods, NAMs, to assess the skin sensitizing potential of a substance. For example, TG442E (OECD, 2023) comprises several *in vitro* NAMs addressing the 3rd key event of the AOP, the activation of dendritic cells. Table 1 provides a comprehensive overview of the assays, the TGs, cell lines employed, and the corresponding key factors addressed within the AOP. Currently,

there are no alternative methods for the fourth key event, the activation and proliferation of T cells.

Table 1: OECD-accepted assays to assess the skin sensitization potential of a chemical.
Listed are the OECD-accepted assays and the corresponding characteristics like the used cell line, read-out parameter and the addressed key factor of the adverse outcome pathway (AOP).

Assay	**OECD TG number**	**Type of method**	**Used cell line**	**Read-out parameter**	**AOP key factor**
Direct Peptide Reactivity Assay (DPRA)	TG 442C (2023)	*In chemico*	-	Concentration of cysteine- or lysine-containing peptides	1. Hapte-nization
ARE-Nrf2 luciferase KeratinoSens™	TG 442D (2022)	*In vitro*	KeratinoSens™ cells	Measurement of luminescence from luciferase under the control of ARE	2. Activation of keratinocytes
ARE-Nrf2 luciferase LuSens	TG 442D (2022)	*In vitro*	LuSens cells	Measurement of luminescence from luciferase under the control of ARE	2. Activation of keratinocytes
Human cell line activation test (h-CLAT)	TG 442E (2023)	*In vitro*	THP-1	Protein expression of CD54 and CD86	3. Activation of dendritic cells
U937 cell line activation test (U-SENS™)	TG 442E (2023)	*In vitro*	U937	Protein expression of CD86	3. Activation of dendritic cells
IL-8 reporter gene assay (IL-8 Luc assay)	TG 442E (2023)	*In vitro*	THP-1-derived IL-8 reporter	Measurement of luminescence from luciferase	3. Activation of dendritic cells

Assay	OECD TG number	Type of method	Used cell line	Read-out parameter	AOP key factor
			cell line (THP-G)	under the control of IL-8 and GAPDH	
Genomic allergen rapid detection (GARD™) for assessment of skin sensitizers (GARD™skin)	TG 442E (2023)	*In vitro*	Subclone of MUTZ-3 cell line (SenzaCell™)	Expression of a defined gene set (196 genes)	3. Activation of dendritic cells

The majority of the *in vitro* NAMs measures the cellular reactions upon sensitizer exposure via the gene and protein expression of characteristic markers or the secretion of inflammatory cytokines. To demonstrate proficiency in executing the test method, the OECD TG 442E (2023) requires testing a set of ten proficiency substances, ensuring comparability of the results. These substances were chosen as they are well understood and have documented reactivity profiles. However, in general, not every substance can be tested due to solubility problems (e.g., chemicals with a high logP value, or some chemical mixtures). Moreover, according to the OECD TG 442E (2023), it should be shown that the assay has a reproducibility over time, involving repeated experiments under the same conditions as well as consistent and reliable results across different time points. In addition, reproducibility should also be confirmed by cross-laboratories studies in which several laboratories perform the same test method to ensure consistent results regardless of the location of the laboratories.

Until now, all OECD-accepted methods only address one of the key factors within the AOP. Due to the complexity of the biological reactions of an ACD, NAMs addressing only one key event are not sufficient as stand-alone methods. Therefore, different methods need to be combined for a defined approach, which is described in the TG 497

(OECD, 2023). A new NAM addressing several key events and mimic the native skin is prone to deliver more reliable results, as it would be more *in vivo* like.

1.5 Advances in the generation of an immunocompetent skin model

Due to the complication of combining different methods to assess the skin sensitization potential of a substance, there are several working groups, which are trying to generate a prediction skin model with a stratified epidermis. Such a skin model would address at least the first three key events of the AOP, from the haptenization to the activation of the keratinocytes as well as dendritic cells. Another advantage of an immersed skin model, which is cultured at the air-liquid interface (ALI), is the dry surface which enables the study of a broader panel of chemicals, e.g., oily substances or cremes and other chemical mixtures.

One example for an immunocompetent skin model is an *ex vivo* skin, obtained from surgical procedures. However, fresh skin biopsies have many limitations, e.g., limited viability (less than one day), the supply of fresh skin and reproducibility (Rodrigues Neves and Gibbs, 2021). Consequently, *ex vivo* skin is not ideally suited for a potential prediction model.

There are already some reconstructed human epidermis models for skin sensitization testing, e.g., the commercially available SENS-IS assay (Cottrez et al., 2015, 2016). Besides having no dermis, these models also only address the first two key events, as no dendritic cell or T cell surrogates are integrated into the epidermis.

Until now, there is no commercially available assay for sensitization testing with an immunocompetent skin model including fibroblasts, keratinocytes, and LC surrogates. However, there are some in-house models (refer to Table 2) with first published results of sensitizer treatment. All published results showed limitations in the prediction of sensitization potential of known sensitizers. Moreover, the respective models cannot be purchased.

Table 2: In-house immunocompetent skin models with LC surrogates.
List of first published results of in-house immunocompetent skin models. [modified from Rodrigues Neves and Gibbs, 2021]

Immunocompetent skin models	**Cell lines and collagen**	**Readout paramter**	**Test substances**	**Reference**
Skin Equivalent-LC (In house, VU medical center)	NHEK and NHFB, Melanocytes, MUTZ-3-derived LC Collagen hydrogel	LC migration (percentage of CD1a cells in epidermis/dermis) LC phenotyping (upregulation CCR7, IL1α transcripts (qPCR); CXCL8 and CD83)	$NiSO_2$, resorcinol, cinnamaldehyde	Santegoets et al. (2008), Dos Santos et al. (2009), Ouwehand et al. (2010)
Reconstructed epidermis with CD34 (+)-derived LCs (in house, L'Oréal Recherche)	NHEK, CD34+-derived LC Episkin® collagen dermal support	LC phenotyping length of dendritic processes, characteristic markers: Langerin, CD1a staining, IL-1β and CD86	TNF-α, IL-1b, DNFB, oxazolone, pPD, NiSO4, eugenol, benzocaine	Facy et al. (2005)
RHS with Mo-LC or MUTZ-LC (In-house model, University of Berlin)	NHEK and NHFB (neonatal) Collagen hydrogel MUTZ-3 or monocyte-derived LC	LC phenotyping characteristic markers: IL-6, IL-8, IL-18, ATF3, IL-1β, CD83, CXCR4, and PD-L1 LC migration (dermal CD1a and CD207 positive cells)	DNCB, pPD, isoeugenol, SDS	Bock et al. (2018)

1.6 Aim of this study

The aim of this study was to generate an immunocompetent skin model by integrating LC-like cells into the Phenion® FT skin model. Such a model could enable the studying of immune reactions, e.g., the biologic reactions after skin exposure to a sensitizer. Furthermore, this study describes important steps for the development of a prediction model to assess the sensitizing potential of a substance. An immunocompetent skin model would be a great achievement for the cosmetic industry, among other industries, to test new substances or mixtures, as animal tests are banned for evaluating substances for the use in cosmetic products.

Before integrating the LC surrogate cells, the MUTZ-LCs, into the Phenion® FT skin model, the differentiation of MUTZ-3 cells into MUTZ-LCs was analyzed, as the published differentiation media differ in differentiation time and medium supplements. To characterize the differentiation process, the phenotype as well as the morphology of MUTZ-3 cells and MUTZ-LCs were analyzed by flow cytometry and microscopy, respectively. In addition, the immunocompetence of the MUTZ-LCs was characterized by sensitizer treatment.

After integrating the analyzed MUTZ-LCs into the Phenion® FT skin model, the structural integrity of the tissue as well as the localization of the MUTZ-LCs was determined. Furthermore, similar to the analysis conducted with the MUTZ-LC suspension cells, the immunocompetence of the skin models with integrated MUTZ-LCs was also addressed. To evaluate this, the skin models were treated with sensitizers, and the resulting potential migration of the MUTZ-LCs was studied with immunofluorescence microscopic images. In addition, Next Generation Sequencing (NGS) was performed on a first set of treated skin models to identify potential read-out parameters to assess the skin sensitization potential of a substance.

2. Materials

2.1 Consumables and chemicals

Consumable or chemical	Manufacturer/Supplier
0.05 % Trypsin-Ethylenediaminetetraacetic acid	Gibco (Thermo Fisher Scientific, Carlsbad, CA, USA)
96 U well plate	VWR (Radnor, PA, USA)
Ammonia/Ethanol	Merck (Darmstadt, Germany)
Antibody Diluent	Agilent Dako (Santa Clara, CA, USA)
Carboxyfluorescein succinimidyl ester (CFSE)	eBioscience Inc. (San Diego, CA, USA)
C-Chip disposable counting chambers	NanoEnTek (Seoul, South Korea)
Caso and Würze agar plates	Sarstedt (Nümbrecht, Germany)
Cell culture dishes, plates and flasks	Cellstar (Greiner Bio-One, Kremsmünster, Austria)
Centrifuge tubes, sterile (15 ml, 50 ml)	Corning (Corning, NY, USA)
Cryogenic vials, CryoTubeTM Vials, 1.8 ml	Nunc (Thermo Fisher Scientific, Roskilde, Denmark)
Cryomold 25 mm x 20 mm x 5 mm	Tissue-Tek (Sakura Finetek, Torrance, CA, USA)
Dimethyl Sulfoxide (DMSO)	PanReac AppliChem (ITW Reagents, Darmstadt, Germany)
Deoxyribonuclease (DNase), RNase-free	Qiagen (Hilden, Germany)
Ethanol 100 %	Merck (Darmstadt, Germany)
Filter of 0.2 µm (aPES membrane)	Thermo Fisher Scientific (Waltham, MA, USA)
Fluorescence mounting medium	Agilent Dako (Santa Clara, CA, USA)
Globulins cohn fraction II, III human	Thermo Fisher Scientific (Waltham, MA, USA)
Haematoxylin 7211	Thermo Fisher Scientific (Waltham, MA, USA)

Microscope slides, frosted (76 x 26 x 1 mm)	Marienfeld (Lauda-Königshofen, Germany)
Phosphate-buffered saline (PBS) with/without calcium and magnesium	Gibco (Thermo Fisher Scientific, Carlsbad, CA, USA)
Pipette tips	Eppendorf (Hamburg, Germany)
Propidium iodide (PI)	Sigma-Aldrich (Merck KGaA, St. Louis, MO, USA)
Proteinase K	Qiagen (Hilden, Germany)
Normal goat serum (10 %)	Thermo Fisher Scientific (Waltham, MA, USA)
Recombinant RNasin®, RNase Inhibitor, 10,000u	Promega (Madison, WI, USA)
Roti®-Histofix 4 %	Carl Roth (Karlsruhe, Germany)
Safe-lock test tubes	Eppendorf (Hamburg, Germany)
Shandon Eosin Y	Thermo Fisher Scientific (Waltham, MA, USA)
Stripette™ Serological Pipets, Polystyrene	Corning (Corning, NY, USA)
TurboFilter 96 Plates (24)	Qiagen (Hilden, Germany)
Thermolysin	Sigma-Aldrich (Merck KGaA, St. Louis, MO, USA)
Tissue freezing medium	Leica (Wetzlar, Germany)
Trypan blue	Sigma-Aldrich (Merck KGaA, St. Louis, MO, USA)
Xylene	Merck (Darmstadt, Germany)

2.2 Antibodies

2.2.1 Antibodies for flow cytometry

Animal derived antibodies

Target	Dilution	Supplier
Allophycocyanin (APC) mouse anti-human CD1	1:167	BD Pharmingen (BD Biosciences, San Diego, CA, USA)
APC mouse anti-human CD86	1:167	BD Pharmingen (BD Biosciences, San Diego, CA, USA)
APC mouse IgG1	1:167	BD Pharmingen (BD Biosciences, San Diego, CA, USA)
Fluorescein isothiocyanate (FITC) mouse anti-human CD14	1:167	BD Pharmingen (BD Biosciences, San Diego, CA, USA)
FITC mouse anti-human human leukocyte antigen-DR isotype (HLA-DR)	1:167	BD Pharmingen (BD Biosciences, San Diego, CA, USA)
FITC mouse IgG2a	1:167	BD Pharmingen (BD Biosciences, San Diego, CA, USA)
Phycoerythrin (PE) mouse anti-human CD34	1:167	BD Pharmingen (BD Biosciences, San Diego, CA, USA)
PE mouse anti-human Langerin	1:167	Miltenyi Biotec (Bergisch Gladbach, Germany)
PE mouse IgG1	1:167	BD Pharmingen (BD Biosciences, San Diego, CA, USA)

Recombinant antibodies

Target	**Article number**	**Dilution**	**Supplier**
Human CD14-Vioblue	130-110-582	1:200	Miltenyi Biotec (Bergisch Gladbach, Germany)
Human HLA-DR-VioGreen	130-111-948	1:200	Miltenyi Biotec (Bergisch Gladbach, Germany)
Human CD34-Viobright515	130-120-522	1:200	Miltenyi Biotec (Bergisch Gladbach, Germany)
Human CD1a-PE	130-112-022	1:200	Miltenyi Biotec (Bergisch Gladbach, Germany)
Human CD207-PE-Vio770	130-112-213	1:200	Miltenyi Biotec (Bergisch Gladbach, Germany)
Human CD54-APC	130-121-342	1:200	Miltenyi Biotec (Bergisch Gladbach, Germany)
Human CD44-APC-Vio770	130-113-339	1:200	Miltenyi Biotec (Bergisch Gladbach, Germany)
Human CD197-Vioblue	130-117-353	1:100	Miltenyi Biotec (Bergisch Gladbach, Germany)
Human CD40-Viobright FITC	130-110-950	1:100	Miltenyi Biotec (Bergisch Gladbach, Germany)
Human CD324-PE	130-111-839	1:100	Miltenyi Biotec (Bergisch Gladbach, Germany)
Human CD18-APC	130-119-091	1:100	Miltenyi Biotec (Bergisch Gladbach, Germany)
Human CD86-APC	130-116-161	1:100	Miltenyi Biotec (Bergisch Gladbach, Germany)
Human CD83-APC-Vio770	130-110-506	1:100	Miltenyi Biotec (Bergisch Gladbach, Germany)
Human CD80-PE	130-123-253	1:100	Miltenyi Biotec (Bergisch Gladbach, Germany)
Human CD184-APC	130-120-708	1:100	Miltenyi Biotec (Bergisch Gladbach, Germany)

REA Control (S)-Vioblue	130-113-442	1:200 or 1:100	Miltenyi Biotec (Bergisch Gladbach, Germany)
REA Control (S)-VioGreen	130-113-444	1:200	Miltenyi Biotec (Bergisch Gladbach, Germany)
REA Control (S)-VioBright FITC	130-113-443	1:100	Miltenyi Biotec (Bergisch Gladbach, Germany)
REA Control (S)-Viobright515	130-113-445	1:200	Miltenyi Biotec (Bergisch Gladbach, Germany)
REA Control (S)-PE	130-113-438	1:200 or 1:100	Miltenyi Biotec (Bergisch Gladbach, Germany)
REA Control (S)-PE-Vio770	130-113-440	1:200 or 1:100	Miltenyi Biotec (Bergisch Gladbach, Germany)
REA Control (S)-APC	130-113-434	1:200 or 1:100	Miltenyi Biotec (Bergisch Gladbach, Germany)
REA Control (S)-APC-Vio770	130-113-435	1:200 or 1:100	Miltenyi Biotec (Bergisch Gladbach, Germany)

2.2.2 Antibodies for immunofluorescence staining

Primary antibodies

Target	**Host**	**Article number**	**Dilution**	**Supplier**
CD1a	Mouse	sc-18885	1:250	Santa Cruz Biotechnology (Dallas, TX, USA)
CD207	Mouse	DDX0361	1:33	Dendritics (Origene Technologies, Rockville, MD, USA)
IgG1	Mouse	14-4714-82	1:250 or 1:33	Invitrogen (Thermo Fisher Scientific, Carlsbad, CA, USA)

Secondary antibodies

Target	Host	Article number	Dilution	Supplier
Anti-mouse IgG, AlexaFluor 488 (FITC)	Goat	A11017	1:200	Invitrogen (Thermo Fisher Scientific, Carlsbad, CA, USA)
4′,6-diamidino-2-phenylindole (DAPI)	-	D9542	1:1000	Sigma-Aldrich (Merck KGaA, St. Louis, MO, USA)

2.3 Materials for flow cytometric analysis

2.3.1 Materials for Accuri Cytometer

Chemical	Supplier
Bacteriostatic concentrate solution (Sheath)	BD Biosciences (San Jose, CA, USA)
Cleaning concentrate solution	BD Biosciences (San Jose, CA, USA)
Running buffer autoMACS	Miltenyi Biotec (Bergisch Gladbach, Germany)
Spherotech 6-Peak validation beads	BD Accuri Cytometers (BD Biosciences, Ann Arbor, MI, USA)
Spherotech 8-Peak validation beads	BD Accuri Cytometers (BD Biosciences, Ann Arbor, MI, USA)

2.3.2 Materials for MACS Quant 10

Chemical	Supplier
Running Buffer	Miltenyi Biotec (Bergisch Gladbach, Germany)
Wash Buffer	Miltenyi Biotec (Bergisch Gladbach, Germany)

Storage Solution	Miltenyi Biotec (Bergisch Gladbach, Germany)
Bleach Solution	Miltenyi Biotec (Bergisch Gladbach, Germany)
Running Buffer autoMACS	Miltenyi Biotec (Bergisch Gladbach, Germany)
Propidium Iodide	Miltenyi Biotec (Bergisch Gladbach, Germany)
Calibration Beads	Miltenyi Biotec (Bergisch Gladbach, Germany)
Tandem Signal Enhancer	Miltenyi Biotec (Bergisch Gladbach, Germany)

2.4 Kits

Name	**Application**	**Order number**	**Company**
TUNNEL assay, In Situ Cell Death Detection Kit, fluorescein	For detection of apoptotic cells in tissue sections	11684795910	Roche (Basel, Switzerland)
RNeasy 96 Kit	For isolating RNA of cells	74181	Qiagen (Hilden, Germany)

2.5 Chemicals for cell and skin model treatment

Chemical	**Supplier** (Article number, location)
1-Chloro-2,4,dinitrobenzen (DNCB), CAS 97-007	Sigma-Aldrich (237329-10g, Merck KGaA, St. Louis, MO, USA)
Imidazolidinyl-Urea, CAS 39236-46-9	Sigma-Aldrich (I5133-25g, Merck KGaA, St. Louis, MO, USA)

Nickel (II)sulfate hexahydrate ($NiSO_4$), CAS 10101-970	Sigma-Aldrich (N4882-250g, Merck KGaA, St. Louis, MO, USA)
Aceton	Merck (Darmstadt, Germany)
PBS without calcium and magnesium	Gibco (Thermo Fisher Scientific, Carlsbad, CA, USA)

2.6 Eukaryotic cells

Name	**Reference**
MUTZ-3 cells	Leibniz Institute DSMZ (German Collection of Microorganisms and Cell Cultures GmbH) (Braunschweig, Germany)
MUTZ-LCs	This work
Fibroblasts	Phenion® (Henkel, Düsseldorf, Germany)
Keratinocytes	Phenion® (Henkel, Düsseldorf, Germany)
5637 cells	Leibniz Institute DSMZ (Braunschweig, Germany)

2.7 Culture media

Fibroblast Medium

Supplement	**Concentration**	**Producer**
Dulbecco´s Modified Eagle Medium (DMEM) + Glutamax/Ham`s F12 Medium	3:1	Invitrogen (Thermo Fisher Scientific, Carlsbad, CA, USA)
Fetal calf serum (FCS) heat inactivated (at 56 °C for 30 min)	10 %	Invitrogen (Thermo Fisher Scientific, Carlsbad, CA, USA)
Ascorbic acid-2-phosphate	1 mM	Sigma-Aldrich (Merck KGaA, St. Louis, MO, USA)

Penicillin	100 IU/ml	Invitrogen (Thermo Fisher Scientific, Carlsbad, CA, USA)
Streptomycin	100 µg/ml	Invitrogen (Thermo Fisher Scientific, Carlsbad, CA, USA)

Keratinocyte Medium

Supplement	**Concentration**	**Producer**
DMEM + Glutamax/Ham`s F12 Medium	3:1	Invitrogen (Thermo Fisher Scientific, Carlsbad, CA, USA)
Adenine	24.3 µg/ml	Sigma-Aldrich (Merck KGaA, St. Louis, MO, USA)
Ascorbic acid-2-phosphate	1 mM	Sigma-Aldrich (Merck KGaA, St. Louis, MO, USA)
Cholera toxin	1×10^{-10} M	Sigma-Aldrich (Merck KGaA, St. Louis, MO, USA)
Epidermal growth factor (EGF)	10 ng/ml	Sigma-Aldrich (Merck KGaA, St. Louis, MO, USA)
Fetalchlone II	10 %	Hyclone (Thermo Fisher Scientific, Logan, UT, USA)
Hydrocorisone	0.4 µg/ml	Sigma-Aldrich (Merck KGaA, St. Louis, MO, USA)
Insulin	0.12 IU/ml	Sigma-Aldrich (Merck KGaA, St. Louis, MO, USA)
Penicillin	100 IU/ml	Invitrogen (Thermo Fisher Scientific, Carlsbad, CA, USA)
Streptomycin	100 µg/ml	Invitrogen (Thermo Fisher Scientific, Carlsbad, CA, USA)
Triiodthyronine	2×10^{-9} M	Sigma-Aldrich (Merck KGaA, St. Louis, MO, USA)

ALI Medium

Supplement	**Concentration**	**Producer**
DMEM + Glutamax / Ham`s F12 Medium	3:1	Invitrogen (Thermo Fisher Scientific, Carlsbad, CA, USA)
Ascorbic acid-2-phosphate	1 mM	Sigma-Aldrich (Merck KGaA, St. Louis, MO, USA)
Bovine serum albumin (BSA)	1.6 mg/ml	Invitrogen (Thermo Fisher Scientific, Carlsbad, CA, USA)
Hydrocortisone	0.4 µg/ml	Sigma-Aldrich (Merck KGaA, St. Louis, MO, USA)
Insulin	0.12 IU/ml	Sigma-Aldrich (Merck KGaA, St. Louis, MO, USA)
Penicillin	100 IU/ml	Invitrogen (Thermo Fisher Scientific, Carlsbad, CA, USA)
Streptomycin	100 µg/ml	Invitrogen (Thermo Fisher Scientific, Carlsbad, CA, USA)

5637 Medium

Supplement	**Concentration**	**Producer**
RPMI 1640		Gibco (Thermo Fisher Scientific, Carlsbad, CA, USA), Biowest
FCS, heat inactivated (at 56 °C for 30 min)	10 %	Biochrom
2-Mercaptoethanol (55 mM)	0-1 % (50 µM)	Gibco (Thermo Fisher Scientific, Carlsbad, CA, USA)
Penicillin 10,000 U/ml, streptomycin 10,000 µg/ml	1 %	Gibco (Thermo Fisher Scientific, Carlsbad, CA, USA)

Maintenance Medium

Supplement	**Concentration**	**Producer**
alpha-MEM (1x)		Gibco (Thermo Fisher Scientific, Carlsbad, CA, USA)
FCS, heat inactivated (at 56 °C for 30 min)	20 %	Merck (Darmstadt, Germany)
Sterile filtered 5637-conditioned medium	10 %	This work
Penicillin 10,000 U/ml, streptomycin 10,000 µg/ml	1 %	Gibco (Thermo Fisher Scientific, Carlsbad, CA, USA)
2-Mercaptoethanol (55 mM)	0.1 % (50 µM)	Gibco (Thermo Fisher Scientific, Carlsbad, CA, USA)

5TT Medium

Supplement	**Concentration**	**Producer**
alpha-MEM (1x)		Gibco (Thermo Fisher Scientific, Carlsbad, CA, USA)
FCS, heat inactivated (at 56 °C for 30 min)	20 %	Merck (Darmstadt, Germany)
Sterile filtered 5637-conditioned medium	10 %	This work
Penicillin 10,000 U/ml, streptomycin 10,000 µg/ml	1 %	Gibco (Thermo Fisher Scientific, Carlsbad, CA, USA)
2-Mercaptoethanol (55 mM)	0.1 % (50 µM)	Gibco (Thermo Fisher Scientific, Carlsbad, CA, USA)
Transforming growth factor (TGF)-β	10 ng/ml	PeproTech (100-21C, Thermo Fisher Scientific, Cranbury, NJ, USA)
Tumor necrosis factor (TNF)-α	2.5 ng/ml	PeproTech (300-01A, Thermo Fisher Scientific, Cranbury, NJ, USA)

5TTG Medium

Supplement	**Concentration**	**Producer**
alpha-MEM (1x)		Gibco (Thermo Fisher Scientific, Carlsbad, CA, USA)
FCS, heat inactivated (at 56 °C for 30 min)	20 %	Merck (Darmstadt, Germany)
Sterile filtered 5637-conditioned medium	10 %	This work
Penicillin 10,000 U/ml, streptomycin 10,000 µg/ml	1 %	Gibco (Thermo Fisher Scientific, Carlsbad, CA, USA)
2-Mercaptoethanol (55 mM)	0.1 % (50 µM)	Gibco (Thermo Fisher Scientific, Carlsbad, CA, USA)
Granulocyte-macrophage colony-stimulating factor (GM-CSF)	100 ng/ml	Miltenyi Biotech (130-093-867, Bergisch Gladbach, Germany)
TGF-β	10 ng/ml	PeproTech (100-21C, Thermo Fisher Scientific, Cranbury, NJ, USA)
TNF-α	2.5 ng/ml	PeproTech (300-01A, Thermo Fisher Scientific, Cranbury, NJ, USA)

TTG Medium (with 20 % FCS)

Supplement	**Concentration**	**Producer**
alpha-MEM (1x)		Gibco (Thermo Fisher Scientific, Carlsbad, CA, USA)
FCS, heat inactivated (at 56 °C for 30 min)	20 %	Merck (Darmstadt, Germany)
Penicillin 10,000 U/ml, streptomycin 10,000 µg/ml	1 %	Gibco (Thermo Fisher Scientific, Carlsbad, CA, USA)
2-Mercaptoethanol (55 mM)	0.1 % (50 µM)	Gibco (Thermo Fisher Scientific, Carlsbad, CA, USA)

GM-CSF	100 ng/ml	Miltenyi Biotech (130-093-867, Bergisch Gladbach, Germany)
TGF-β	10 ng/ml	PeproTech (100-21C, Thermo Fisher Scientific, Cranbury, NJ, USA)
TNF-α	2.5 ng/ml	PeproTech (300-01A, Thermo Fisher Scientific, Cranbury, NJ, USA)

TTG Medium (with 5 % FCS)

Supplement	**Concentration**	**Producer**
alpha-MEM (1x)		Gibco (Thermo Fisher Scientific, Carlsbad, CA, USA)
FCS, heat inactivated (at 56 °C for 30 min)	5 %	Merck (Darmstadt, Germany)
Penicillin 10,000 U/ml, streptomycin 10,000 µg/ml	1 %	Gibco (Thermo Fisher Scientific, Carlsbad, CA, USA)
2-Mercaptoethanol (55 mM)	0.1 % (50 µM)	Gibco (Thermo Fisher Scientific, Carlsbad, CA, USA)
GM-CSF	100 ng/ml	Miltenyi Biotech (130-093-867, Bergisch Gladbach, Germany)
TGF-β	10 ng/ml	PeproTech (100-21C, Thermo Fisher Scientific, Cranbury, NJ, USA)
TNF-α	2.5 ng/ml	PeproTech (300-01A, Thermo Fisher Scientific, Cranbury, NJ, USA)

TTG Medium (with 4 % Ultroser G)

Supplement	Concentration	Producer
alpha-MEM (1x)		Gibco (Thermo Fisher Scientific, Carlsbad, CA, USA)
Ultroser G	5 %	Pall BioSepra (Cergy, France)
Penicillin 10,000 U/ml, streptomycin 10,000 µg/ml	1 %	Gibco (Thermo Fisher Scientific, Carlsbad, CA, USA)
2-Mercaptoethanol (55 mM)	0.1 % (50 µM)	Gibco (Thermo Fisher Scientific, Carlsbad, CA, USA)
GM-CSF	100 ng/ml	Miltenyi Biotech (130-093-867, Bergisch Gladbach, Germany)
TGF-β	10 ng/ml	PeproTech (100-21C, Thermo Fisher Scientific, Cranbury, NJ, USA)
TNF-α	2.5 ng/ml	PeproTech (300-01A, Thermo Fisher Scientific, Cranbury, NJ, USA)

2.8 Laboratory equipment

Instrument	Manufacturer
Accuri C6 Flow Cytometer	BD Biosciences (San Jose, CA, USA)
Cryostat SM 1900	Thermo Fisher Scientific (Waltham, MA, USA)
Fluorescence & light microscope (inverse microscope CKX41 and fluorescence microscope BX51)	Olympus (Tokyo, Japan)
Gemini AS automated slide stainer	Thermo Fisher Scientific (Waltham, MA, USA)
Heraeus Multifuge X3R	Thermo Fisher Scientific (Waltham, MA, USA)

Incubator	BINDER (Tuttlingen, Germany)
Laminar flow hood	Thermo Fisher Scientific (Waltham, MA, USA) / Holten LaminAir
MACS Quant 10	Miltenyi Biotec (Bergisch Gladbach, Germany)
Microscope digital cameras DP71 and XC10, magnification 0.5x	Olympus (Tokyo, Japan)
Multimode microplate reader Tecan Spark®	Tecan (Männedorf, Switzerland)
Nanodrop ND-1000 Spectrophotometer	PEQLAB (VWR, Erlangen, Germany)
Optical cohrerence tomography imaing system	Thorlabs (Newton, NJ, USA)
Pipettes	Eppendorf (Hamburg, Germany)
Water Bath	Memmert (Schwabach, Germany)

2.9 Programs and software

Program/Software	**Supplier**
MACS Quantify	Miltenyi Biotec (Bergisch Gladbach, Germany)
Microsoft Office 365	Microsoft (Redmond, WA, USA)
Fiji/ImageJ 1.52i	NIH (Bethesda, MD, USA)
SparkControlTM Software	Tecan (Männedorf, Switzerland)
CellSense Dimension	Olympus (Tokyo, Japan)

3. Methods

3.1 Cell culture

All cell culture was performed in an incubator at 37 °C with 5 % CO_2 and humidified atmosphere. For working with the cells, a laminar flow hood was used to ensure aseptic conditions. The suspension cells, MUTZ-3 cells and MUTZ-LCs were cultured in a 12-well flat-bottomed plate with 2 ml cell suspension per well. In contrast, all used adherent cells, fibroblasts, keratinocytes and 5637 cells, were cultured in 175 cm^2 flasks with 25 ml cell suspension per flask. The general cell culture (refer to 3.1.1, 3.1.3, 3.1.4) of the fibroblasts and keratinocytes was conducted according to the Standard Operation Procedure (SOP) documents provided by Henkel. These protocols are also used for the Phenion® Full-Thickness (FT) skin model production. The supplements of the used cell culture media are listed in 2.7. The cells were centrifuged for 5 min at 200 rcf and room temperature, except fibroblasts and keratinocytes, which were centrifuged for 3 min at 200 rcf. In order to determine the number of viable cells, the cells were stained with trypan blue, which stains dead cells blue (product data sheet, Sigma-Aldrich). After that, the cells were transferred in disposable counting chamber enabling a reliable counting of viable and blue-stained dead cells under the microscope.

3.1.1 Thawing of frozen cells

As dimethyl sulfoxide (DMSO) is toxic above 4 °C (Bouroncle et al., 1967), the cells were quickly thawed in a 37 °C water bath. As soon as only small clumps of ices were left, the cells were diluted with pre-warmed fresh medium to minimize the toxic effect of DMSO. After that, the cells were centrifuged, counted, and transferred into the required volume of medium. Depending on the cell line, the adjusted cell suspension was then split into new 12-well plates or 175 cm^2 flasks.

3.1.2 Splitting of suspension cells

As suspension cells, the MUTZ-3 cells and MUTZ-LCs, were splitted by centrifuging and counting the cells. After adjusting the cell suspension with pre-warmed medium accordingly to ~5 x 10^5 MUTZ-3 cells or ~2.5 x 10^5 MUTZ-LCs per ml, the cells were transferred into 12-well plates.

3.1.3 Splitting of adherent cells

After aspirating the medium, the cells were washed once with phosphate-buffered saline (PBS) to remove any remaining culture medium. To detach the cells, 5 ml trypsin was added to each flask and the cells were incubated at 37 °C for 7 min (5637 cells) or at room temperature for 2 min (fibroblasts). For the splitting of keratinocytes, which were cultured on feeder cells, the growth-inhibited fibroblasts needed to be removed at first. To accomplish this, 5 ml trypsin was added to the cells, which were then incubated for 2 min at room temperature. Subsequently, the fibroblast suspension was removed. Afterward, 5 ml trypsin was added again and the cells were incubated for 5 min at 37 °C to detach the keratinocytes.

Once the cells were detached, the trypsin was inactivated by adding 10 ml pre-warmed medium (including serum). Following centrifugation and cell counting, the appropriate volume of medium was added, and the adjusted cell suspension was transferred into 175 cm^2 flasks (3.0 x 10^6 5637 cells per flask, 5.5 × 10^5 keratinocytes, fibroblasts or growth-inhibited fibroblasts per flask).

3.1.4 Freezing of cells

Adherent cells were detached with trypsin, following the described protocol in 3.1.3. The detached adherent cells or the suspension cells were centrifuged, counted, resuspended in culture medium, and transferred into cryogenic vials (500 µl per vial). After that, the cell suspension was diluted with an equal volume of culture medium containing 20 % DMSO. DMSO functions as a cryoprotective agent, as it reduces the formation of ice crystals and

thus, prevents cell death (Chen and Thibeault, 2013). The cells were not directly resuspended in culture medium supplemented with 10 % DMSO in order to minimize the cell exposure time to the toxic DMSO. The cryogenic vials were stored for approximately one day at -80 °C, before being stored in the air phase of liquid nitrogen.

3.1.5 5637-conditioned medium

In order to obtain the 5637-conditioned medium (5637CM), which was required for the culture of MUTZ-3 cells, 5637 cells were cultured in a 175 cm^2 flask at a cell density of 3.0 x 10^6 cells per ml in 5637 medium. The cells were cultured for at least two weeks after thawing the cells and splitting the cells three times a week. Next, the conditioned medium was collected when passaging the 5637 cells after two days of culturing. The collected medium was filtered through a sterile filter of 0.2 µm to exclude contaminating non-adherent cells. The 5637CM was stored as 5-15 ml aliquots at -80 °C.

3.1.6 Culture of MUTZ-3 cells

The MUTZ-3 cells were purchased at the Leibniz Institute DSMZ. They were cultured at ~5 x 10^5 MUTZ-3 cells per ml in a 12 well plate. The cells were cultured in maintenance medium and split every three or four days, so twice a week, which is within the time period recommended by the Leibnitz Institute DMSZ (four to six days).

3.1.7 Differentiation of MUTZ-3 cells into MUTZ-LCs

To generate a surrogate cell line for Langerhans cells (LCs), the MUTZ-3 cells were differentiated into LC like cells (called MUTZ-LCs). Before starting the differentiation, the MUTZ-3 cells were cultured for at least two weeks to ensure enough recovering time for the cells after the thawing process. Upon reaching the required quantity of MUTZ-3 cells, it was essential to ensure that the cell count exceed approximately twice the desired number of MUTZ-LCs, considering the potential loss in cell viability during differentiation. At this stage, the differentiation could be started.

During this study, various differentiation protocols were tested. The MUTZ-3 cells were differentiated either over 7 or 14 days (with changing the medium after 7 days). In addition, the effect of different medium supplements was tested: granulocyte-macrophage colony-stimulating factor (GM-CSF), 5736CM and fetal calf serum (FCS). The tested differentiation media are listed in 2.7 (5TT, 5TTG, TTG – with varying FCS concentration). In the optimized and thus final differentiation protocol the MUTZ-3 cells were differentiated into MUTZ-LCs for seven days in TTG medium supplemented with 5 % FCS.

3.1.8 Labelling of MUTZ cells with CFSE

One method to track the MUTZ-LCs within the Phenion® FT skin model is the cell labeling with the fluorescent cell staining dye carboxyfluorescein ester (CFSE). The staining was conducted based on the CFSE manufacturer´s product data sheet ("CFSE cell labeling protocol", eBioscience Inc.). First, the cells were washed twice with PBS (without calcium and magnesium) and were then resuspended in 1 µM CFSE (in PBS without calcium and magnesium, ~5-10 x 10^6 cells per ml). After incubating the cells for 10 min at 37 °C in the dark, the labelling was stopped by adding four times the amount of serum-containing medium. Next, the cells were incubated on ice for 5 min, washed twice with medium containing serum and resuspended in the culture medium. One aliquot with at least 2×10^5 cells was measured with flow cytometry to evaluate the fluorescence intensity of the CFSE-labeled cells.

3.1.9 Treating MUTZ-LCs with sensitizers

To test, whether the MUTZ-LCs can be activated with a sensitizer, the cells were treated for 24 h with 1-Chloro-2,4,dinitrobenzene (DNCB), an extreme sensitizer, and imidazolidinyl urea (I. Urea), a weak sensitizer. The chemical solutions were freshly prepared on the same day of measurement. To identify the sensitizer concentration corresponding to a cell viability (CV) of 75 % compared to the vehicle control, a dose finding assay was performed, based on the one for the h-CLAT assay (OECD TG 442E, 2023). After treating the cells (analogous to the described protocol below) with a dilution

series of the chemical, the cells were stained with propidium iodide (PI) and flow cytometrically analyzed (refer to 3.2) to measure the viability of the cells.

First, the cells were collected, centrifuged, and counted. The cells were resuspended with differentiation medium to achieve a cell density of ~6 x 10^5 cells per ml. The adjusted cell suspension was transferred into a 24 well flat-bottomed plate with 500 µl per well. Subsequently, the cell suspension was diluted with the same volume of differentiation medium with or without chemical (500 µl per well). Besides the negative control (untreated cells), the cells were treated with DNCB and the corresponding vehicle control DMSO as well as I. Urea and the corresponding vehicle control PBS. After the 24 h incubation time in an incubator at 37 °C with 5 % CO_2 and humidified atmosphere, the expression levels of characteristic surface proteins were analyzed with flow cytometry (refer to 3.2).

3.2 Flow cytometric analysis – Staining of surface antigens

The first experiments of this study were performed with antibodies from BD and the flow cytometer Accuri C6. After that, recombinant antibodies (REAfinity™) from Miltenyi Biotec were used as well as the flow cytometer MAQS Quant 10 from Miltenyi Biotec. This switch occurred, since it was associated with some advantages: For one, the MACS Quant 10 has more channels than the Accuri and the recombinant antibodies are offered with various fluorochromes, which enabled a parallel staining with different antibodies (large multi-panel). In addition, Miltenyi Biotec claims that the recombinant antibodies have a higher specificity and lower background signals compared to other antibodies (product data sheet, Miltenyi Biotec). The used antibodies are listed in 2.2.1.

The staining protocol differs depending on the used antibodies. PI was added to the samples before starting the measurement to stain and thus exclude the dead cells from the analysis.

With animal-derived antibodies from BD and the Accuri C6 flow cytometer:
First, the cells were washed twice with MACS Flow Buffer. Next, a blocking solution containing 0.1 % Globulins Cohn Fraction I, II (in PBS) was added to block non-specific Fc-mediated interactions. After an incubation for 10 min at 4 °C, the samples were washed with MACS Flow Buffer and transferred into the required number of flow cytometer tubes (100 µl per tube) or wells in a 96 well plate (50 µl per well). Except for the unstained control, the antibody was added to the cell suspension (6 µl per tube and respectively 3 µl per well) and incubated for 30 min at 4 °C in the dark. Next, the cells were washed twice with MACS Flow Buffer and resuspended in 150 µl MACS Flow Buffer containing 0.625 µg/ml PI to label dead cells (without PI for the unstained control). The cells were measured with the Accuri C6 Flow Cytometer.

With recombinant antibodies from Miltenyi Biotec and MACS Quant flow cytometer:
This protocol is based on the one recommended by Miltenyi Biotec (product data sheet REAfinity™ antibodies, "Cell surface flow cytometry staining protocol", Miltenyi Biotec). First, the cells were washed once with MACS Flow Buffer and then transferred into the required number of flow cytometer tubes or wells in a 96 well plate. After centrifuging the cells again, they were resuspended in 100 µl MACS Flow Buffer containing the antibodies (or without antibodies as an unstained control). Subsequently, the cells were incubated for 10 min at 4 °C in the dark. The cells were washed once with MACS Flow Buffer, resuspended in 200 µl MACS Flow Buffer and then measured with the MACS Quant flow cytometer. The MACS Quant was set to automatically add 1:100 PI to each sample (except the unstained control) before starting the measurement. This way, it was guaranteed, that every sample had the same incubation time with PI.

3.3 Generation of Phenion® Full-Thickness skin model

3.3.1 Established protocol to produce the Phenion® Full-Thickness skin model

The protocol to produce Phenion® FT skin models was already published by Phenion® (www.phenion.com), as described by Mewes et al. (2007). To generate a Phenion® FT skin model, human fibroblasts and keratinocytes were used from the same donor. The

supplements of the used media are listed in 2.7. In total, it takes at least seven weeks to produce a standard Phenion® FT skin model. The protocol can be divided into six sections:

I. Washing the matrix
II. Culture of fibroblasts
III. Seeding fibroblasts on the matrix
IV. Culture of keratinocytes
V. Seeding keratinocytes on the dermis model
VI. Transferring the skin models in the Air-Liquid Interface (ALI)

An overview of the timeframe and protocol steps is depicted in Figure 6. First, the IP-protected matrices were incubated with 70 % ethanol for one hour, washed with PBS and lastly were incubated with fibroblast medium. In parallel, the culture of fibroblasts started. For that, the fibroblasts were thawed and cultured at a cell density of 5.5 x 10^5 cells per 175 cm^2 flask in fibroblast medium. After three days, the medium was changed with fresh fibroblast medium. On the fourth day, the fibroblasts were detached with trypsin (as described in 3.1.3), centrifuged, resuspended with pre-warmed fibroblast medium and counted. The cell suspension was adjusted to 5 × 10^5 cells per ml with fibroblast medium. 1 ml of the adjusted cell suspension was added to each matrix. The medium of the "dermis models" was exchanged every other day. One week after the fibroblast seeding, the culture of the keratinocytes started. For that, fibroblasts, which were growth-inhibited with mitomycin C, were used as feeder cells for the keratinocytes, as the fibroblasts secrete cytokines which are crucial for keratinocyte growth (Jubin et al., 2011). The cells were seeded at a density of 5.5 x 10^5 cells per flask and cultured in keratinocyte medium. After two days, the keratinocytes were added to the conditioned medium (5.5 x 10^5 cells per flask). The keratinocytes were cultured for five days before they were harvested. The medium of the dermis models was removed and 0.45 × 10^6 keratinocytes per model were added (in keratinocyte medium). The medium was exchanged the next day. The day after that, the skin models were transferred in ALI phase. For that, the skin models were positioned on a filter paper, which was placed on a spacer in a petri dish (78.5 cm^2) filled with ~35 ml ALI medium. The volume of the ALI medium needed to be adjusted so that it was level with the filter paper to enable a continuous supply of medium. After three days of ALI culture, the medium was removed, and the

skin models were “starved” for ~24 h. This “starving” process was repeated two days later. After that, the medium was changed three times a week.

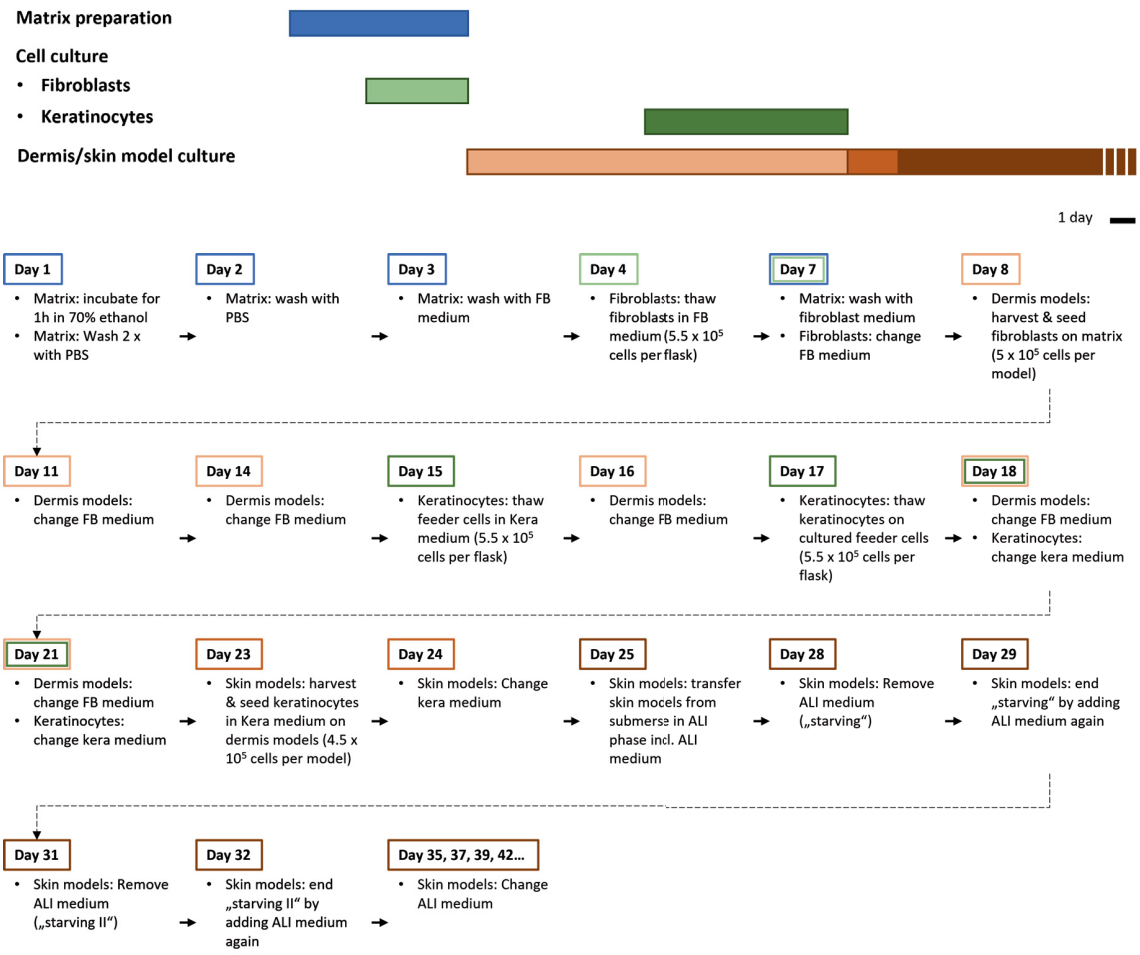

Figure 6: Overview of the Phenion® Full-Thickness skin model production.
Depicted is the protocol of the Phenion® Full-Thickness skin model production, which can be divided into matrix preparation, cell culture (fibroblasts and keratinocytes) and dermis as well as skin model production. The detailed daily timeline is also shown. Scale bar represents 1 day, applicable to the bar charts.

3.3.2 Integrating MUTZ-LCs into the Phenion® Full-Thickness skin model

To generate an immunocompetent skin model with integrated MUTZ-LCs, slight modifications of the established skin model production protocol (refer to 3.3.1) were done. During the first experiments, the MUTZ-LCs (1×10^6 cells per model), unlabeled or labeled with CFSE, were seeded together with keratinocytes (0.45×10^6 cells per model) on the dermis models. However, the MUTZ-LCs were not successfully integrated with this protocol. Therefore, the MUTZ-LCs (1×10^6 cells per model) and keratinocytes

(0.25×10^6 cells per model) were seeded on the dermis model. After one hour, another layer of 0.25 x 10^6 keratinocytes was seeded to integrate the MUTZ-LCs. Furthermore, to ensure an adequate medium supply for the increased number of cells, the original volume of 1 ml keratinocyte medium was increased to 2 ml. Moreover, the skin models were not "starved" for 24 h in ALI phase, as the effect of the "starving" on the MUTZ-LC integration is not known. After at least ten days of culturing in ALI phase, the skin models were analyzed.

3.3.3 Treating the Phenion® Full-Thickness skin models with sensitizers

In order to analyze the immunocompetence of the Phenion® FT skin models, they were treated with the sensitizers DNCB (in PBS) and $NiSO_4$ (in Acetone). Untreated skin models and skin models treated with the vehicle controls, PBS and Acetone, served as controls. To determine the highest sensitizer concentration, which still corresponds to viability comparable to the controls, a dose finding assay was performed. For that, the skin models were treated with dilution series of the sensitizers. The viability was analyzed with a MTT assay (refer to 3.4.2), and the tissue integrity was studied with hematoxylin-eosin-stained (HE-stained) frozen sections (refer to 3.4.5).

Before starting the treatment, the skin models were transferred from being cultured on a filter with three to five other skin models to a stand-alone culture. This was done to prevent potential cross-contamination of chemicals between the skin models. The skin models were transferred on a filter paper, which was placed on a spacer in a 100/20 mm petri dish filled with 5.6 ml ALI medium. After preparing the chemical solutions, 50 µl of the chemical solution was evenly applied to the surface of each skin model without damaging the models. Next, the skin models were incubated for 20 h in an incubator at 37 °C with 5 % CO_2 and humidified atmosphere. Finally, the skin models were shortly emerged in PBS to remove any chemical residues on the surface. The skin models were either histological prepared (refer to 3.4.4) or the RNA was isolated for further analyses (refer to 3.4.9).

3.4 Analyzing the Phenion® Full-Thickness skin model without and with MUTZ-LCs

3.4.1 Optical coherence tomography images

Before further analyzing the Phenion® FT skin models after at least ten days of culture in the ALI phase, optical coherence tomography (OCT) images were taken. The OCT images enabled an evaluation the structure of the skin models without being invasive.

3.4.2 MTT assay

To assess the viability of the skin models, a thiazolyl blue tetrazolium blue (MTT) assay is a commonly used colorimetric method, first described by Mosmann et al. (1983). Hereby, the cellular metabolic activity is measured by mitochondrial NAD(P)H-dependent oxidoreductase, which convert the MTT into formazan. While the MTT produces a yellow-colored solution, the formazan is dark-blue and hydrophobic. The blue „formazan crystals“ are solubilized with isopropanol. Consequently, the supernatant of vital skin models is deeply purple colored after eluting with isopropanol. In contrast, the solution becomes increasingly transparent/clear with an elevated degree of damage to the skin models. Subsequently, the quantification of the respective color intensities is performed by measuring the supernatants at 570 nm.

The MTT assay was performed as described in the SOP from Henkel. On day seven of ALI phase, four days before starting the MTT assay, the ALI medium was changed to phenol red-free ALI medium. This was done to prevent interfere from phenol red in the photometric measurement. The skin models were first washed by emerging the models completely in PBS (in a 12 well plate). This washing step was performed to get rid of any medium or substances, in case the skin models were treated before with a chemical. After briefly drying the skin models on a paper tissue, they were quartered with a scalpel and transferred into a 24 well plate. Next, 1 ml of the 0.5 mg/ml MTT solution (diluted in PBS with calcium and magnesium) were added to each skin model. The skin models were incubated for three hours in an incubator at 37 °C with 5 % CO_2 and humidified atmosphere. This was followed by another washing step with PBS (with calcium and magnesium). After drying the skin models on a paper tissue, the skin models were

transferred in a new 24 well plate. 1 ml isopropanol (99.8 %) was added to each skin model. The plate was closed with parafilm and incubated overnight at 4 °C. On the next day, the plate was placed on a shaker for approximately 30 min to reach room temperature. After removing the skin models, at least two times 200 µl of each sample was transferred into a 96 well plate with flat bottom. Lastly, the samples were measured in a microtiter plate (Tecan) at 570 nm. If the measured absorption was outside the instrument measurement plate, the samples were diluted 1:2 with isopropanol and measured again at 570 nm.

The viability of the skin models was calculated as a percentage, based on the controls, which were usually untreated skin models. Phenol red-free ALI medium served as a blank and the mean of the blank replicates was used to correct the optical density of the measured skin model samples.

3.4.3 Separation of epidermis

In order to enable an independent analysis of the epidermis and dermis of the Phenion® FT skin models, it was necessary to first separate the skin layers. This was done enzymatically, as described by Reisinger et al. (2018), by placing the skin models with the epidermis facing upward in 12 well plates containing 300 µl thermolysin per well or one half of the skin model in 24 well plates filled with 150 µl thermolysin. The skin models were incubated for one to two hours at 4 °C before separating the layers with the help of tweezers. Subsequently, the RNA was isolated from the layers (refer to 3.4.9) or the epidermis was embedded in fluorescence mounting medium and examined under a fluorescence microscope to visualize the integrated CFSE-labeled MUTZ-LCs.

3.4.4 Preparation of frozen tissue section

At least one half of the Phenion® FT skin models was used to further analyze the tissue architecture of the skin models. For that, one half of the skin model was embedded in tissue freezing medium in cryomolds. Next, it was frozen at -20 °C and cut into ~8 µm sections with a cryostat SM 1900. Subsequently, the tissue sections were then further stained (refer to 3.4.5 and 3.4.6).

3.4.5 Haematoxylin and eosin staining of frozen tissue

The haematoxylin and eosin (HE) staining is a commonly used method, which enables the distinction of various tissue structures. Hematoxylin stains acidic and basophile structures blue, e.g., nucleus (the nucleic acids) and ribosomes, while eosin stains basic and acidophile structures pink/red, e.g., cytoplasm and extracellular matrix (the collagen fibers and proteins) (Chan, 2014). The combination of the two dyes was first described by Wissowzky (1877).

The prepared frozen tissue sections were stained with HE in an automated slide stainer (HistoTek), as described in the SOP from Henkel. For that, the following protocol was programmed:

I. 3 min incubation in Roti®-Histofix
II. 2 min incubation in Roti®-Histofix
III. 3 min incubation in Roti®-Histofix
IV. 3 min incubation in distilled water
V. 2 min incubation in haematoxylin
VI. 2 min incubation in distilled water
VII. 30 s incubation in 70 % ethanol
VIII. 20 s incubation in ammonia/ethanol
IX. 1 min incubation in eosin
X. 1 min incubation in 100 % ethanol
XI. 1 min incubation in 100 % ethanol
XII. 3 min incubation in xylene
XIII. 2 min incubation in xylene
XIV. Storage in xylene

After drying the slides under the fume hood, the tissue sections were covered with Cytoseal mounting medium to prevent the fading of the color and mounted with a cover glass. Lastly, the tissue sections were visualized under a microscope (BX51 with a microscope-mounted camera DP71).

3.4.6 Immunofluorescence staining of frozen tissue

The used immunofluorescence antibodies are listed in 2.2.2. The immunofluorescence staining was performed indirectly in two steps, as published by Phenion® ("Protocol Phenion® FT Skin Model Histology – Immunofluorescent labelling", www.phenion.com) with minor changes regarding incubation time and washing steps. First, the primary antibody was added to bind the target protein. The secondary antibody is conjugated with a fluorochrome and binds to the primary antibody. The negative controls were only stained with the secondary antibody to identify potential unspecific background staining of the secondary antibody.

First, the tissue sections were fixed by incubating the slides in pre-cooled Acetone at -20 °C for at least 15 min. After drying the slides under the fume hood, the tissue sections were outlined with a hydrophobic pen to contain the staining solutions within the sections. Next, the tissue sections were incubated with an anti-goat serum for at least 30 min at room temperature in a humidified chamber to block non-specific binding of the antibodies. The blocking solution was removed and the appropriately diluted primary antibody in DAKO antibody diluent was added (~70 µl per tissue section). However, for the negative control, only DAKO antibody diluent was applied without any antibody addition. This was followed by an incubation for at least one hour at 4 °C in a humidified chamber. After removing the primary antibody solution, the sections were washed three times with PBS (each time the slide were incubated for 10 min in PBS). The appropriate secondary antibody solution diluted in DAKO antibody diluent including 0.1 % 4′,6-diamidino-2-phenylindole (DAPI) was added to each section (~70 µl per tissue section). DAPI was added to the solution to enable a staining of the cell nuclei. Following the incubation for one hour at room temperature in a humidified chamber, the solution was removed, and the sections were washed three times in PBS. Each washing step included a 10 min incubation in the dark. After the incubation with the secondary antibody, the subsequent steps were predominantly conducted in the dark to account for the light sensitivity of the fluorochromes. Lastly, the tissue sections were covered with DAKO fluorescence mounting medium to preserve the fluorescence intensity, mounted with a cover glass and examined under a fluorescence microscope (BX51 with a microscope-mounted digital camera DP71).

3.4.7 Quantification of the epidermal thickness of Phenion® Full-Thickness skin model with and without integrated MUTZ-LCs

The analysis of the epidermal thickness of Phenion® FT skin model was performed using HE-stained images of tissue sections and the open access program ImageJ. To determine the thickness, lines were drawn and adjusted to the epidermal boundary at a specified distance. In order to account for commonly observed thickness variations within the skin models, a total of eleven lines were measured (if possible).

3.4.8 TUNEL assay on frozen tissue

To identify apoptotic cells in the skin models and to compare untreated and treated skin models, a terminal deoxynucleotidyl transferase-mediated dUTP-X nick end labeling (TUNEL) assay was performed on frozen tissue samples. This assay is based on labeling deoxyribonucleic acid (DNA) strand breaks (nicks), which is an early stage of apoptosis. The modified nucleotides can bind to the breaks, which is catalyzed by the enzyme terminal deoxynucleotidyl transferase. The modified nucleotides are coupled with fluorescein, enabling a detection of the apoptotic cells under a fluorescence microscope.

An *in situ* cell death detection kit with fluorescein was used and the protocol was performed according to the manufacturer's product data sheet ("Treatment of cryopreserved tissue", Roche). All TUNEL solutions, label and enzyme solution, were kept on ice until use. The frozen tissues were fixed for 20 min at room temperature in 4 % PFA (in TBS). To remove the fixation solution, the tissue sections were washed for 30 min in TBS. For the labeling, 200 µl 0.1 % Triton X-100 were added to the sections, followed by a 2 min incubation at room temperature. Subsequently, the solution was removed, and the tissue sections were washed twice in TBS (for 3 min each). In addition, to generate a positive control, one slide with frozen tissue sections were incubated for 10 min at room temperature in 3 U/ml Deoxyribonuclease I (Dnase I) (diluted in DNA Digest Buffer RDD) to induce DNA strand breaks.

Next, the TUNEL mix assay was prepared by diluting the TUNEL enzyme 1:10 in the TUNEL label solution. 50 µl TUNEL mix was added to each section, which were then enclosed with a coverslip. For the negative control, the sections were covered with the

label solution without enzymes. The sections were incubated for 60 min at 37 °C in the dark. After carefully removing the liquid, the sections were washed three times for 3 min in TBS in the dark. The slides were covered with 50 µl - 100 µl PI (1 µg/ml) and incubated for 5 min at room temperature in the dark. The toxic PI solution was removed, and the section were washed for 5 min in TBS in the dark. Lastly, the tissue sections were covered with DAKO fluorescence mounting medium to prevent fading of the fluorescence, mounted with a cover glass and examined under a fluorescence microscope (BX51 with a microscope-mounted digital camera DP71).

3.4.9 RNA isolation and Next Generation Sequencing of skin models

To study the molecular reaction of the skin models upon sensitizer treatment, a Next Generation Sequencing (NGS) with ribonucleic acid (RNA) samples was conducted. With this sequencing method it is possible to identify characteristic genes and thus read-out parameters to identify the sensitizing potential of a substance. To enable an individual analysis of the epidermis and dermis, the epidermal layer of one half of the skin models was enzymatically separated, as described in 3.4.3. Next, the isolation of RNA started using the RNeasy Mini kit (Qiagen), as described in the SOP from Henkel. The tissue samples were lysed by transferring the samples into 2 ml Eppendorf tubes and adding 150 µl RLT buffer. Next, the tissue samples were vortexed and shaken for at least 30 min in a lab shaker to disrupt the cells. The samples were stored at -20 °C until further processed. After thawing and vortexing the samples, 300 µl Proteinase K (20 mg/ml in RNA-free water) was added to each tube for protein degradation. The samples were incubated for 1 hour at 55 °C in a lab shaker. To precipitate the RNA, 500 µl 99 % ethanol was added. This was followed by mixing the samples through pipetting and transferring them onto RNease Mini Spin Columns. To save time, a QIAvec 96 top plate was used for a vacuum-based purification instead of centrifuging the samples. The vacuum was applied until every column was empty. The flowthrough was discarded, as the RNA and DNA remained on the column. Subsequently, the samples were washed by adding 500 µl RW1 buffer and applying vacuum until the columns were empty. In order to remove the DNA, 80 µl DNase1 (diluted in RDD buffer, 341 Kunitz units/ml) was added to each column. After a 15 min incubation at room temperature, the columns were washed again with 500 µl RW1 buffer. Next, the cells were washed twice with 500 µl RPE buffer. The samples were centrifuged at 13,000 rpm for 5 min to remove any liquid from the columns.

To elute the RNA, the columns were placed onto new collection tubes and 30 µl RNase-free water was added on each column membrane. Finally, the samples were centrifuged again at 13,000 rpm for 5 min. The RNA concentration of the samples was photometrically determined with a Nanodrop at 260 nm. In addition, the optical density (OD) was measured at 280 nm to detect any protein residues. Thus, the quotient OD260 nm/OD280 nm indicates the purity of the sample. A sample was considered free of contamination if the quotient value was between 1.8 and 2.0. The samples were stored at -20 °C. The transfer to Life & Brain GmbH was performed on dried ice with same-day delivery. Life & Brain GmbH conducted the NGS.

4. Results

The aim of this project is to generate a 3D immunocompetent skin model with dendritic cells. Native Langerhans cells (LCs) have a limited viability in culture and the disadvantage of donor variabilities. Thus, the human acute myeloid leukemia cell line MUTZ-3 was chosen as LC surrogate. Three main work packages were addressed in this project:

I. Differentiation of MUTZ-3 cells into MUTZ-LCs
II. Testing the immunocompetence of MUTZ-LCs
III. Integration of MUTZ-LCs into the Phenion® Full-Thickness (FT) skin model
IV. Testing the immunocompetence of Phenion® FT skin models integrated with MUTZ-LCs

4.1 Differentiation of MUTZ-3 cells into MUTZ-LCs

To get suitable surrogates for LCs, MUTZ-3 cells had to be differentiated with a cytokine cocktail into LC-typical cells, the MUTZ-LCs. There are already some published differentiation protocols, which differ in culture time and medium supplements. Thus, different protocols were tested to generate an optimized protocol. The impact of some medium supplements like granulocyte-macrophage colony-stimulating factor (GM-CSF), 5637-conditioned medium (5637CM) and fetal calf serum (FCS) on the MUTZ-LC differentiation and the differentiation time were studied. The aim was to maximize the yield of differentiated MUTZ-LCs, while improving the standardization of the protocol. The effect on cell morphology was analyzed microscopically. Furthermore, the expression of characteristic markers was studied with flow cytometry.

4.1.1 The effect of granulocyte-macrophage colony-stimulating factor on MUTZ-LC differentiation

In a previous study conducted at Henkel in the framework of a bachelor thesis, the MUTZ-3 cells were cultured for seven days in a differentiation medium supplemented with 20 % FCS, 10 % 5637CM, tumor necrosis factor alpha (TNF-α) and transforming growth factor beta (TGF-β) (5TT medium) (Cox, 2016). However, literature research has shown that besides TNF-α and TGF-β, GM-CSF is also known to induce dendritic cell development (Inaba et al., 1992) and is already frequently supplemented to the differentiation medium by published protocols (e.g., Santegoets et al., 2006; Nelissen et al., 2009; Kosten et al., 2015; Bock et al., 2018). Thus, to verify the effect of GM-CSF on MUTZ-LC differentiation, an initial cell passage was split and cultured in two differentiation media: 5TT (without GM-CSF) and 5TTG (with GM-CSF). The differentiation status was analyzed over three weeks to identify the optimal time frame for the differentiation.

Microscopic images of MUTZ-3 cells in maintenance medium (Figure 7A) showed mostly round-shaped cells and a few slightly elongated ones. The MUTZ-3 cells grew in suspension and as single cells. After 14 days of differentiation in 5TT and 5TTG medium, there were more dead cells and debris in the differentiation media (Figure 7B, C) compared to the maintenance medium. Moreover, an increase in cell size and an enhanced granularity was observed during differentiation, especially in 5TTG medium (Figure 7C). In contrast to the differentiation without GM-CSF, most of 5TTG-differentiated cells built cluster-like formations.

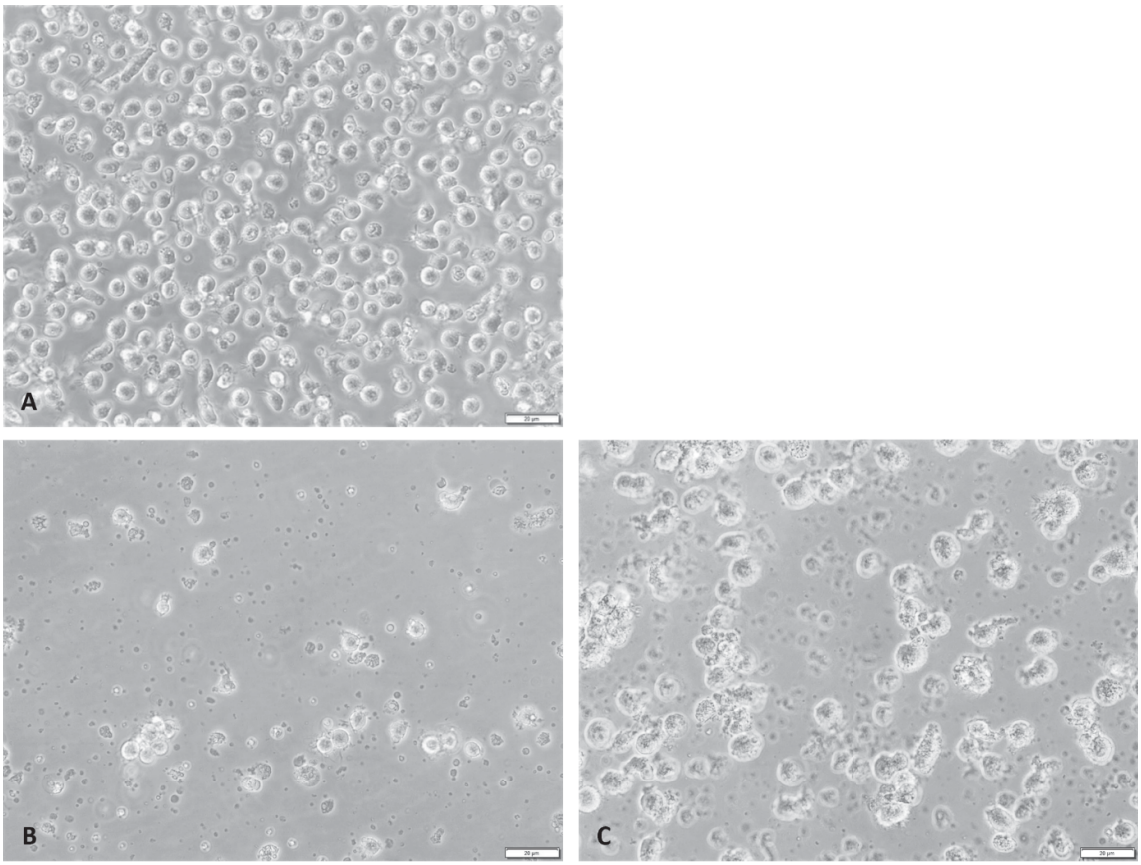

Figure 7: Morphological characteristics of MUTZ-3 cells and MUTZ-LCs.
Representative phase-contrast microscopic images showing MUTZ-3 cells cultured in maintenance medium (A) as well as 5TT- (B) and 5TTG-differentiated MUTZ-LCs (C) after 14 days of culture. Differentiation resulted in an increased number of dead cells and debris. An increase in cell size and granularity was observed in 5TTG medium. Scale bars represent 20 µm. Taken and modified from the author´s master thesis (Böttcher, 2019).

Flow cytometry analysis after seven days showed a *de novo* expression of the LC-typical markers CD1a and CD207 (Figure 8). On all measured time points, the expression was at least two-fold more pronounced in the medium with GM-CSF than in 5TT. However, after two weeks of differentiation, the numbers of positive cells stagnated or even decreased in both differentiation media. The expression of CD14 was lost after two weeks in 5TTG medium. In contrast, in 5TT medium CD14-positive cells were detected on all time points. After one week, the CD14 expression even increased in 5TT medium, with nearly 70 % positive MUTZ-LCs especially high in one of the two experiments. The number of CD86-positive cells increased from 20 % to approximately 80 % in 5TTG medium after seven days of differentiation and then stagnated. Initially, the CD86 expression remained the same during the first week in 5TT medium and then increased to only 60 % in the second week. After three weeks, CD86 expression in 5TT-differentiated MUTZ-LCs was discordant between two independently performed

experiments. In one experiment nearly 50 % of MUTZ-LCs were positive for CD86, while in the other one nearly no CD86-positive cell was detected. The course of the HLA-DR expression profiles was similar to the CD86 ones. Both markers were more expressed when differentiating the cells in the presence of GM-CSF in the differentiation medium. However, the initial HLA-DR expression of the MUTZ-3 cells was higher than the CD86 expression. Thus, the increase in HLA-DR expression was less pronounced. After three weeks, the numbers of HLA-DR-positive cells were more scattered in 5TT medium compared to every other time point.

Overall, the expression profiles of the differentiating cells changed during the first two weeks and then mostly stagnated in the third week. In addition, differentiating the cells with GM-CSF resulted in higher numbers of CD1a- and CD207-positive cells, indicating a more LC-like phenotype. Thus, for all following experiments GM-CSF was always added to the differentiation medium, while the differentiation time was set on two weeks.

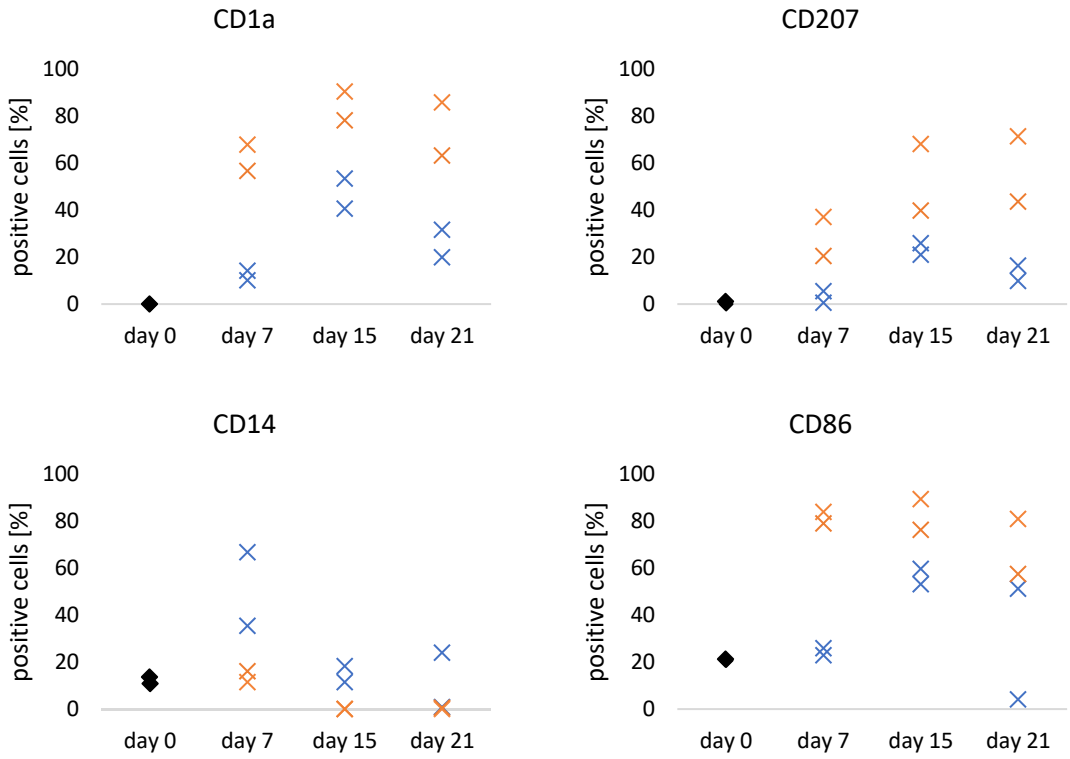

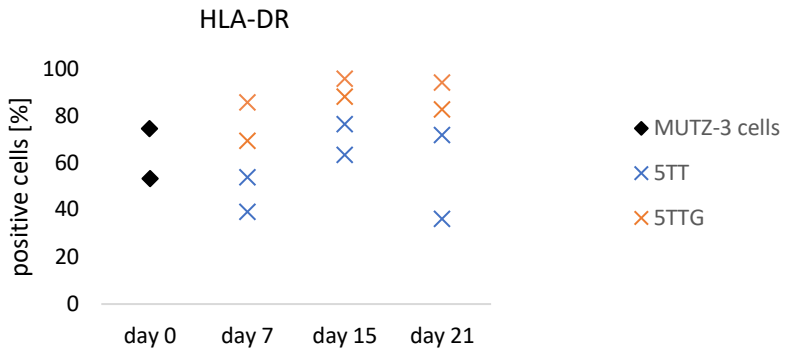

Figure 8: Changes in marker expression during MUTZ-LC differentiation with and without granulocyte-macrophage colony-stimulating factor over three weeks.
Floy cytometry analysis of the initial cell population, the MUTZ-3 cells, on day zero (black rhombus) and the differentiation in 5TT (blue crosses) and 5TTG (orange crosses) medium over three weeks. Cells were stained for the following markers: CD1a, CD207, CD14, CD86 and HLA-DR. A gate for propidium iodide (PI)-negative cells was drawn and a total of 10,000 PI-negative cells were analyzed. N=2, one symbol equals one experiment. Taken and modified from the author´s master thesis (Böttcher, 2019).

4.1.2 The effect of 5637-conditioned medium on MUTZ-LC differentiation

The supplier of the MUTZ-3 cells, the DSMZ, recommends adding 5637CM, the conditioned medium of a urinary bladder tumor cell line culture, to the cell culture medium during maintenance culture. However, to the author´s knowledge, it is not yet published whether this undefined cytokine cocktail has also a positive effect on LC differentiation. For that, two differentiation media were compared: TTG (without 5637CM) and 5TTG (with 5637CM).

Microscopic images of 5TTG- and TTG-differentiated MUTZ-LCs showed similar morphological characteristics (Figure 9). Both differentiation protocols resulted in cells similar in size, with an enhanced granularity and cluster-like formations, as described in 4.1.1.

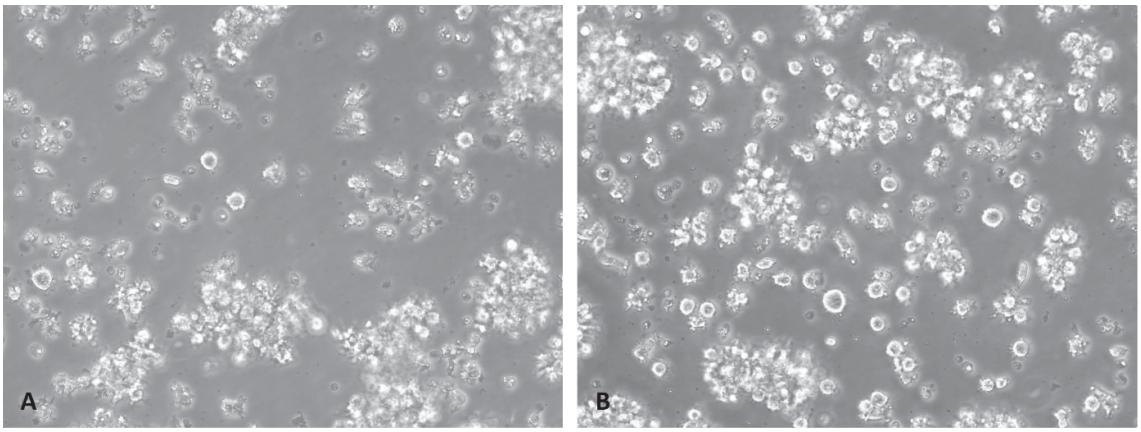

Figure 9: Effect of 5637-conditioned medium (5637CM) on the morphological characteristics of differentiated MUTZ-LCs.
Representative phase-contrast microscopic images in phase contrast of MUTZ-LCs differentiated in 5TTG (with 5637CM, A) and TTG (without 5637CM, B) after 14 days differentiation to observe the effect of 5637CM on MUTZ-LC differentiation. The bright-field phase-contrast images were taken at 20x object magnification.

Flow cytometry analysis revealed nearly identical expression profiles of all tested markers (Figure 10), independent of the composition of the differentiation medium in which the MUTZ-3 cells had been cultured. The viability of the cells decreased from approximately 90 % of the initial MUTZ-3 cell population to around 60 % on day seven and then to nearly 50 % after two weeks differentiation. A *de novo* expression of the surface proteins CD1a and CD207 was detected on the MUTZ-LCs after one week of differentiation. On day 14 nearly every MUTZ-LC was positive for the LC-typical markers. CD184 was also *de novo* expressed on the MUTZ-LCs, however, on day 14 only around 10 % of MUTZ-LCs were CD184-positive. The expression of CD34 as well as CD14 was lost during differentiation. The percentage of CD18-positive cells halved over time. A four-fold increase to nearly 90 % CD86-positive cells was detected after seven days of differentiation. Independent of the time of measurement, nearly all MUTZ-3 cells of the initial cell population and all MUTZ-LCs during the course of differentiation were positive for CD54 and CD44. After seven days of differentiation, CD80 expression increased from about 0 % to 30 % positive cells. A three-fold enrichment of CD80-positive cells was detected in the second week of differentiation. Around 15 % of the initial MUTZ-3 cell population were CD40-positive. During the differentiation, the percentage of CD40-postive MUTZ-LCs increased to approximately 60 % on day 7 and to about 90 % on day 14. Two thirds of MUTZ-3 cells were positive for HLA-DR, which increased to 85 % during differentiation, while none of the cells were positive for CCR7.

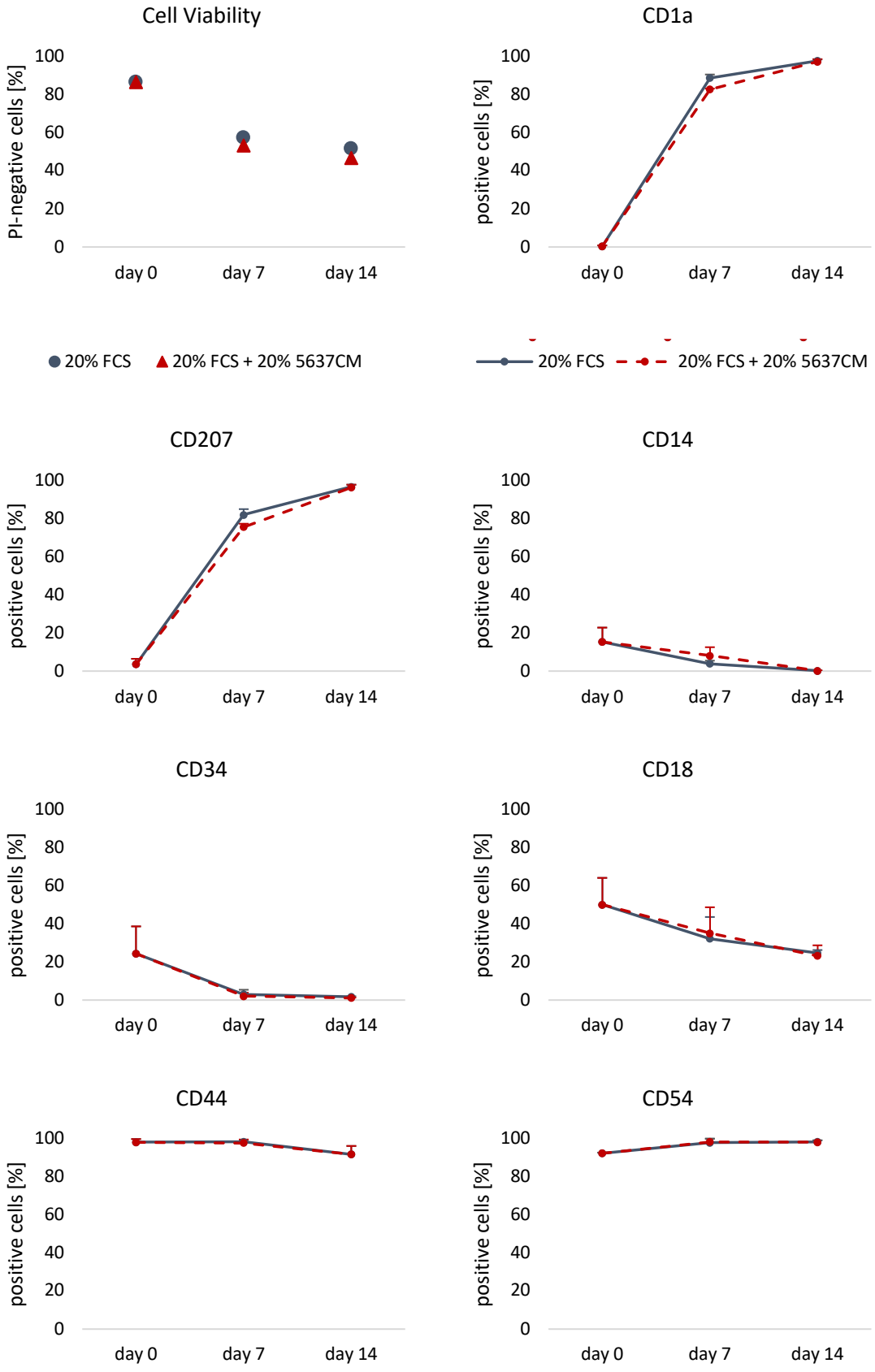
Cell Viability
PI-negative cells [%]
100
80
60
40
20
0
day 0
day 7
day 14
20% FCS
20% FCS + 20% 5637CM
CD1a
positive cells [%]
100
80
60
40
20
0
day 0
day 7
day 14
20% FCS
20% FCS + 20% 5637CM
CD207
positive cells [%]
100
80
60
40
20
0
day 0
day 7
day 14
CD14
positive cells [%]
100
80
60
40
20
0
day 0
day 7
day 14
CD34
positive cells [%]
100
80
60
40
20
0
day 0
day 7
day 14
CD18
positive cells [%]
100
80
60
40
20
0
day 0
day 7
day 14
CD44
positive cells [%]
100
80
60
40
20
0
day 0
day 7
day 14
CD54
positive cells [%]
100
80
60
40
20
0
day 0
day 7
day 14

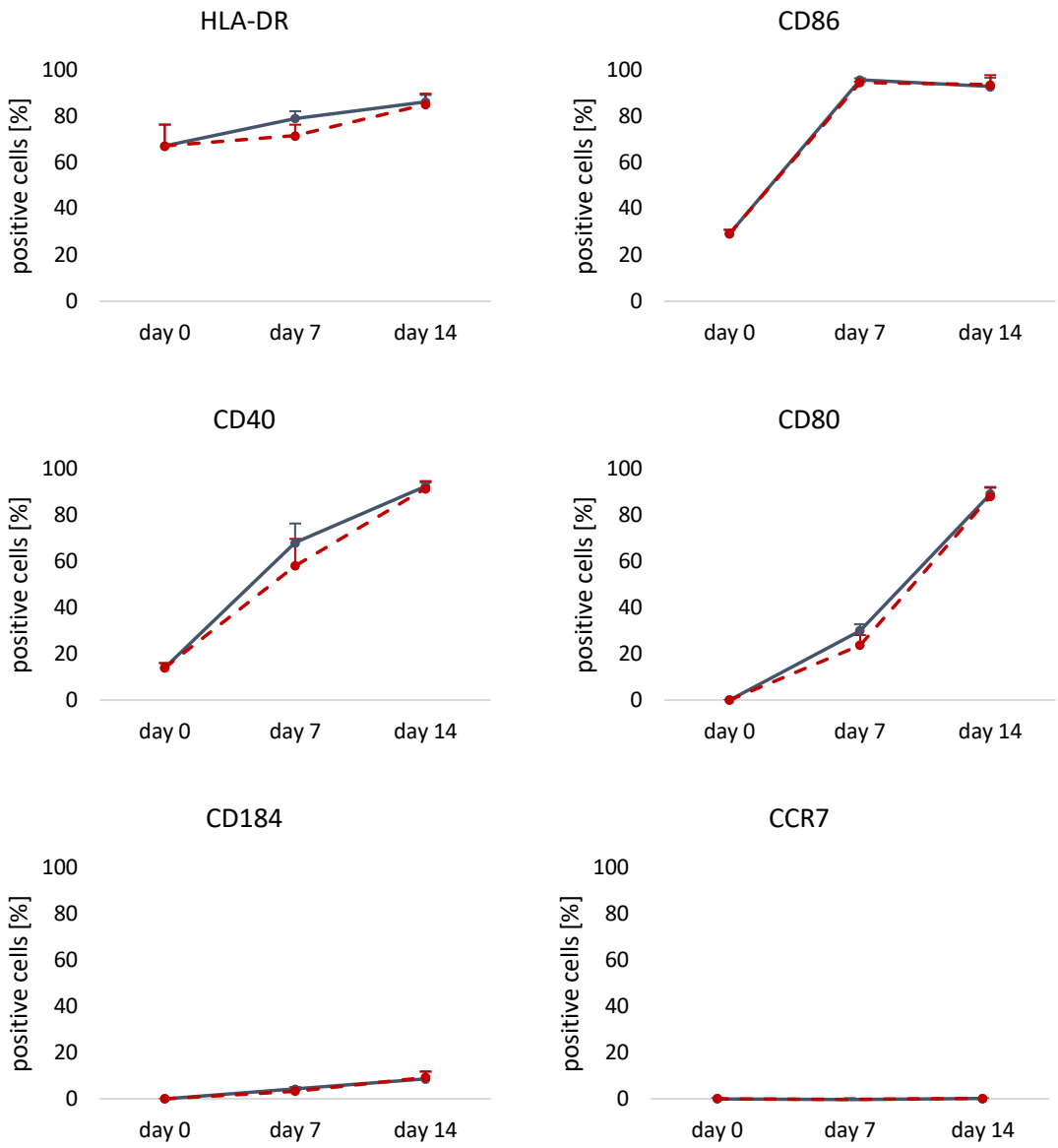

Figure 10: Changes in marker expression during MUTZ-LC differentiation with and without 5637-condiioned medium (5637CM) over two weeks.
Flow cytometry analysis of MUTZ-LCs differentiated in 5TTG (red triangle and red dotted line) and TTG (blue circle and blue solid line) medium. Day 0 represents the initial cell population, MUTZ-3 cells, before starting LC differentiation (day 7, 14). Cells were labeled with specific recombinant antibodies to identify the following proteins: CD1a, CD207, CD14, CD34, CD18, CD44, CD54, HLA-DR, CD86, CD40, CD80, CD184 and CCR7. A gate for propidium iodide (PI)-negative cells was drawn and a total of 10,000 PI-negative cells were analyzed. N=3, error bars represent standard deviation.

To sum it up, differentiating the MUTZ-LCs in culture medium without 5637CM seemed to have no impact on cell morphology and on the expression of proteins known to be expressed by LCs. As 5637CM is a biological product, it is likely that the composition of cytokines varies between the lots and passages of 5637 cells, which might hinder the reproducibility of the differentiation protocol. Hence, 5637CM was excluded from the differentiation medium for all following experiments.

4.1.3 Effects of FCS reduction on MUTZ-LC differentiation

In the next case study, the FCS effect on MUTZ-LC differentiation was analyzed. Four differentiation media were compared, all supplemented according to TTG medium with GM-CSF, TGF-β and TNF-α, but with different FCS concentration: 0 %, 5 %, 10 % and 20 % FCS. In the following, the media are named based on their FCS content.

After seven days of differentiation, the morphology of MUTZ-LCs differed depending on the FCS concentration in the medium (Figure 11). For one, only a few apparently viable cells and mostly debris were found when differentiating the cells completely without FCS (Figure 11A). 5 % FCS- (Figure 11B) and 10 % FCS-differentiated MUTZ-LCs for one week (figure 11C) were morphological similar to the cells cultured with 20 % FCS for two weeks (Figure 9B). Some of the cells formed long dendritic processes, which were more pronounced than in 20 % FCS-supplemented differentiation medium. However, in contrast to the previous reported observations for 20 % FCS-differentiated cells after 14 days, nearly no cluster-like formations nor adherent MUTZ-LCs with dendritic processes were observed after seven days of differentiation in 20 % FCS-supplemented differentiation medium (Figure 11D).

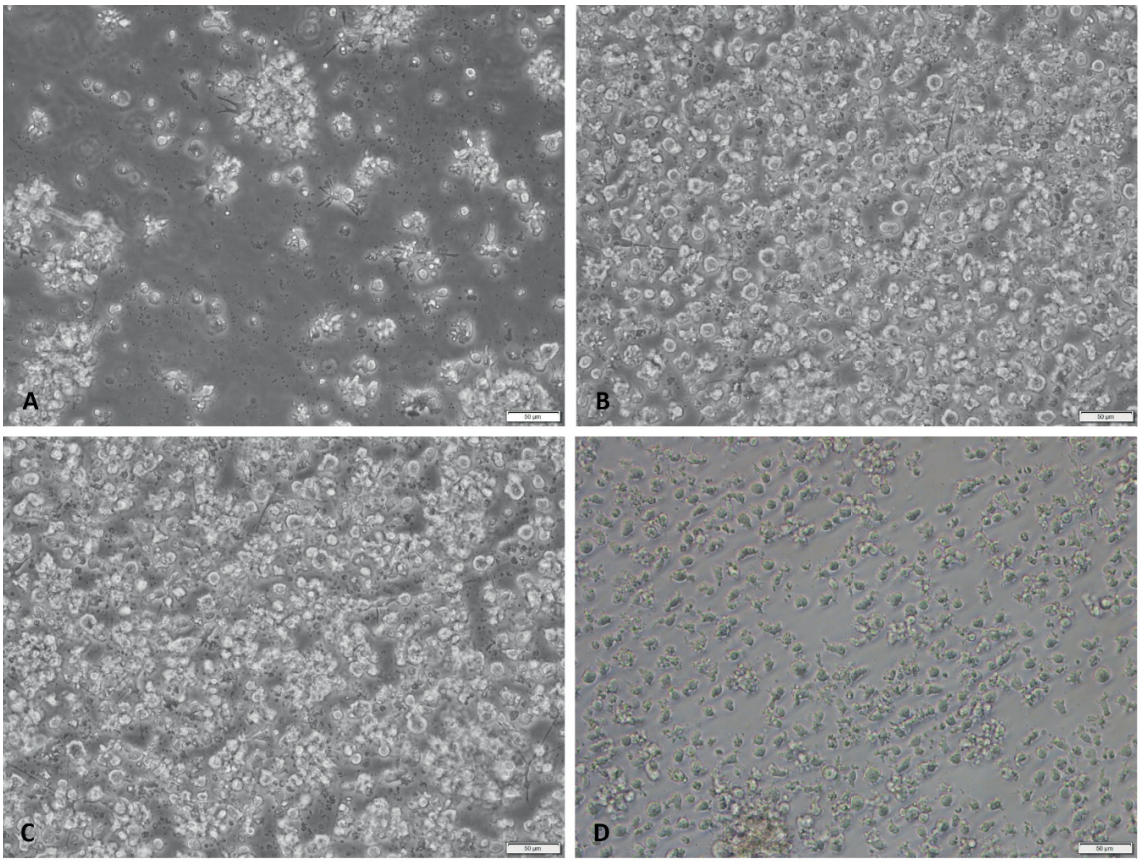

Figure 11: Morphological characteristics of 0 %, 5 %, 10 % and 20 % FCS-differentiated MUTZ-LCs.
Representative phase-contrast microscopic images of MUTZ-LCs differentiated in 0 % (A), 5 % (B), 10 % (C) and 20 % FCS (D) after seven days differentiation to observe the effect of FCS content on MUTZ-LC differentiation. Scale bars represent 50 µm.

Flow cytometry analysis showed a decrease of cell viability over the course of differentiation (Figure 12A). Compared to the initial MUTZ-3 cell population, a loss of cell viability by approximately 20 % for 20 % FCS- and nearly 30 % for 10 % FCS- as well as 5 % FCS-differentiated cells occurred. After the first week of differentiation, it was observed that slightly more than half of the 20 % FCS-differentiated cells remained viable. When the cells were exposed to a differentiation medium with reduced FCS content, the viability of the cells further declined, with fewer cells remaining viable (~45 %) compared to the 20 % FCS condition. During the second week, cell viability in all culture conditions decreased even further, falling below 40 %.

There is no data of 0 % FCS-differentiated MUTZ-LCs depicted, as the absence of FCS resulted in such a high cell death, that the number of viable cells was insufficient to perform a flow cytometry analysis. Apart from the increasing number of dead cells, the increase in cell debris, observed in the microscopic images, could also be confirmed by

flow cytometry analysis. The representative side vs. forward scatter plot showed more than 40 % of the detected events to be debris (Figure 12B).

The expression profiles of the differentiated MUTZ-LCs differed only in the marker expression of CD1a and CD207 (Figure 12C). On day seven, the typical LC markers were more expressed in 5 % FCS- and 10 % FCS- than in 20 % FCS-supplemented medium. After two weeks of differentiation, the numbers of CD1a- and CD207-positive MUTZ-LCs in 20 % FCS medium increased to the level of 5 % and 10 % FCS-differentiated cells at day seven.

CD34 expression was lost by all differentiated cells after the first week. On day seven, there were nearly no CD14-positive MUTZ-LCs detected in 5 % FCS- as well as 10 % FCS-supplemented medium (4.1 % and 2.5 %, respectively). In the 20 % FCS condition, 11.2 % of the cells expressed CD14. Thus, the decrease of CD14 expression occurred later in 20 % FCS-supplemented medium than in the reduced FCS condition. Regardless of the differentiation time and FCS content, nearly every MUTZ-LC was positive for CD44, CD54 and CD86.

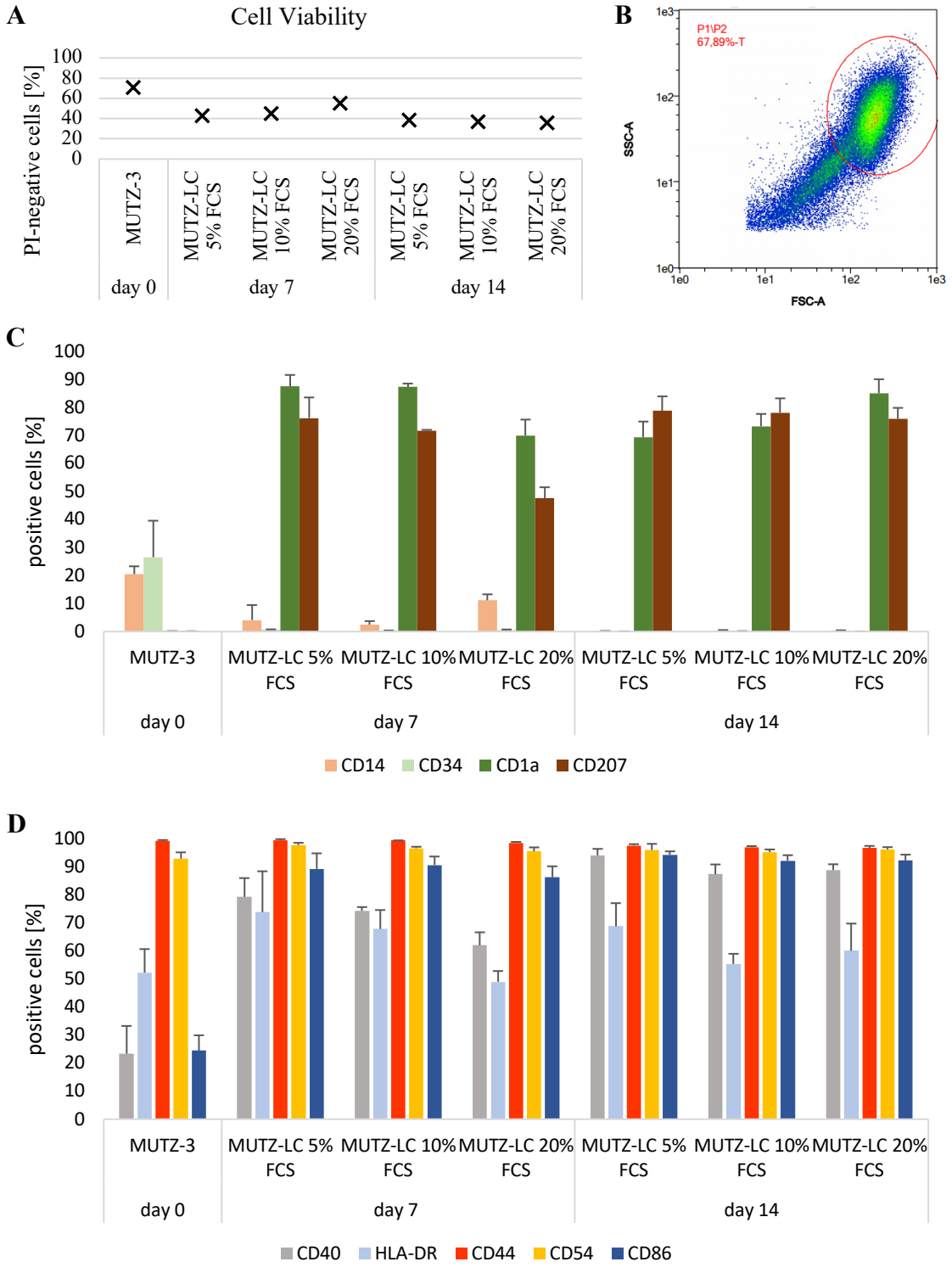

Figure 12: Changes in marker expression during MUTZ-LC differentiation with 5 %, 20 % and 20 % FCS over two weeks.
Flow cytometry analysis of MUTZ-LCs differentiated in 5 %, 10 % and 20 % FCS medium. Day 0 represents the initial cell population, MUTZ-3 cells, before starting LC differentiation (day 7 and 14). The viability of cells represents the percentage of propidium iodide (PI)-negative cells (A). Representative side vs. forward scatter plot of single cells showing gate P2 around the cell population to exclude cell debris (B). Cells were stained for the following markers: CD14, CD34, CD1a and CD207 (C); CD40, HLA-DR, CD44, CD54 and CD86 (D). A gate for PI-negative cells was drawn and a total of 10,000 PI-negative cells were analyzed. N=4, error bars represent standard deviation.

Overall, the expression profiles of MUTZ-LCs, cultured in 5 % and 10 % FCS, were similar during differentiation. Moreover, the FCS-reduced differentiation media accelerated the induction of LC-typical markers compared to the original 20 % FCS differentiation medium. For the following experiments, 5 % FCS was supplemented to the differentiation medium.

4.1.4 Effect of Ultroser G on MUTZ-LC differentiation

One aim of this project was to improve the standardization of the differentiation protocol and reducing the use of animal-derived products. The differentiation without FCS resulted in a high cell death. Thus, Ultroser G, a commercially available and non-animal-derived alternative for FCS, was tested. Two TTG differentiation media were compared: one supplemented with 5 % FCS, and the other one with 4 % Ultroser G medium. The Ultroser G concentration was set based on the originally recommended 20 % FCS supplement, which is described to be equivalent to 4 % Ultroser G (product data sheet, Pall BioSepra).

When differentiating the cells with 4 % Ultroser G, only few cells with small dendritic processes were observed (Figure 13A). In contrast to Ultroser G, 5 % FCS-differentiated MUTZ-LCs were bigger in size, and numerous cells adhered to the bottom of the well, thereby exhibiting long, branched dendritic processes (Figure 13B). Cell granularity was increased in both differentiation media compared to the MUTZ-3 cells (Figure 7A).

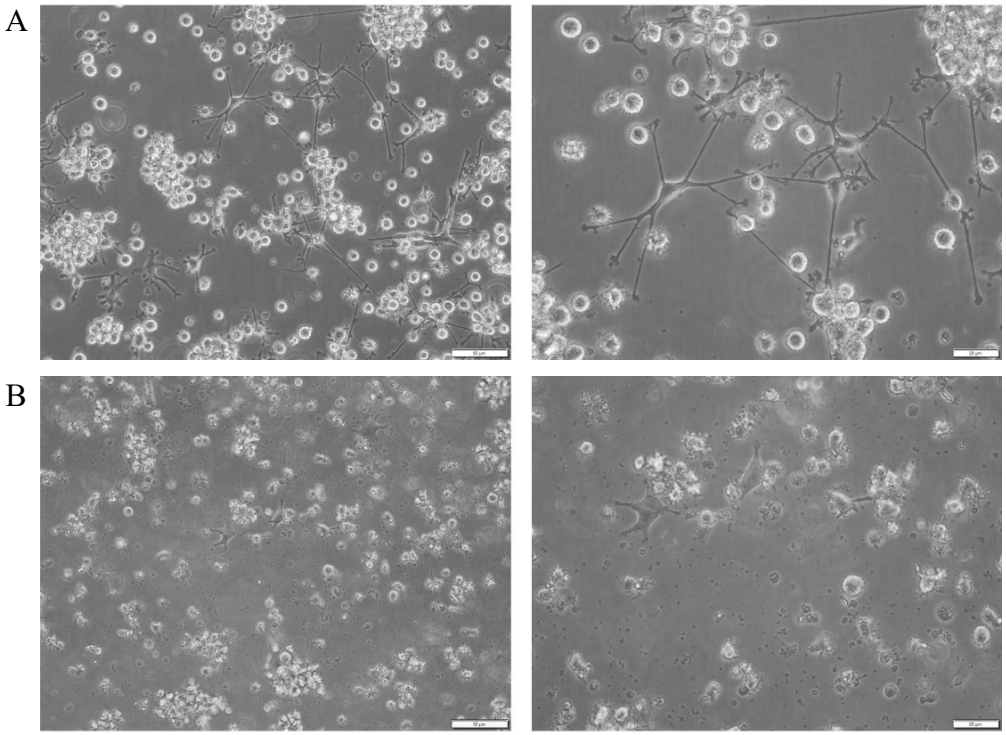

Figure 13: Morphological characteristics of 5 % FCS- and 4 % Ultroser G-differentiated MUTZ-LCs.
Representative phase-contrast microscopic images of MUTZ-LCs differentiated for seven days in 5 % FCS (A) and 4 % Ultroser G (B). Scale bars on the left side represent 50 µm and on the right side 20 µm.

After seven days 67.4 % ± 7.3 were viable in 4 % Ultroser G and 49.1 % ± 7.3 were viable in 5 % FCS medium. The viability of cells represented the percentage of propidium iodide (PI)-negative cells. On day seven, flow cytometry analysis (Figure 14) revealed a slight CD14 expression on 4 % Ultroser G-differentiated MUTZ-LCs, while no CD14-positive cells were found in 5 % FCS medium. In some experiments there were still CD34-positive MUTZ-LCs in 4 % Ultroser G medium, but overall, the CD34 expression was mainly lost as in the 5 % FCS medium. Moreover, when differentiating the cells in 4 % Ultroser G, the percentage of CD1a-positive cells were nearly halved and only one third of the MUTZ-LCs were positive for CD207 compared to the numbers of 5 % FCS-differentiated cells. The CD40 and HLA-DR expression of 4 % Ultroser G-differentiated cells was on average 20 % lower than in 5 % FCS medium. In contrast, the expression levels of CD44, CD54 and CD86 were high in both differentiation media. The CD18 expression was slightly higher in 4 % Ultroser G medium than in 5 % FCS medium. Compared to the 5 % FCS-differentiated cells, only one tenth of the 4 % Ultroser G-differentiated MUTZ-LCs expressed the costimulatory factor CD80. The numbers of positive cells for CD184 and CCR7 were low and comparable in both differentiation media.

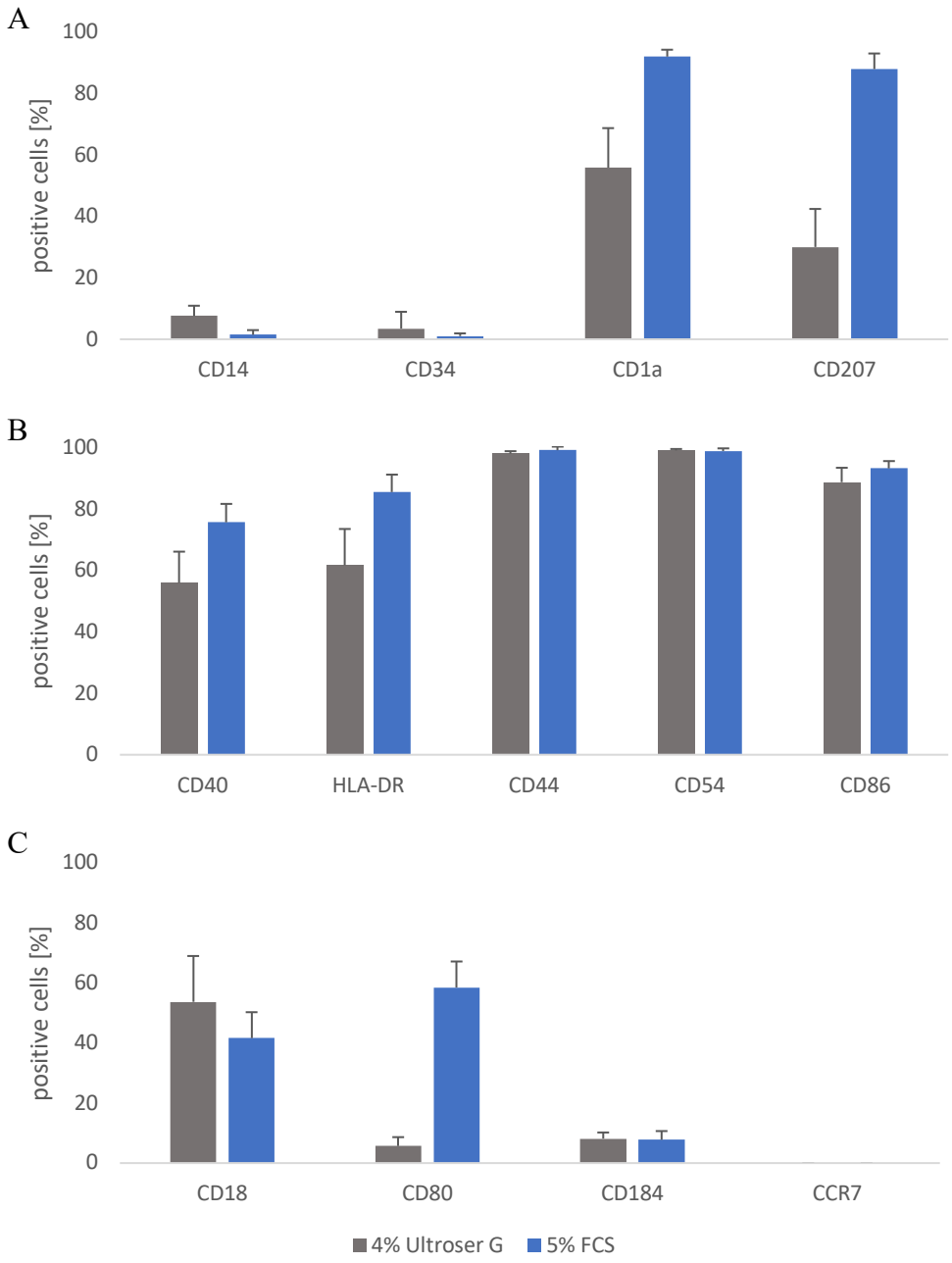

Figure 14: Marker expression comparison of 5 % FCS- and 4 % Ultroser G-differentiated MUTZ-LCs on day seven.
Flow cytometry analysis of MUTZ-LCs differentiated for seven days in 5 % FCS (blue) and 4 % Ultroser G (grey). MUTZ-LCs were stained for the following markers: CD14, CD34, CD1a and CD207 (A); CD40, HLA-DR, CD44, CD54 and CD86 (B); CD18, CD80, CD184 and CCR7 (C). A gate for propidium iodide (PI)-negative cells was drawn and a total of 10,000 PI-negative cells were analyzed. N=8, error bars represent standard deviation.

4.2 Treatment of MUTZ-LCs with sensitizers

To identify whether the differentiated MUTZ-LCs could be activated and thus be used for skin sensitizations assays, the cells were treated with sensitizers. 2,4-Dinitrochlorobenzene (DNCB) was chosen as a known extreme sensitizer and imidazolidinyl urea (I. Urea) as a weak sensitizer. Both chemicals are listed as proficiency chemicals for the h-CLAT assay (OECD TG 442E, 2023). According to this OECD-accepted h-CLAT assay (OECD TG 442E, 2023), sensitizers were used in a concentration, which resulted in approximately 75 % cell viability compared to the vehicle control after 24 h treatment. The concentrations were determined with a dose range finder (data not presented here). DNCB was dissolved in DMSO and I. Urea in phosphate-buffered saline (PBS). The sensitizers were used in different concentration for 5 % FCS- and 4 % Ultroser G-differentiated MUTZ-LCs. The measured cell viabilities are depicted in Table 3.

Table 3: Viability of DNCB- and imidazolidinyl urea-treated (I. Urea) MUTZ-LCs, differentiated in 5 % FCS- and 4 % Ultroser G-supplemented medium.
Viability of treated MUTZ-LCs based on the viability of the corresponding vehicle control. Cells were differentiated for seven days in medium supplemented with 5 % FCS or 4 % Ultroser G. 5 % FCS-differentiated MUTZ-LCs were treated with 2.5 µg/ml and 3.5 µg/ml DNCB as well as 40 µg/ml I. Urea. 4 % Ultroser G-differentiated MUTZ-LCs were treated with 1.5 µg/ml DNCB and 25 µg/ml I. Urea. After 24 h treatment, the viability of MUTZ-LCs was detected with propidium iodide (PI)-staining. 10,000 PI-negative (viable) cells were measured with flow cytometry.

Differentiation medium	Treatment	Relative viability [%] ± standard deviation
5 % FCS	2.5 µg/ml DNCB	95.88 ± 5.32
	3.5 µg/ml DNCB	80.42 ± 10.88
	40 µg/ml I. Urea	78.88 ± 11.17
4 % Ultroser G	1.5 µg/ml DNCB	75.30 ± 1.29
	25 µg/ml I. Urea	75.73 ± 10.68

4.2.1 Effect of DNCB treatment on 5 % FCS- and 4 % Ultroser G-differentiated MUTZ-LCs

The impact of DNCB treatment on cell viability could also be observed microscopically (Figure 15C, D), showing more dead cells compared to untreated cells and the vehicle control (Figure 15A, B). In addition, when treating 5 % FCS-differentiated MUTZ-LCs with DNCB, there were fewer adherent cells with dendritic processes found than in the controls. This could not be observed for the DNCB treatment of 4 % Ultroser G-differentiated MUTZ-LCs, as almost none of the untreated cells expressed dendritic processes. Apart from that, the sensitizer treatment had no visible effect on the formation of the typical cell-aggregates.

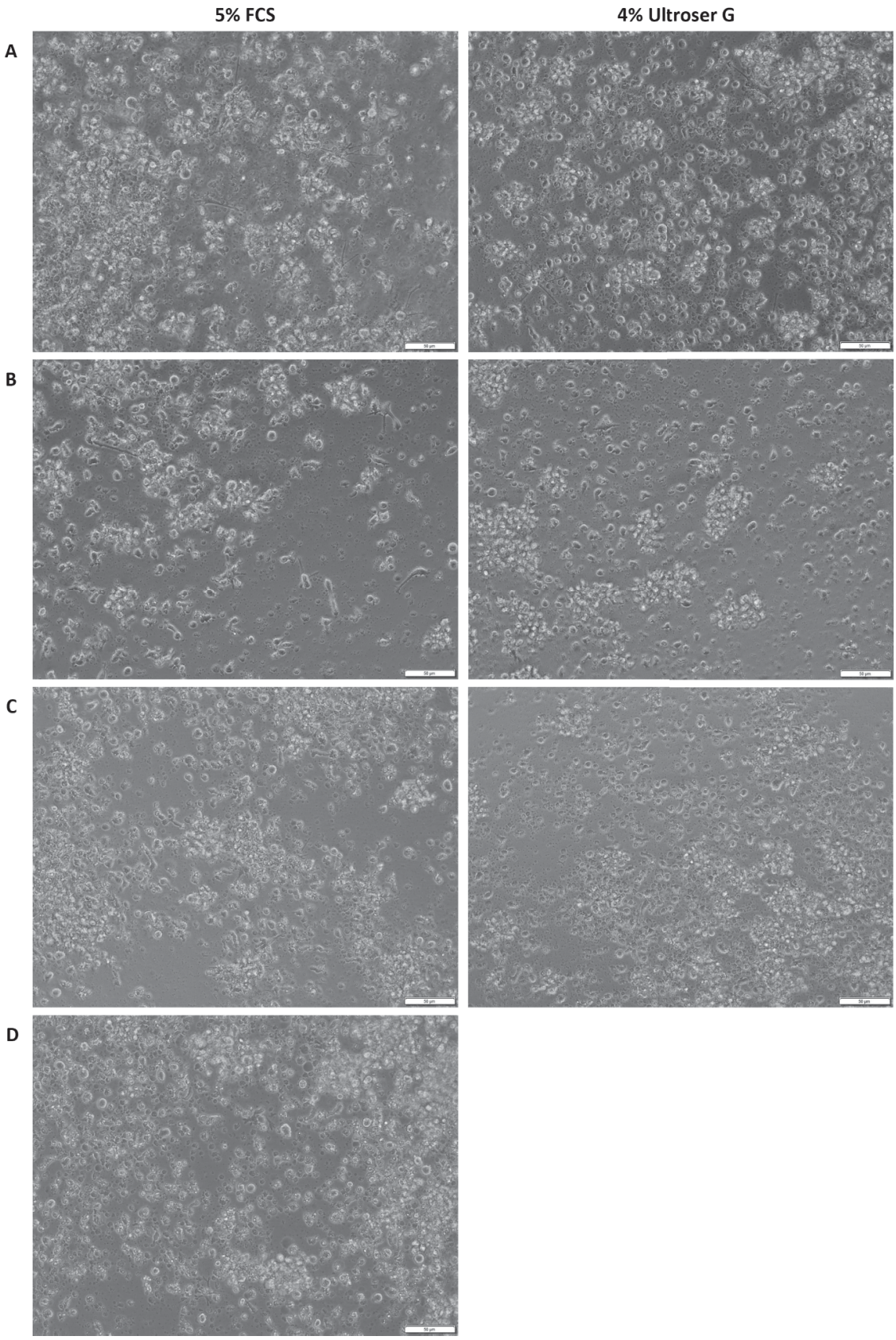

Figure 15: Morphological characteristics of untreated and DNCB-treated MUTZ-LCs, differentiated in 5 % FCS or 4 % Ultroser G.
Representative phase-contrast microscopic images of MUTZ-LCs differentiated in 5 % FCS (left side) and 4 % Ultroser G (right side) after seven days differentiation. The cells were untreated (A) as well as treated for 24 h with 1:500 DMSO (B), 2.5 µg/ml DNCB (C, left side,) or 1.5 µg/ml DNCB (C, right side) and 3.5 µg/ml DNCB (D). Scale bars represent 50 µm.

The flow cytometry analysis showed mostly no differences in marker expression after DNCB treatment (Figure 16). The expression of LC-typical markers, CD14, CD34, CD1a and CD207, remained unchanged (Figure 16A) compared to MUTZ-LCs not exposed to the sensitizer (expression levels were already described in 4.1.3 and 4.1.4). Similarly, no changes in the expression of chosen markers, known for their relevance in the process of LC maturation, were detected: CD40, CD44, CD54, CD86, CD80, CD18, E-Cadherin and CCR7 (Figure 16B, C). Representative histograms of CD54 and CD86, used, e.g., as sensitization markers in the h-CLAT assay (OECD TG 442E, 2023), showed no differences in signal distribution and intensity (Figure 16D). The expression of two of these markers, CD207 and CD40, showed minor changes in 4 % Ultroser G-differentiated MUTZ-LCs, but with relatively high standard deviations and thus minimizing the differences.

However, CD83 showed a three-fold and respectively four-fold increase after 2.5 µg/ml and 3.5 µg/ml DNCB treatment of 5 % FCS-differentiated MUTZ-LCs. The difference in the expression levels could also be seen in the representative histograms of CD83 (Figure 16D). There was no change in CD83 expression observed on 4 % Ultroser G-differentiated MUTZ-LCs.

A

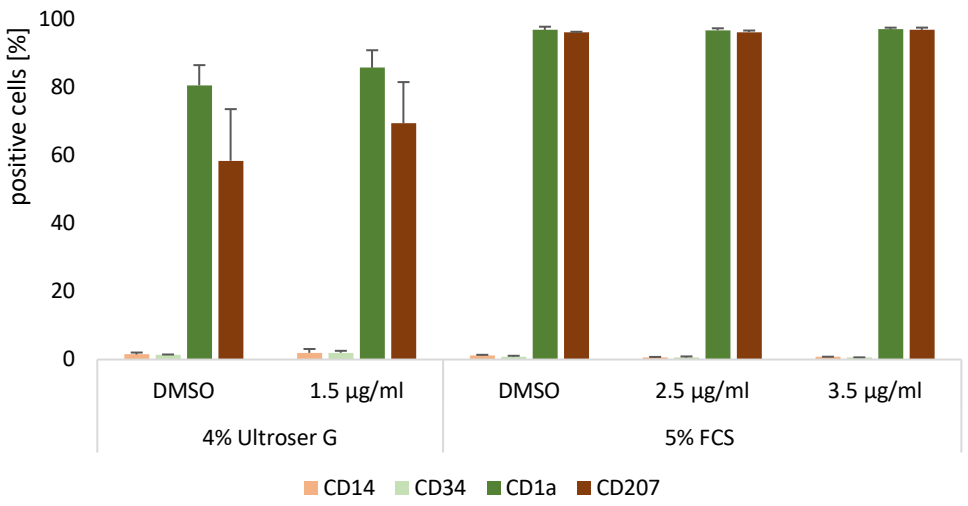

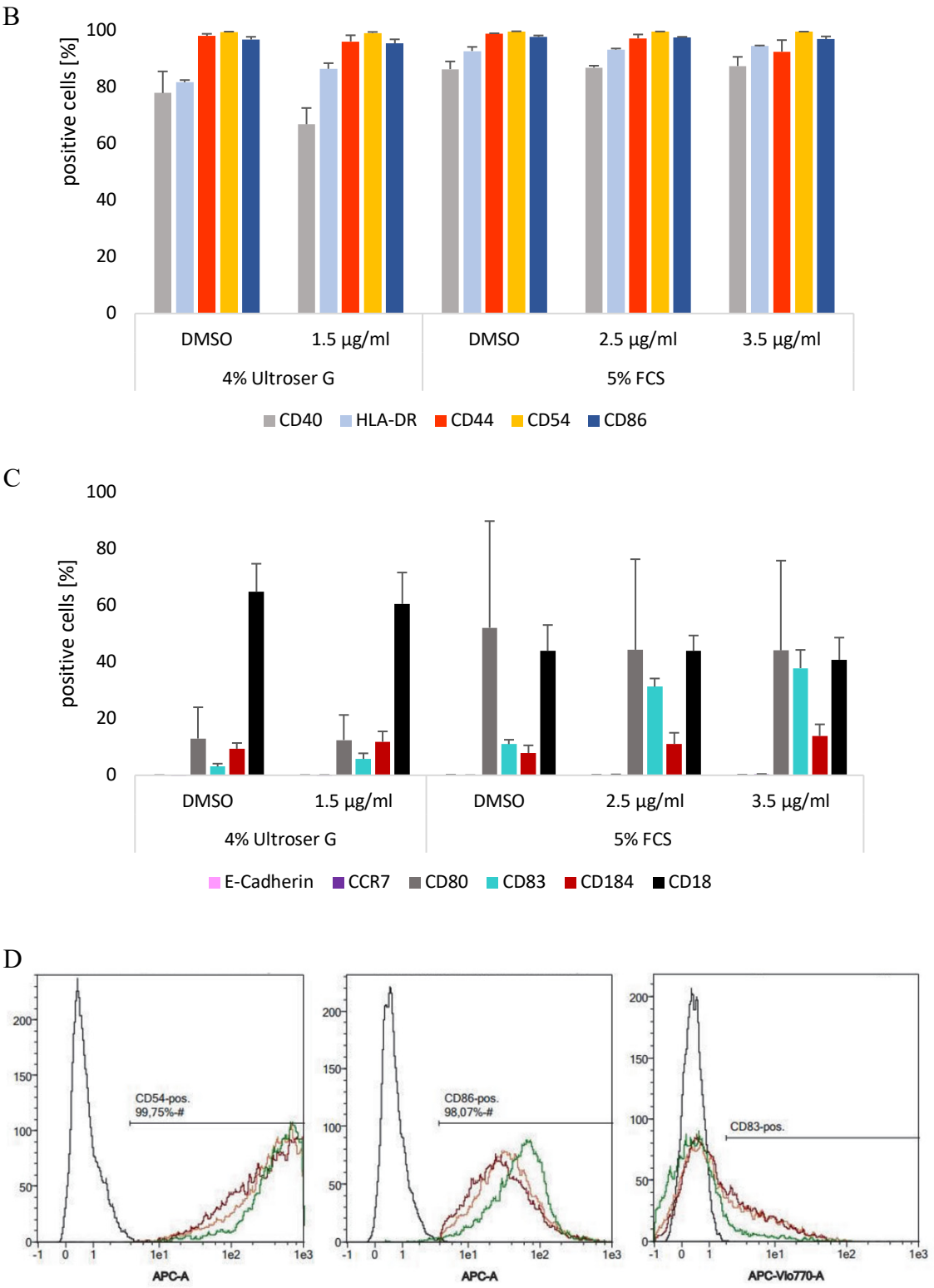

Figure 16: Changes in marker expression of 5 % FCS- and 4 % Ultroser G-differentiated cells after DNCB treatment.

Flow cytometry analysis of MUTZ-LCs differentiated for seven days in 5 % FCS and 4 % Ultroser G medium. 5 % FCS-differentiated MUTZ-LCs were treated for 24 h with 2.5 µg/ml and 3.5 µg/ml DNCB and 4 % Ultroser G-differentiated cells with 1.5 µg/ml DNCB. DMSO (0.2 %) was used as a vehicle control. Cells were stained for the following markers: CD14, CD34, CD1a and CD207 (A); CD40, HLA-DR, CD44, CD54 and CD86 (B); E-Cadherin, CCR7, CD80, CD83, CD184 and CD18 (C). Error bars represent standard deviation. Representative histograms of 5 % FCS-differentiated MUTZ-LCs stained with CD54, CD86 and CD83 showed an increase in CD83-positive cells after DNCB treatment (D): vehicle control (green), 2.5 µg/ml (orange) and 3.5 µg/ml DNCB (red).

4.2.2 Effect of imidazolidinyl urea treatment on 5 % FCS- and 4 % Ultroser G-differentiated MUTZ-LCs

Besides DNCB, the MUTZ-LCs, differentiated for seven days in either 5 % FCS- or 4 % Ultroser G-supplemented medium, were also treated for 24 h with I. Urea. After I. Urea treatment, there were more dead cells found under both culture conditions (Figure 17B) compared to the vehicle control (Figure 17A). It could be observed that the DNCB treatment resulted in a reduction of adherent cells with dendritic processes (Figure 16). In contrast, I. Urea treatment did not exhibit a similar effect (Figure 17).

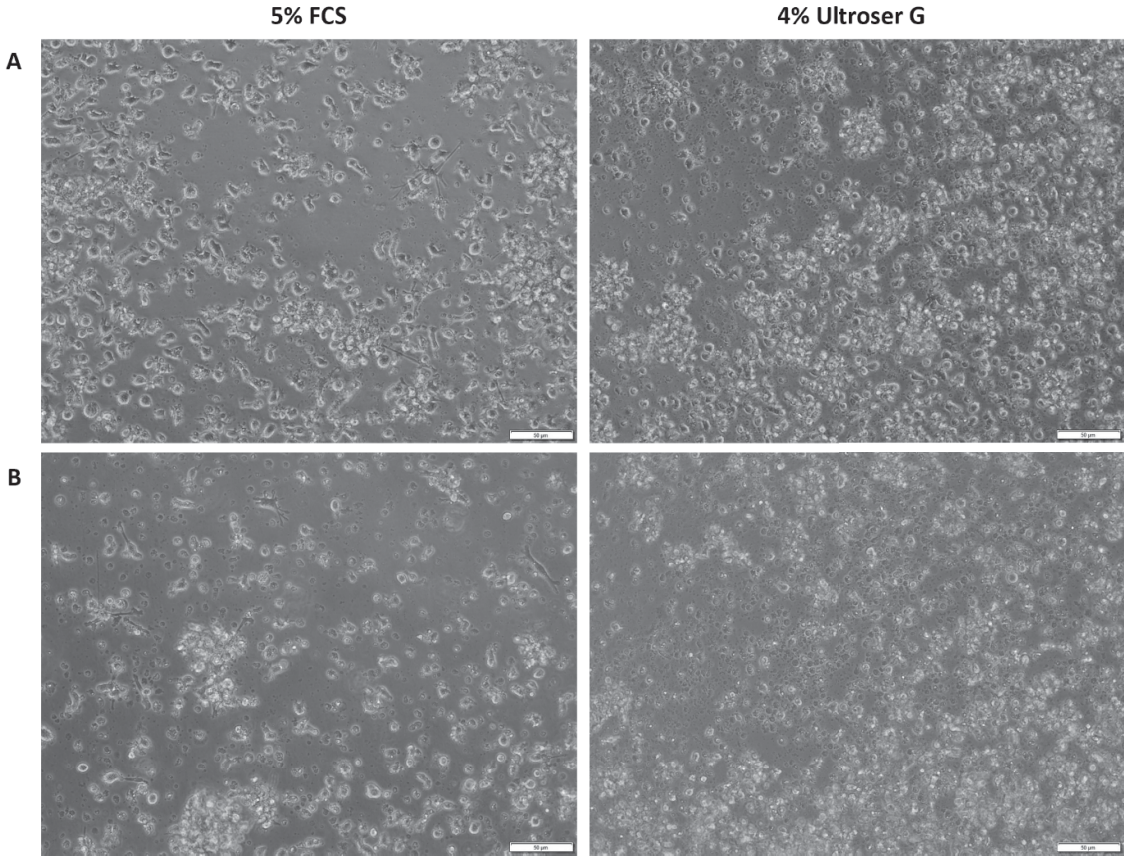

Figure 17: Morphological characteristics of PBS- and imidazolidinyl urea (I. Urea)-treated MUTZ-LCs, differentiated in 5 % FCS- or 4 % Ultroser G-supplemented medium.
Microscopic images of MUTZ-LCs differentiated in 5 % FCS- (left side) and 4 % Ultroser G-supplemented medium (right side) after seven days differentiation. The cells were treated for 24 h with 1:500 PBS (A) – the vehicle control for I. Urea –, 40 µg/ml (B, left side) or 25 µg/ml I. Urea (B, right side). Scale bars represent 50 µm.

Flow cytometry analysis showed that I. Urea treatment affected only the expression of HLA-DR and CD40, while all other marker expressions remained unchanged (Figure 18).

The percentage of HLA-DR increased in 4 % Ultroser G medium by approximately 5 percentage points from 80 % to 85 % positive cells and in 5 % FCS medium from 90 % to 95 %. The expression of CD40 was only increased on 5 % FCS-differentiated MUTZ-LCs from 80 % to 85 %. However, the changes observed in the expression levels of the previously described markers were relatively minor compared to the three-fold increase of CD83 expression after the DNCB-treatment of 5 % FCS-differentiated MUTZ-LCs (Figure 16).

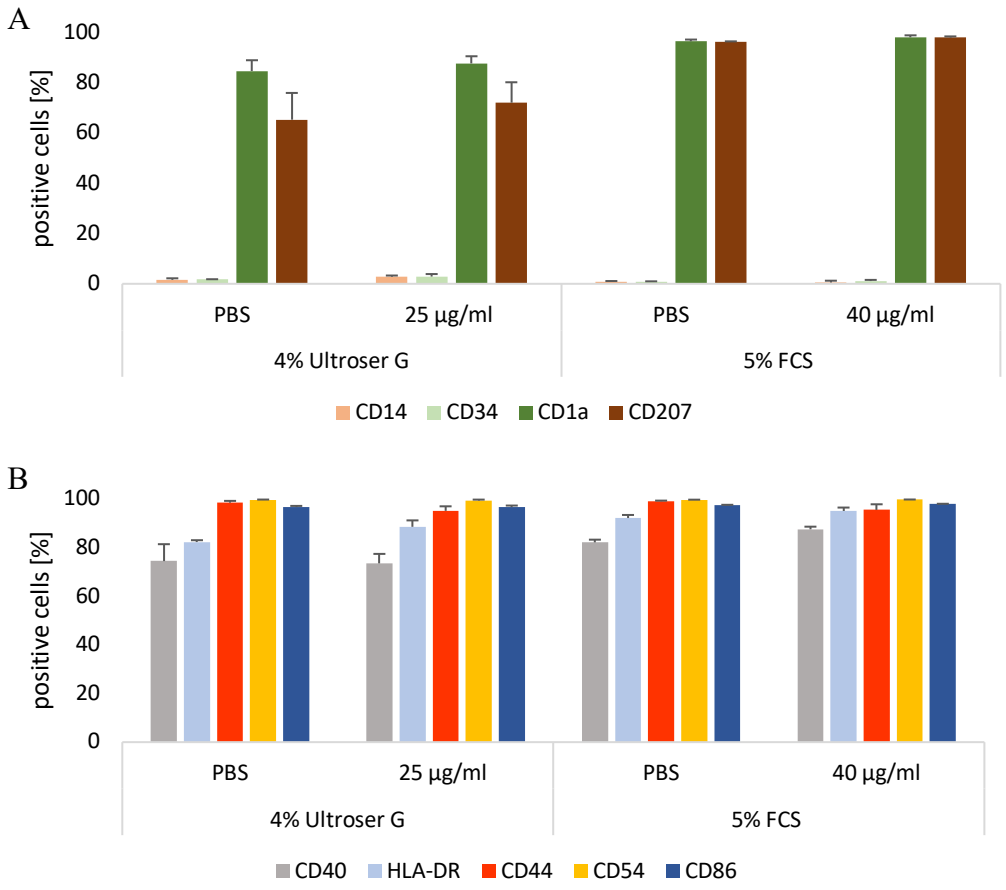

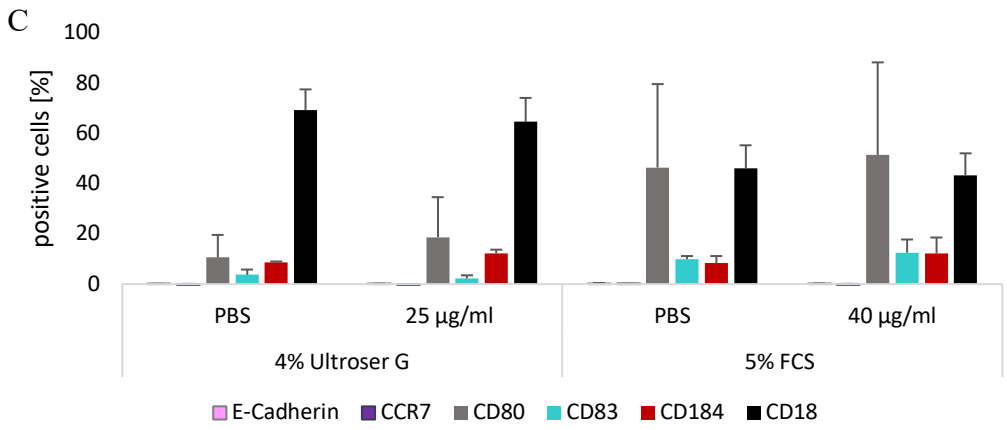

Figure 18*:* Changes in marker expression of 5 % FCS- and 4 % Ultroser G-differentiated cells after imidazolidinyl urea (I. Urea) treatment.

Flow cytometry analysis of MUTZ-LCs differentiated for seven days in 5 % FCS- and 4 % Ultroser G-supplemented medium. 5 % FCS-differentiated MUTZ-LCs were treated for 24 h with 40 µg/ml I. Urea and 4 % Ultroser G-differentiated cells with 25 µg/ml I. Urea. PBS (0.2 %) was used as a vehicle control. Cells were stained for the following markers: CD14, CD34, CD1a and CD207 (A); CD40, HLA-DR, CD44, CD54 and CD86 (B); E-Cadherin, CCR7, CD80, CD83, CD184 and CD18 (C). N=3, error bars represent standard deviation.

Overall, after DNCB treatment of 5 % FCS-differentiated MUTZ-LCs, an increased CD83 expression was detected, which was the only marker affected by the treatment. In addition, less adhered 5 % FCS-differentiated MUTZ-LCs with dendritic processes were found upon DNCB exposure compared to the controls. This could not be observed for the treatment with the weaker sensitizer I. Urea and for none of the treatments of 4 % Ultroser G-differentiated MUTZ-LCs.

4.3 Integration of MUTZ-LCs into the Phenion® Full-Thickness skin model and the effect on skin model differentiation

After optimizing the differentiation of MUTZ-LCs, the next step to generate a 3D immunocompetent skin model was the integration of MUTZ-LCs into the Phenion® FT skin model. First, a successful MUTZ-LC seeding protocol had to be developed. For that, different MUTZ-LC seeding protocols were designed and tested. When seeding the MUTZ-LCs (1E+6 cells) together with the keratinocytes (~0.5E+6 cells) on the dermis model, no MUTZ-LCs could be found in the fully differentiated skin models (no immunofluorescence signal of CD1a- or CD207-stained tissue sections; black images not

shown). To enable a better integration, 1E+6 MUTZ-LCs were seeded simultaneously with 2.5E+5 keratinocytes, followed by an additional seeding of 2.5E+5 keratinocytes after one to two hours. The results achieved with this procedure are explained in the following chapters.

The impact of the MUTZ-LC integration on the differentiation of the skin model was studied with optical coherence images (OCT) images as well as on hematoxylin-eosin-stained (HE-stained) histological sections. To determine the localization of the integrated MUTZ-LCs, the cells were stained with different methods.

In order to study the structural integrity of the skin models with and without integrated MUTZ-LCs, OCT images were taken of the skin models after being cultured for ten days at the air-liquid interface (ALI). The OCT images of skin models without and with integrated MUTZ-LCs showed an even epidermal surface (Figure 19). In addition, the epidermis and dermis could be clearly distinguished due to the change in OCT contrast (arrows, Figure 19A, B). By comparing skin models without MUTZ-LCs (control; Figure 19A) with skin models with integrated MUTZ-LCs (Figure 19B), no apparent differences were visible.

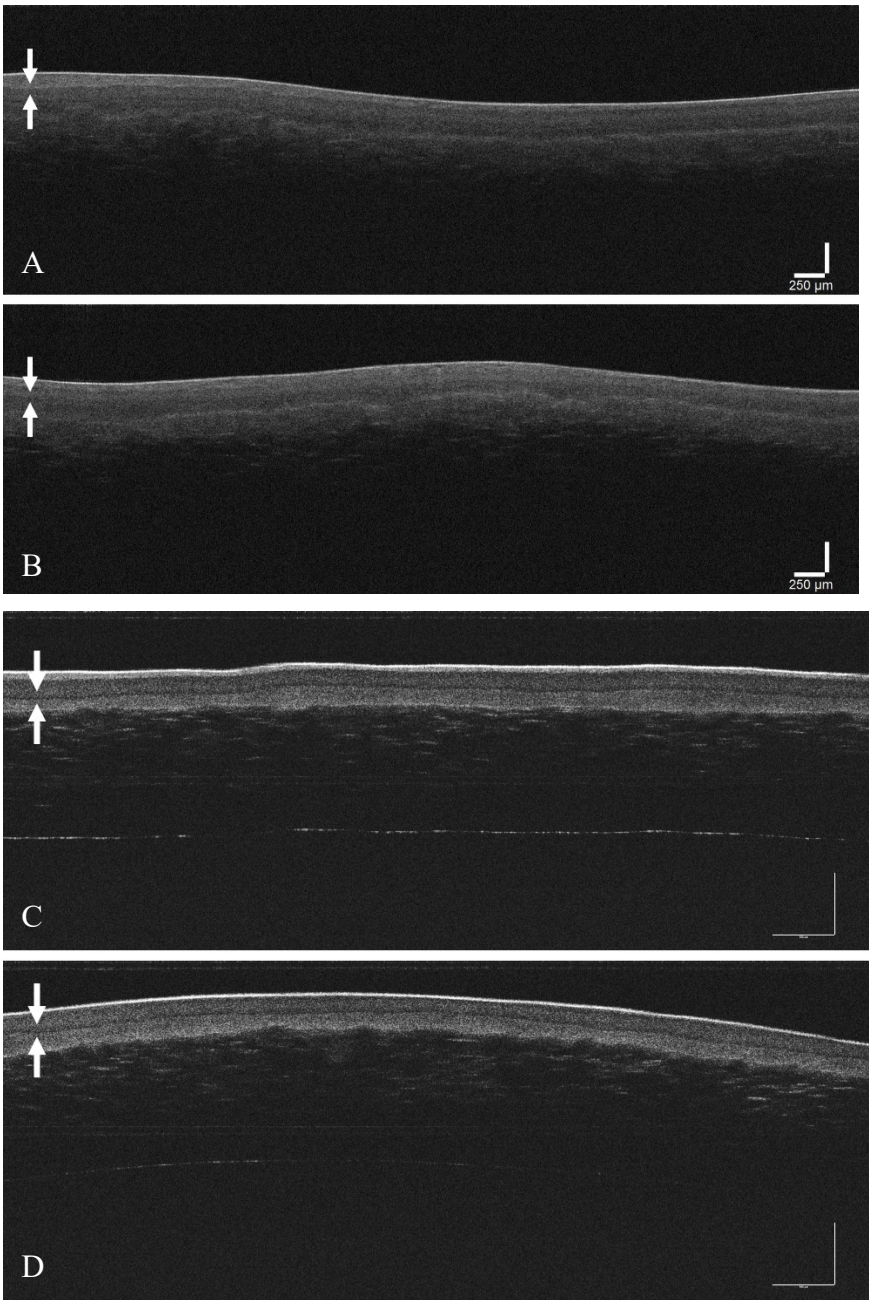

Figure 19: Optical coherence tomography images of a Phenion® Full-Thickness standard and LONG-LIFE skin model without and with integrated MUTZ-LCs.
Optical coherence tomography image of a standard (A, B) or LONG-LIFE (C, D) Phenion® Full-Thickness skin model, which was cultured for eleven days in air-liquid interface culture. Skin models were either without (A, C) or with integrated 20 % FCS-differentiated MUTZ-LCs (B, D). The junction between the epidermis and dermis can be identified due to the change in OCT contrast (junction is highlighted with arrows). Scale bars represent 250 µm (A, B) or 500 µm (C, D).

Tissue integrity and correct epidermal and dermal differentiation was also confirmed in detail on histological sections of the skin models (Figure 20). All epidermal layers characteristically for native human skin were correctly developed, including a multi-layered stratum corneum, independent of the additional seeded MUTZ-LCs. Directly underneath the epidermis, a zone of newly synthesized extracellular matrix proteins was

visible in both models, with and without MUTZ-LCs. The dermal region defined by the extent of the collagen matrix looked also similar, the pores were filled with ECM fibers in which the fibroblasts were embedded.

Apart from the standard Phenion® standard skin models (Figure 20A, B), it was also tested whether the MUTZ-LCs can be integrated into the LONG-LIFE version of the Phenion® FT skin model. This model enables with 50 days a four-times longer experimental test phase than the standard skin models. Similar to the results with the standard models, OCT images (Figure 19C, D) and HE staining (Figure 20C, D) of the tissues showed no differences in histological architecture between the skin models without and with integrated MUTZ-LCs.

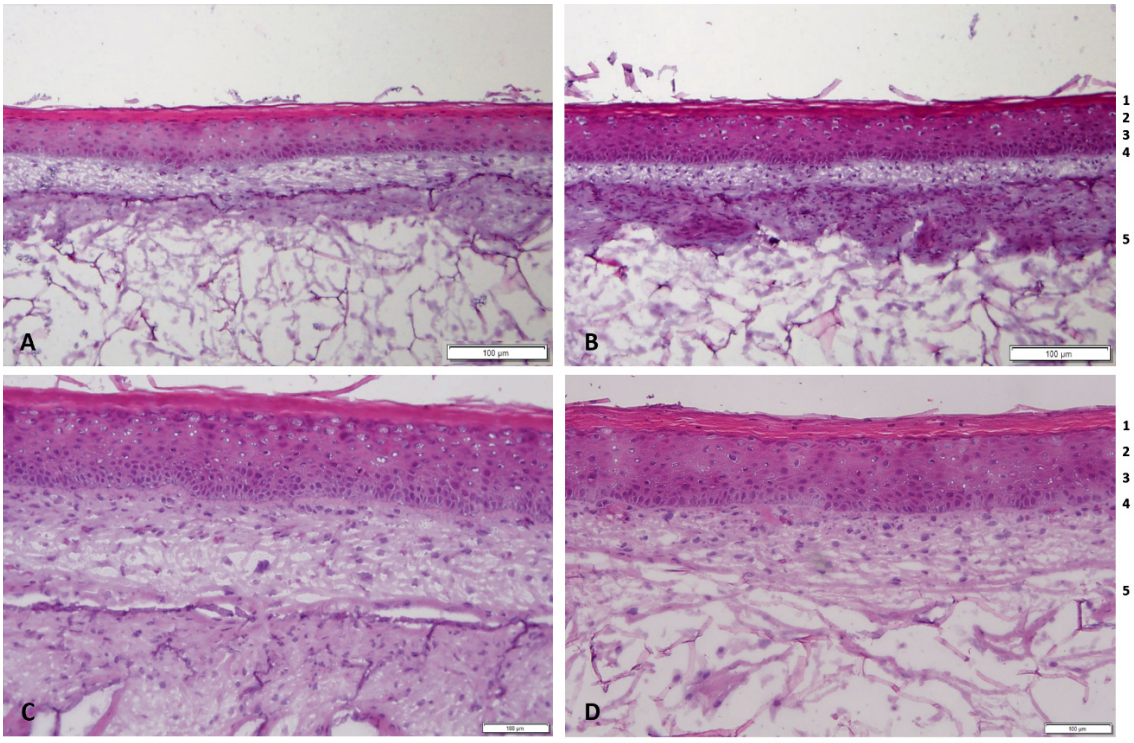

Figure 20: Effect of MUTZ-LC integration on the structure of Phenion® Full-Thickness skin models, standard and LONG-LIFE version.
Hematoxylin-eosin staining of frozen sections of Phenion® Full-Thickness skin models, standard (A, B) and LONG-LIFE version (C, D). Depicted are skin models without (A, C) or with MUTZ-LCs (B, D), which were differenitated for 14 days in 20 % FCS before being integrated into the skin models. The structure of the skin models shows the different epidermal layers: stratum corneum (1), stratum granulosum (2), stratum spinosum (3) and stratum basale (4). Below the epidermis is the dermis formed on the collagene matrix (5). Scale bars represent 100 µm.

Although the skin models with and without integrated MUTZ-LCs looked identical in terms of tissue architecture based on histological analyses, the MUTZ-LCs themselves could not be identified within the epidermal layers. If they had been successfully incorporated in a significant number, they seemed to be indistinguishable from the keratinocytes. To enable visual observation of the MUTZ-LCs, they were stained with carboxyfluorescein succinimidyl ester (CFSE) prior their integration into the skin model. CFSE is a widely used fluorescent dye that emits a distinct and detectable fluorescence signal, allowing the tracking of cells throughout an experiment. First, the CFSE staining was performed in 2D cell culture (Figure 21) to validate the staining success as well as the staining intensity. For that, MUTZ-3 cells instead of MUTZ-LCs were labelled, as the MUTZ-3 culture is more cost- and time-effective. All MUTZ-3 cells in the phase-contrast microscopic image (Figure 21A) emitted a green fluorescence signal in the green channel (Figure 21B), which is also shown in the merged image (Figure 21C).

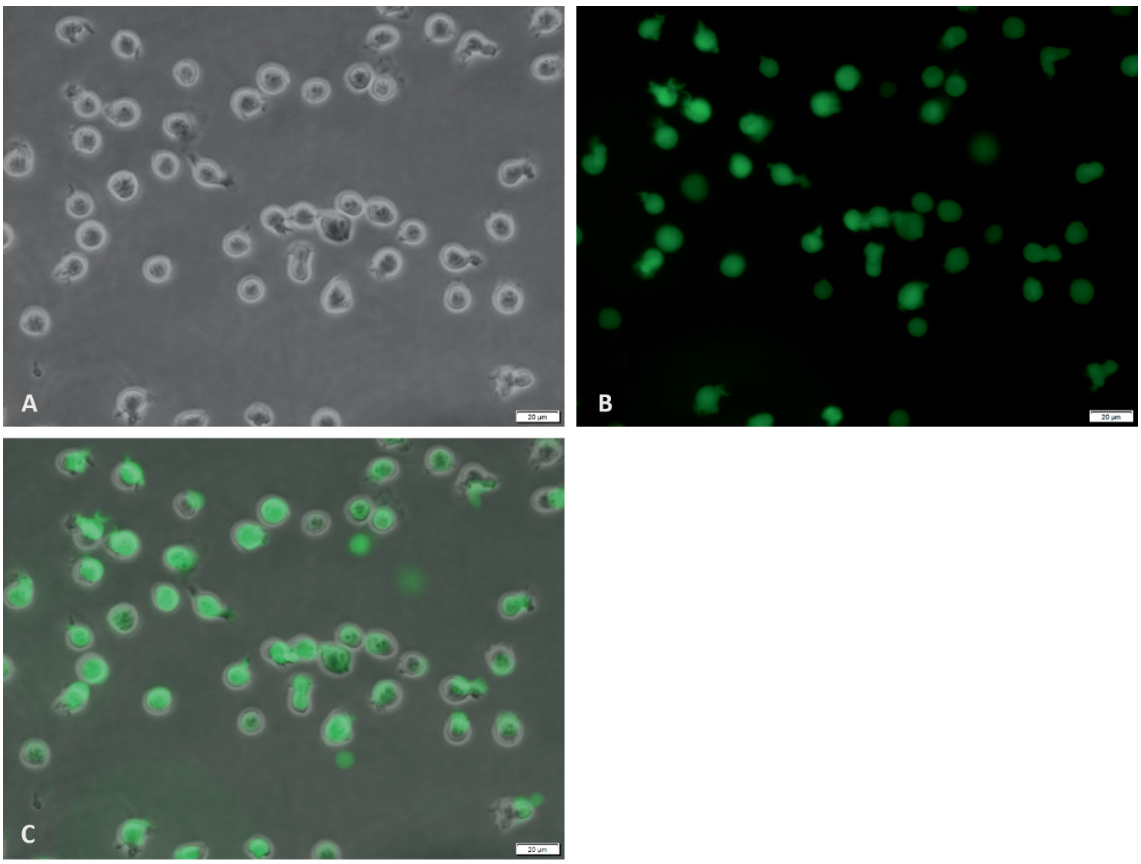

Figure 21: CFSE-labeled MUTZ-3 cells.
Representative microscopic images of CFSE-labeled MUTZ-3 cells. Depicted is an image in bright-field (A) and the green channel (B) as well as a merged image of the two channels (C) showing a successful CFSE staining of all cells. Scale bars represent 20 µm.

To test whether CFSE-labeled MUTZ-LCs could be identified in the epidermal tissue of the skin models based on their fluorescence signal, two analyses were performed, each conducted with one half of a skin model. For one, the epidermis of the skin models was enzymatically separated from the dermis and scanned for labeled cells with fluorescence microscopy (Figure 22). Skin models without integrated MUTZ-LCs served as controls, with no specific signals detected in the epidermal tissues (Figure 22B). Taking the overall pattern and distribution in the tissues into account, the faint fluorescing areas can be attributed to unspecific background signals emitted by intrinsic cellular molecules (Figure 22B). The tissue samples with integrated CFSE-labeled MUTZ-LCs emitted bright fluorescence signals (Figure 22D). The MUTZ-LCs seemed to form aggregates in the skin model, as they were mainly found in cluster-like formations. However, it was not possible to identify in which epidermal stratum the MUTZ-LCs were integrated.

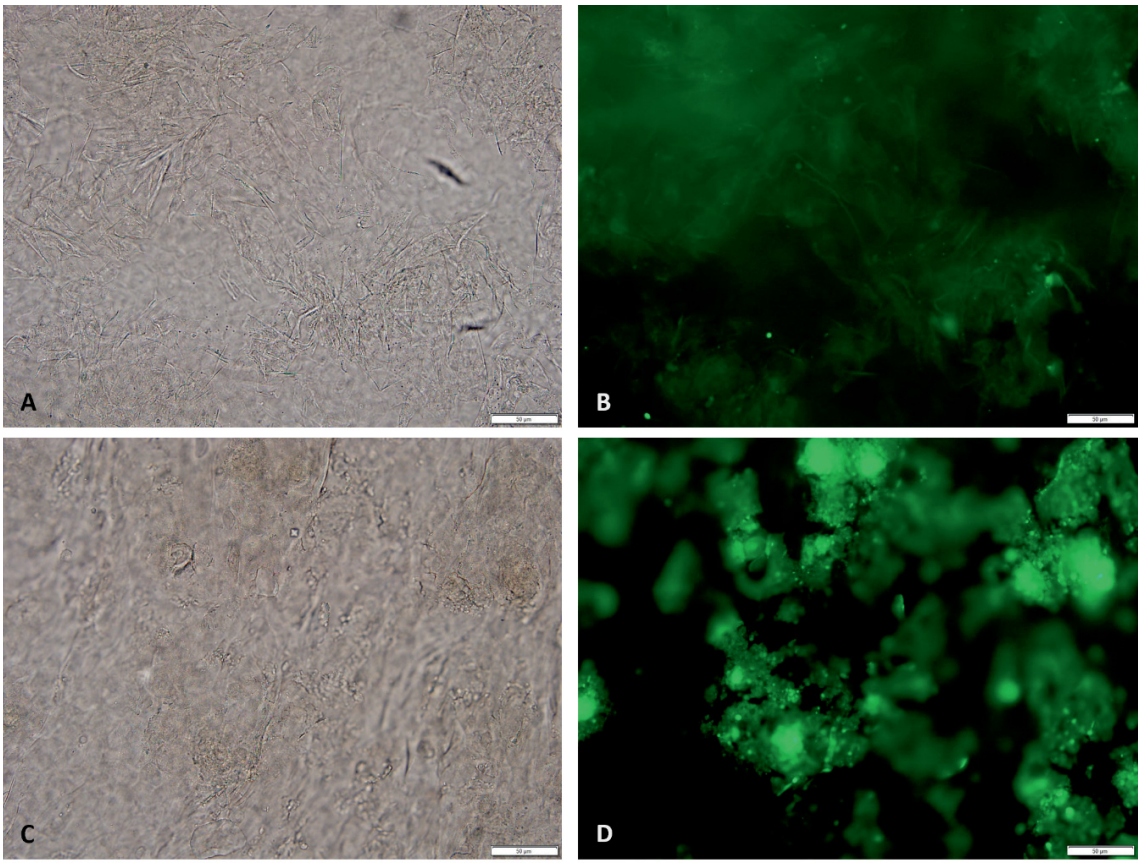

Figure 22: Separated epidermis of Phenion® Full-Thickness skin models without or with CFSE-labeled MUTZ-LCs.
Representative microscopic images of epidermis, enzymatically separated on day 11 from Phenion® Full-Thickness skin models without (A, B) and with MUTZ-LCs (C, D), which were differentiated for 14 days in 20 % FCS medium and labeled with CFSE before being integrated into the skin models. Scale bars represent 50 µm.

To determine the localization of MUTZ-LCs more precisely, frozen tissue sections of the other half of skin model were generated. However, microscopic images of tissue sections with CFSE-labeled MUTZ-LCs showed no fluorescence signal (black images not shown). Thus, an immunofluorescence staining for the LC-typical markers CD1a and CD207 on frozen sections was performed. Figure 23 depicts the CD1a staining of Phenion® Full-Thickness standard (A, C-F) and LONG-LIFE skin models (B, G, H). The staining of Phenion® FT skin models without integrated MUTZ-LCs showed no CD1a-staining (Figure 23A, B), while the skin models with integrated MUTZ-LCs exhibited CD1a-positive MUTZ-LCs, equally distributed in the epidermis (Figure 23C, D), independent of the skin model version (standard or LONG-LIFE). The stained MUTZ-LCs exhibited the LC-typical long multiple cytoplasmic projections. Only a few positive signals were found in the dermis underneath the basement membrane, which were smaller in size than the epidermal MUTZ-LCs. More extended fluorescence signals in the lower parts of the dermis were false-positive signals, emitted from the collagen matrix. The fluorescence microscopic images of CD207-stained skin models with integrated MUTZ-LCs showed similar results (Supplemental Figure 1).

Furthermore, the integration of MUTZ-LCs differentiated with the original protocol (20 % FCS) (Figure 23C, D, G, H) and the optimized protocol (5 % FCS) (Figure 23E, F) was compared. The CD1a immunofluorescence-stained frozen sections showed no apparent differences. With both differentiation protocols, the MUTZ-LCs were observed with dendritic processes in the epidermal layers.

Overall, MUTZ-LCs could be detected in in the Phenion® FT Standard and LONG-LIFE skin models without apparently interfering with skin differentiation. Although LONG-LIFE skin models enable a longer experimental test period, further experiments were done with standard skin models, as they needed less time to be produced and were more cost-effective.

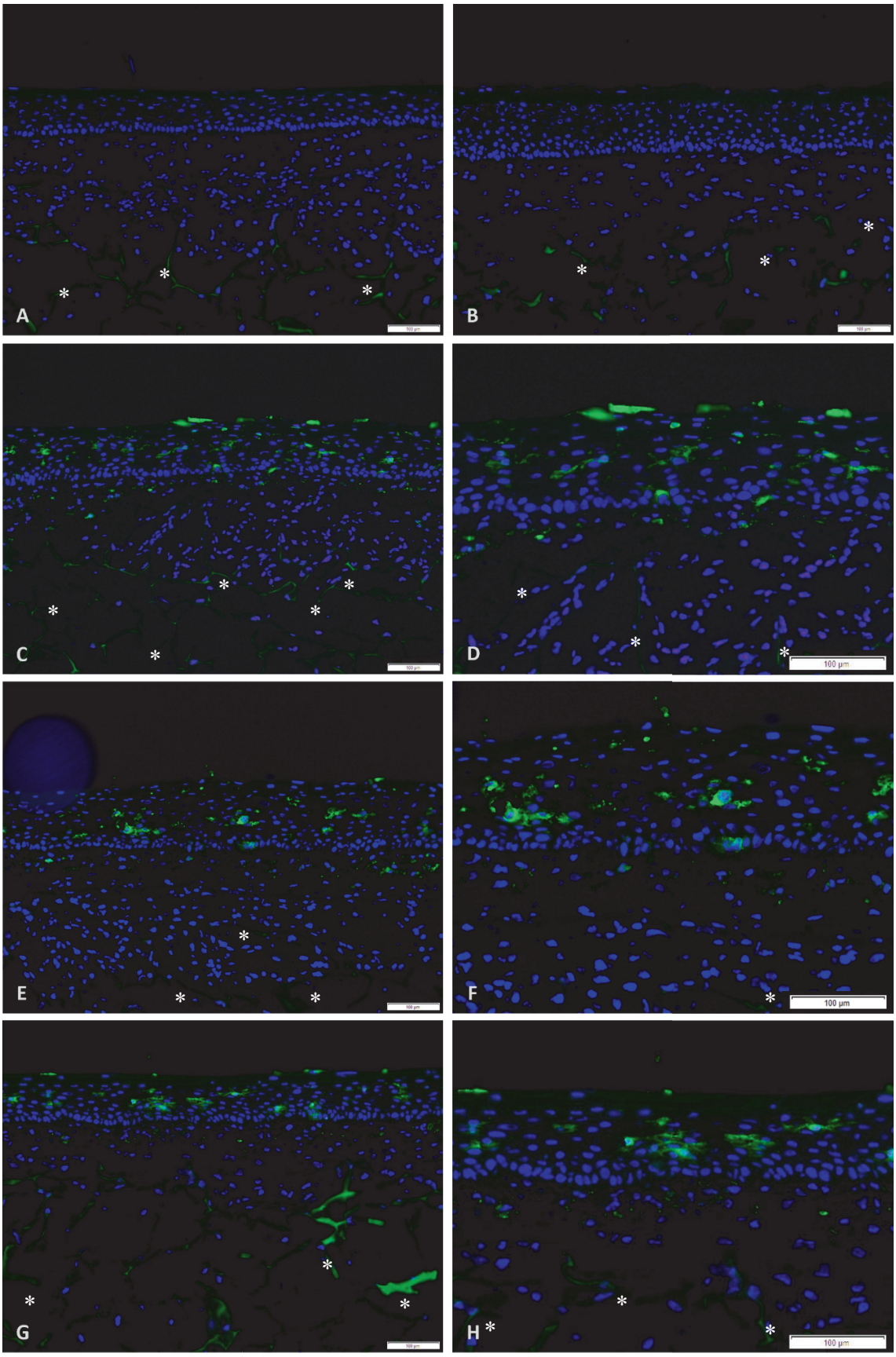

Figure 23: CD1a expression in standard Phenion® Full-Thickness skin models with and without integrated 20 % FCS- or 5 % FCS-differentiated MUTZ-LCs as well as a comparison of Phenion® Full-Thickness standard and LONG-LIFE skin models.

Representative microscopic images of frozen sections of Phenion® Full-Thickness skin models after ten days in air-liquid interface with an immunofluorescence staining for CD1a, which is expressed by MUTZ-LCs. A comparison of Phenion® Full-Thickness standard (A, C-F) and LONG-LIFE skin models (B, G, H). Skin model without integrated MUTZ-LCs (A, B) and skin models with integrated MUTZ-LCs, which were differentiated for 14 days in 20 % FCS (C, D, G, H) or for 7 days in 5 % FCS medium (E, F). A magnification of the images is depicted to illustrate the morphological features (D, F, H). CD1a-stained MUTZ-LCs were mainly found in the epidermis and expressed long dendritic processes. CD1a is depicted in green (FITC) and nuclei in blue (DAPI). Green, fluorescent signals in the lower part of dermis were false-positive ones, emitted by the matrix (signals are highlighted with asterisks, not exhaustive). Scale bars represent 100 µm.

4.4 Sensitizer treatment of Phenion® Full-Thickness skin models with integrated MUTZ-LCs

After successfully integrating MUTZ-LCs into the Phenion® FT skin models, their immunological competence needed to be verified. To accomplish that, the skin models were topically treated with chemicals of different skin-sensitizing potency. One possible read-out parameter to characterize the sensitization potential of a chemical could be the migration of MUTZ-LCs, if the surrogates behave in the same way as LCs do in the native skin after sensitizer exposure. In addition, a Next Generation Sequencing (NGS) was performed to identify genes which might serve as promising and reliable indicators for the cellular sensitization reaction.

Skin models were treated for 20 h with two sensitizers, the extreme sensitizer DNCB and the moderate sensitizer $NiSO_4$. First, a dose range finder with a serial dilution of the sensitizer was performed to find a suitable concentration, which did not result in a high cytotoxicity. The cytotoxicity was analyzed with an MTT test and the affected structural integrity with HE staining of the skin models. During the MTT assay, which is a commonly used method to assess cell viability, the skin models were treated with various concentrations of DNCB and $NiSO_4$ (Figure 24). Skin models treated with DNCB exhibited varying levels of viability that were dependent on the used concentration (Figure 24A). The treatment with 0.1 % DNCB exerted a viability comparable to the untreated skin models. However, DNCB treatments with concentrations of 0.2 % and higher resulted in a reduction of cell viability compared to the untreated skin models. In contrast, all $NiSO_4$ treatments (2 mM to 15 mM $NiSO_4$) resulted in a viability comparable to that of untreated skin models (Figure 24B).

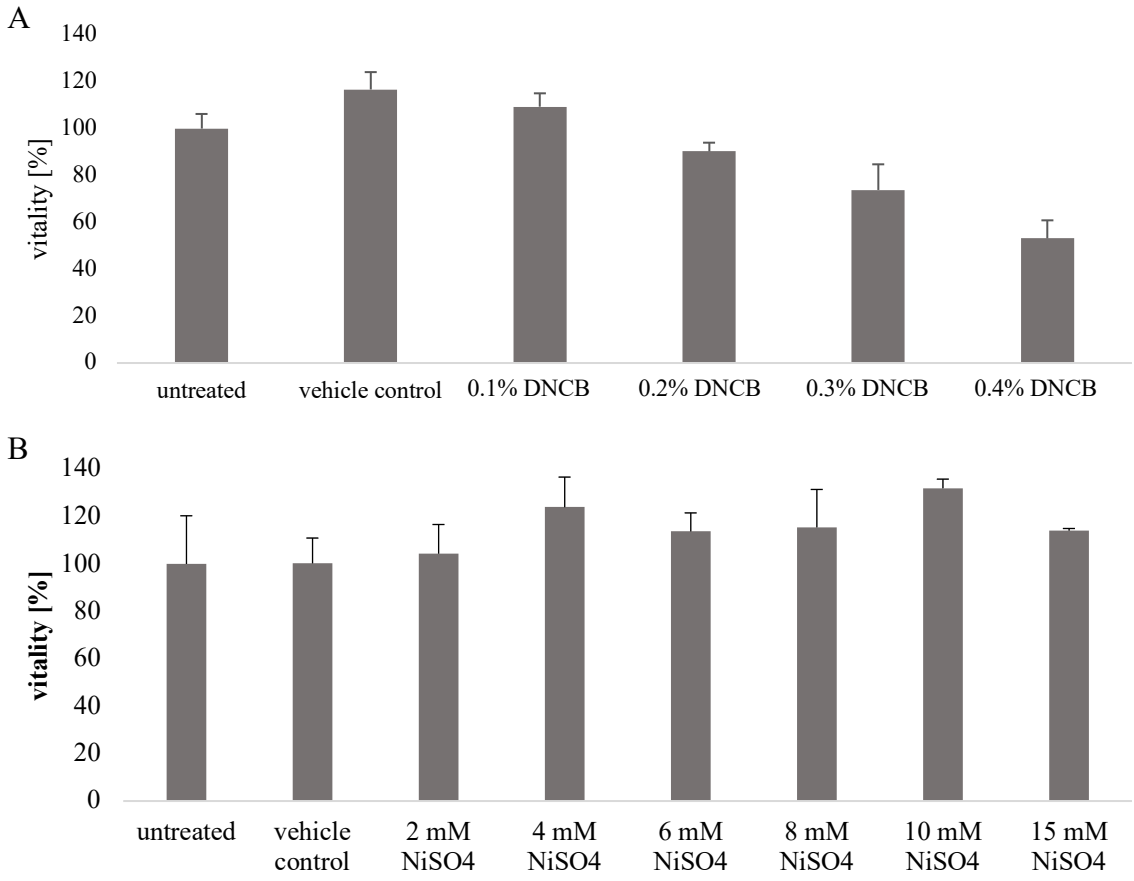

Figure 24: Effect of DNCB and $NiSO_4$ treatment on viability of Phenion® Full-Thickness skin models. Phenion® Full-Thickness skin models were treated on day 11 of air-liquid interface for 20 h. The skin models were treated with the vehicle control for DNCB (Acetone), as well as 0.1 %, 0.2 %, 0.3 % and 0.4 % DNCB (A). In addition, skin models were treated with the vehicle control for $NiSO_4$ (PBS), as well as 2 mM, 4 mM, 6 mM, 8 mM, 10 mM and 15 mM $NiSO_4$ (B). Vitality of skin models were measured with MTT assay. Percent vitality was calculated as cell vitality relative to untreated skin models. N=3, error bars represent standard deviation.

Contrary to the MTT results, it was observed that the washing steps of the MTT protocol led to the detachment of the epidermis of some DNCB- and $NiSO_4$-treated skin models. This detachment indicates a damaged skin model with a compromised structural integrity.

Besides the MTT assay, HE staining of DNCB- and $NiSO_4$-treated skin models were performed to validate the histological architecture of the skin models. HE staining of the skin models treated with 0.1 % DNCB showed an irregular stratum basale (Figure 25B) compared to the vehicle control (Figure 25A). This was also observed in the HE staining of 2 mM $NiSO_4$-treated skin models (Figure 25D) vs. the vehicle control (Figure 25C). In addition, the epidermis of the 2 mM $NiSO_4$-treated skin models was thinner and more dead cells were found compared to the vehicle control. In contrast, according to the MTT, the skin models treated with 0.1 % DNCB or 2 mM $NiSO_4$ were as vital as the untreated

ones (Figure 24A, B). Only when treating the skin models with 0.01 % DNCB and 0.5 mM $NiSO_4$, one tenth and one thirtieth of the MTT-determined concentration, the skin models showed primarily minor stressed or damaged characteristics (Figure 26D, G).

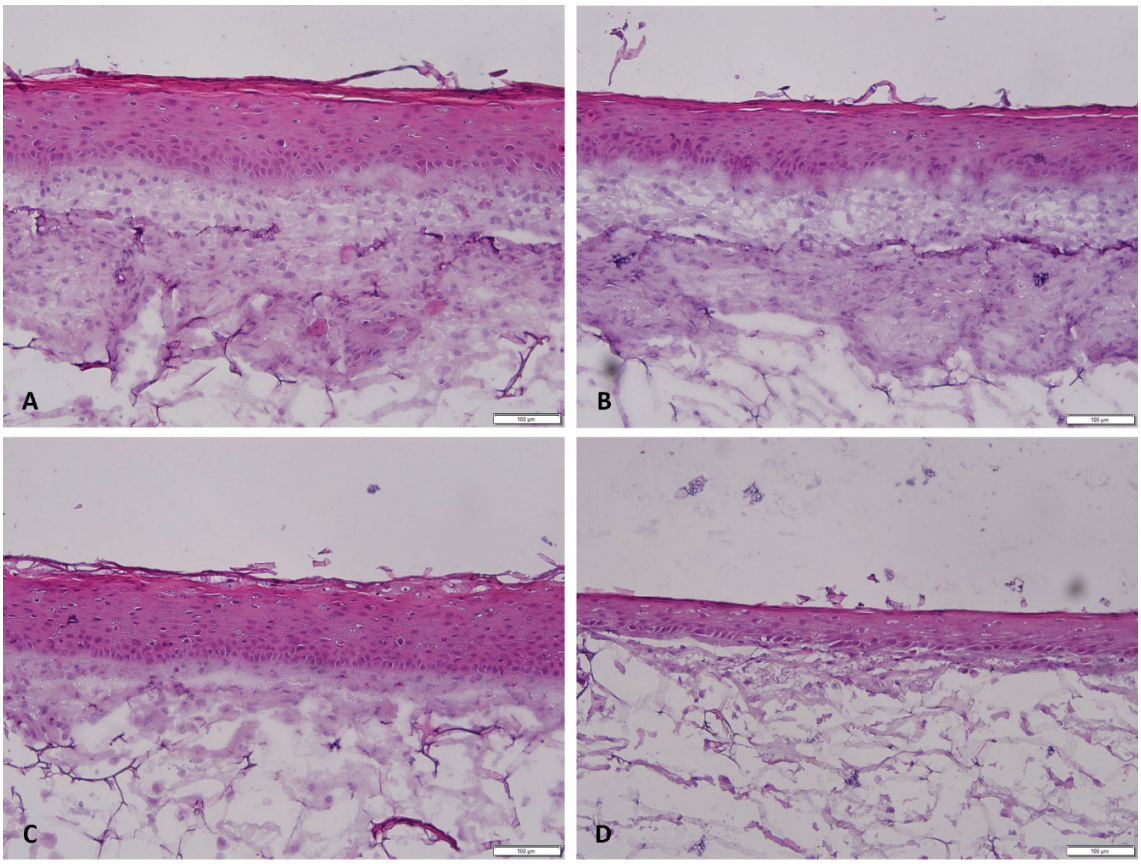

Figure 25: Effect of 0.1 % DNCB and 2 mM $NiSO_4$ treatment on the histological architecture of the Phenion® Full-Thickness skin models.
Hematoxylin-eosin staining of frozen sections of Phenion® Full-Thickness skin models. Skin models were integrated with MUTZ-LCs, which were differenitated for seven days in 5 % FCS. Skin models were treated on day 11 of air-liquid interface for 20 h with Acetone -vehicle control for DNCB- (A), 0.1 % DNCB (B), PBS -vehicle contol for $NiSO_4$- (C) and 2 mM $NiSO_4$ (D).

Due to the huge discrepancy of the MTT results and the effect of sensitizer treatment on the skin model structure, the sensitizer concentration was set based on the HE staining. The chosen concentrations for the following experiments were based on the aim of identifying the highest concentration of the sensitizer that did not have any detrimental effects on the structure of the skin models. In this regard, 0.01 % DNCB was chosen. However, for $NiSO_4$, two concentrations were selected, 0.1 mM and 0.5 mM $NiSO_4$. This decision was driven by experimental observations, which indicated that 0.5 mM $NiSO_4$ occasionally had a negative impact on the histological architecture of the skin models.

4.5 Effect of hydrocortisone on MUTZ-LC behavior in the immunocompetent Phenion® Full-Thickness skin model

According to the theory of skin sensitization elicitation, after getting in contact with a sensitizer, the LCs start migrating out of the epidermis to the nearest lymph node. Hence, the tissue sections of the DNCB- and $NiSO_4$-treated skin models were screened for indications of MUTZ-LC migration in the Phenion® FT skin model with integrated MUTZ-LCs. This was analyzed with immunofluorescence staining for CD1a of frozen tissue samples. When culturing the skin models with the same medium as the commercially available skin models, no clear migration of the MUTZ-LCs could be observed after sensitizer treatment (Figure 27, left side). As the read-out parameter could not be observed, the medium supplements were reviewed, in case one of them could be interfering with the immune reaction of MUTZ-LCs. One medium supplement, which is an integral component of the ALI medium for the Phenion® FT skin models, was identified as a possible inhibitor/candidate: hydrocortisone (HC). HC is a known immunosuppressor, often used in ointments, creams or lotions to treat inflamed skin areas (Mehta et al., 2016). Thus, two ALI culture conditions of skin models were tested: ALI medium with and without HC (Figure 26 and 27, left and right side).

First, it was analyzed whether the absence of HC influenced the differentiation of the skin model. Comparing the HE staining of untreated skin models cultured with and without HC, no apparent differences regarding the structure of the skin model could be observed (Figure 26A). All layers were correctly differentiated. This was also the case for the treated skin models (vehicle controls, DNCB, $NiSO_4$), which showed no apparent differences when being cultured with or without HC during ALI culture (Figure 26B-G). In some cases, an apparent increase in formed extracellular matrix was observed in skin models cultured without HC during ALI phase compared to the ones with HC, but not in every skin model.

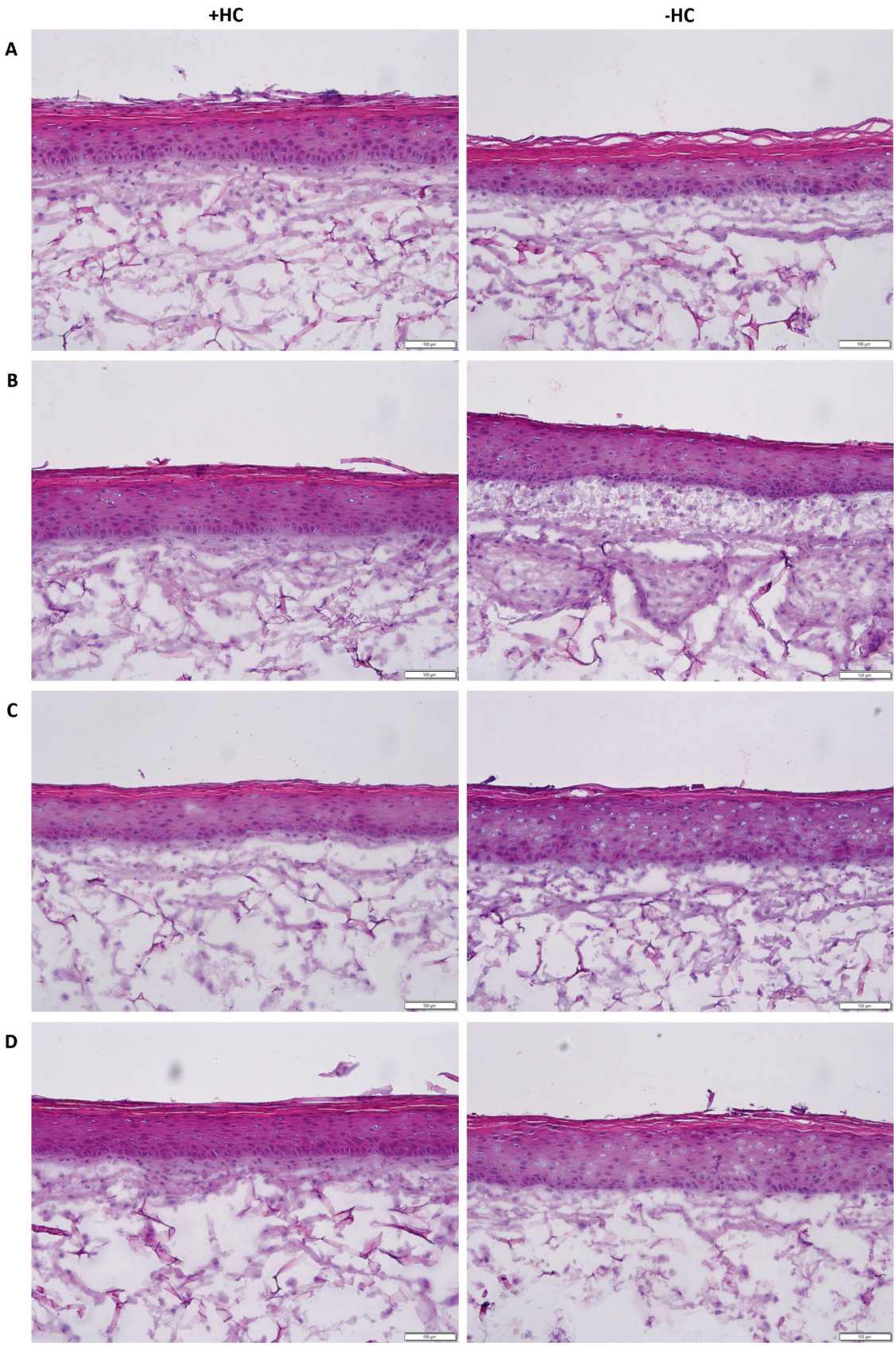
+HC
-HC
A
B
C
D

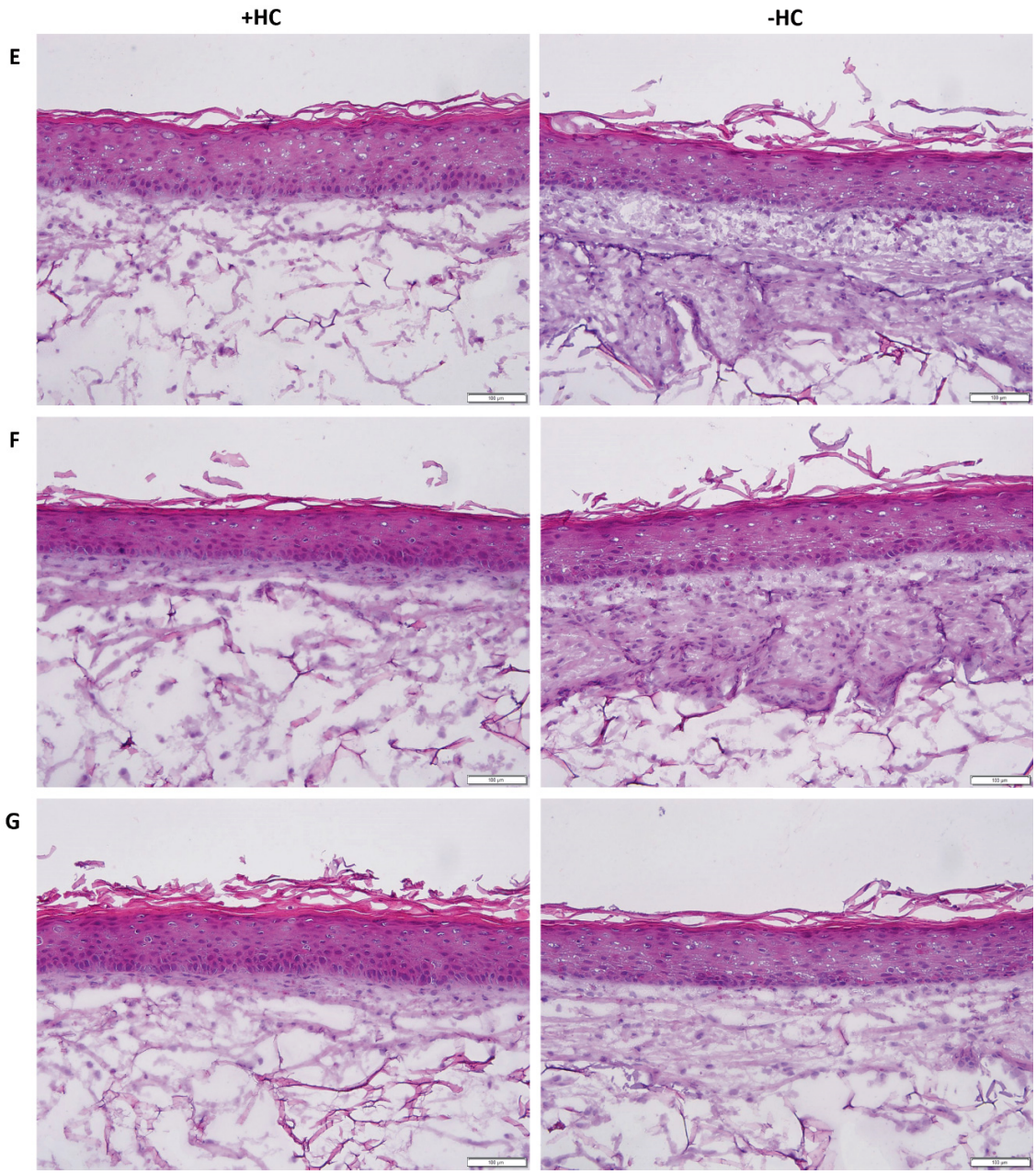

Figure 26: Effect of DNCB and $NiSO_4$ treatment on the structure of Phenion® Full-Thickness skin models, cultured with and without hydrocortisone (HC).
Hematoxylin-eosin staining of frozen sections of Phenion® Full-Thickness skin models. Skin models, cultured with (left side) or without HC (right side), were either without (A) or with inegrated MUTZ-LCs (B-G), which were differenitated for seven days in 5 % FCS before being integrated. Skin models were untreated (A, B) or treated on ALI day 11 for 20 h with Acetone -vehicle control for DNCB- (C), 0.01 % DNCB (D), PBS -vehicle contol for $NiSO_4$- (E), 0.1 mM $NiSO_4$ (F) and 0.5 mM $NiSO_4$ (G).

Next, the presence and distribution of MUTZ-LCs in the skin models under different experimental conditions was analyzed on tissue sections labeled with anti-CD1a antibodies. Skin models without MUTZ-LCs, cultured with and without HC, emitted no fluorescence signal except for the intrinsic fluorescence emitted from the collagen matrix (Figure 27A). CD1a-stained cells with dendritic processes were found in the epidermis of

every skin model with integrated MUTZ-LCs (Figure 27B-G), regardless of the culture condition (similar to Figure 23). Nevertheless, some differences could be observed across all treatment conditions when culturing the skin models with integrated MUTZ-LCs without HC compared to the original culture with HC (with HC left side, without HC right side, Figure 27B-G): For one, the signal intensity of the CD1a-staining was increased. Furthermore, the size of the signals, and thus the size of the cells, appeared to be larger. The integrated MUTZ-LCs seemed to exhibit longer dendritic processes. Additionally, a substantial increase in the overall number of signals was observed.

Apart from the overall noticeable changes of the culture without HC, additional noticeable changes could be observed between the untreated and treated skin models with integrated MUTZ-LCs. In the untreated skin models, the majority of the CD1a-stained MUTZ-LCs were found in the epidermis. However, comparing the culture conditions, more fluorescent signals were detected in the dermis of HC-free cultured, untreated skin models (Figure 27B). These dermal signals were less and smaller compared to the ones in the epidermis.

Furthermore, the skin models with integrated MUTZ-LCs were treated with Acetone (Figure 27C), which is the vehicle control for DNCB. The majority of the signals were detected in the epidermal layers with a few signals in the dermis. These observations were comparable to the microscopic images of untreated skin models.

The DNCB treatment of HC-free cultured skin models exerted strong fluorescent signals in the dermis and also some signals in the epidermis (Figure 27D, right side). The dermal signals were more and with higher intensity than in the skin models treated with Acetone, while the epidermal signals were comparable to the vehicle control. In contrast, only a few CD1a-stained MUTZ-LCs were found in the epidermis and dermis of HC-cultured and 0.01 % DNCB-treated skin models (Figure 27D, left side). Compared to the vehicle control, far less signals could be observed in total.

The distribution of the fluorescent signals within epidermis and dermis in the skin models treated with PBS, the vehicle control for $NiSO_4$, is depicted in Figure 27E. For both culture conditions with and without HC, the majority of CD1a-stained MUTZ-LCs was

detected in the epidermis, with only a few positive signals in the dermis. These results were similar to the Acetone-treated skin models.

When treating the HC-free cultured skin models with 0.1 mM $NiSO_4$, nearly half of the fluorescent signals were detected in the dermis (Figure 27F, right side). However, the signals in the epidermis and dermis were smaller than the ones detected in the PBS-treated skin models. Compared to the DNCB-treated skin models, 0.1 mM $NiSO_4$ treatment resulted in more fluorescent signal in the dermis of HC-free cultured skin models. In 0.1 mM $NiSO_4$-treated skin models, cultured with HC, nearly all fluorescent signals were located in the epidermis (Figure 27F, left side). Only a few signals were detected in the dermis, which was comparable to the signals of the corresponding vehicle control. Increasing the $NiSO_4$ concentration to 0.5 mM, most of the CD1a-positive signals were observed in the epidermis of HC-cultured skin models with some signals in the dermis (Figure 27G, left side). Compared to the 0.1 mM $NiSO_4$-treated skin models, more signals were detected in the dermal tissue. In the culture condition without HC, nearly half of the signals were found in the dermis of the 0.5 mM $NiSO_4$-treated skin models (Figure 27G, right side). This observation was similar to the HC-free cultured skin models treated with 0.1 mM $NiSO_4$.

To sum it up, the DNCB and $NiSO_4$ treatment of Phenion® FT skin models, cultured without HC, resulted in more CD1a-stained MUTZ-LCs in the dermis compared to the ones that were cultured with HC.

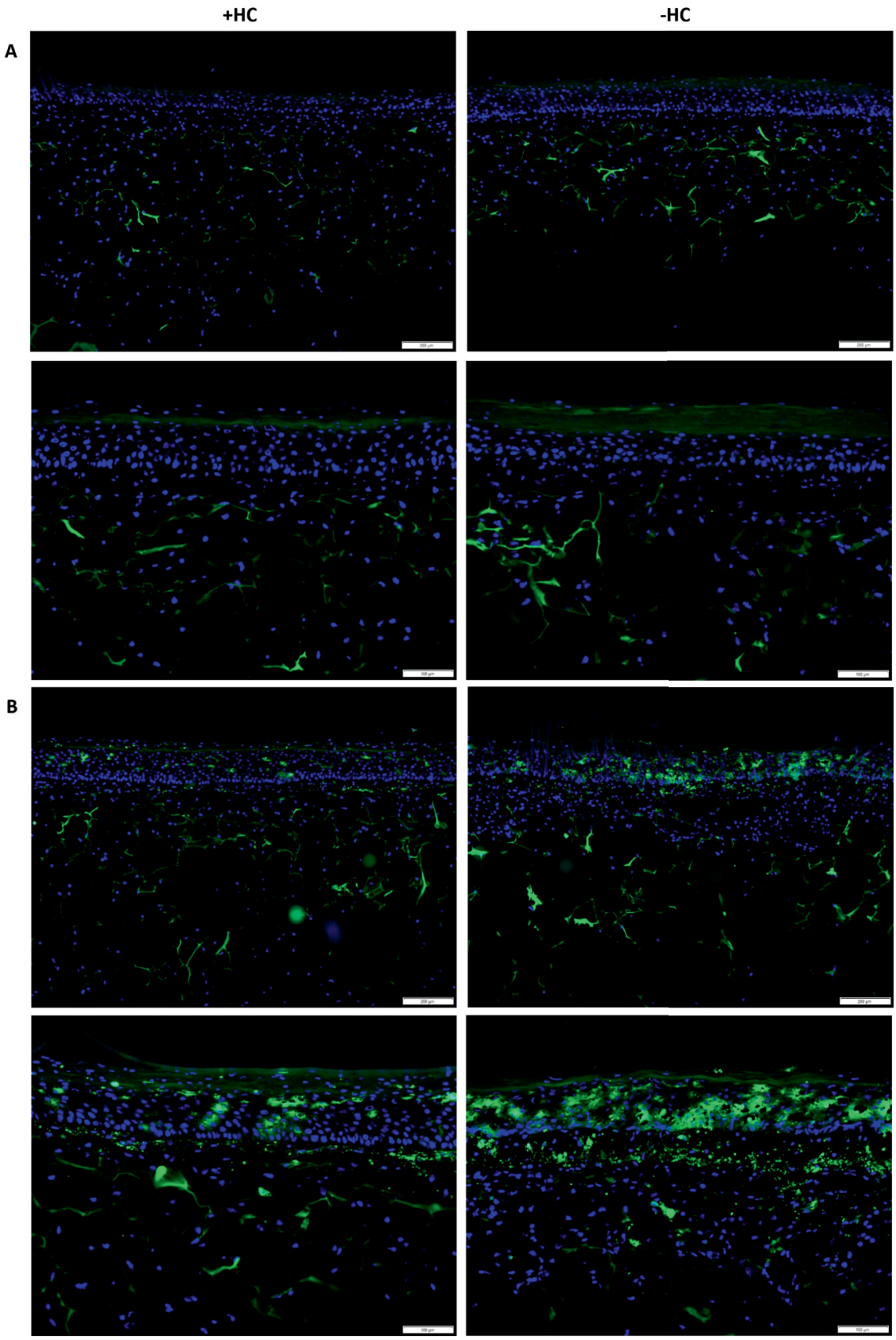
+HC
-HC
A
B

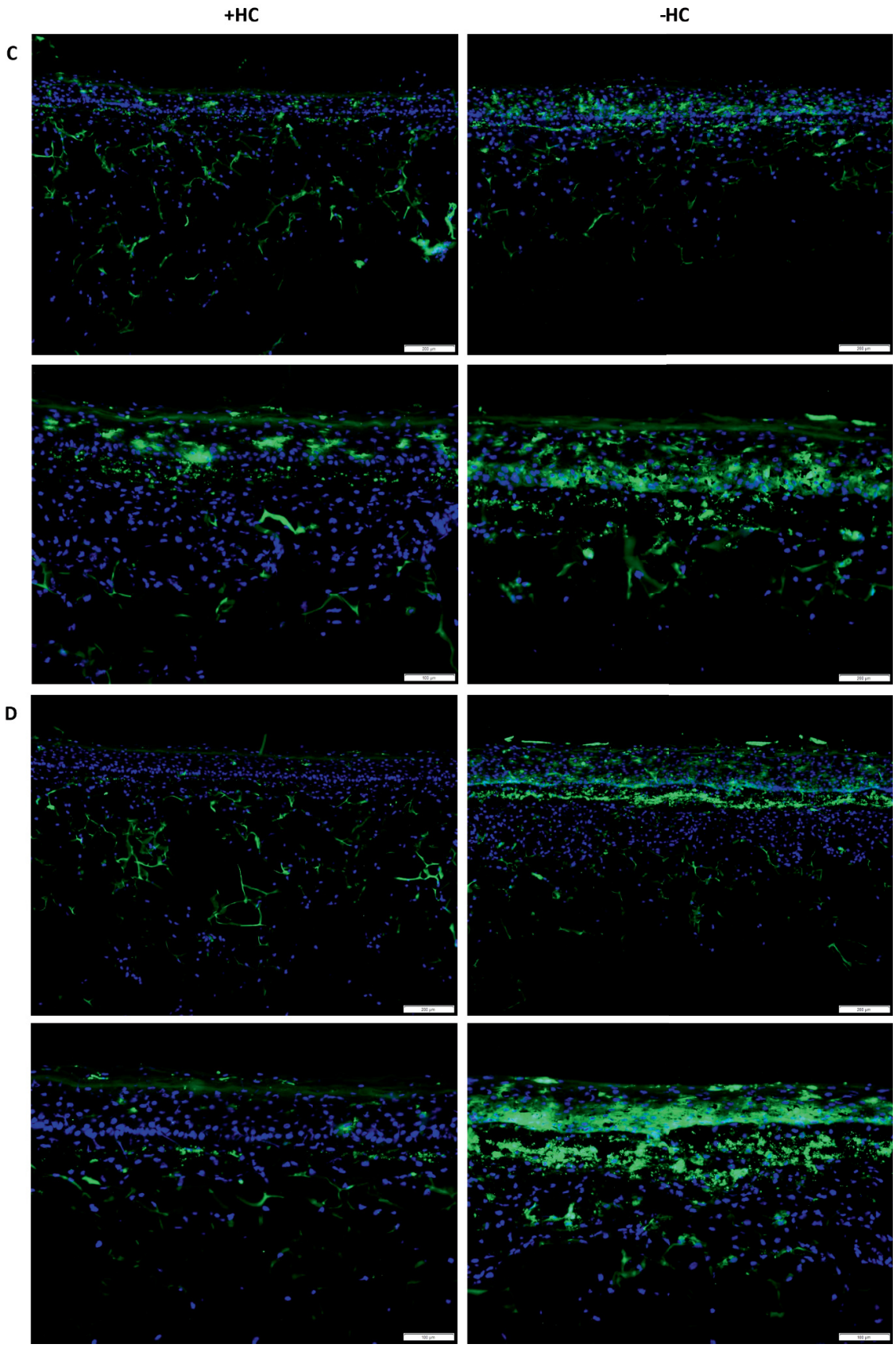
+HC
-HC
C
D

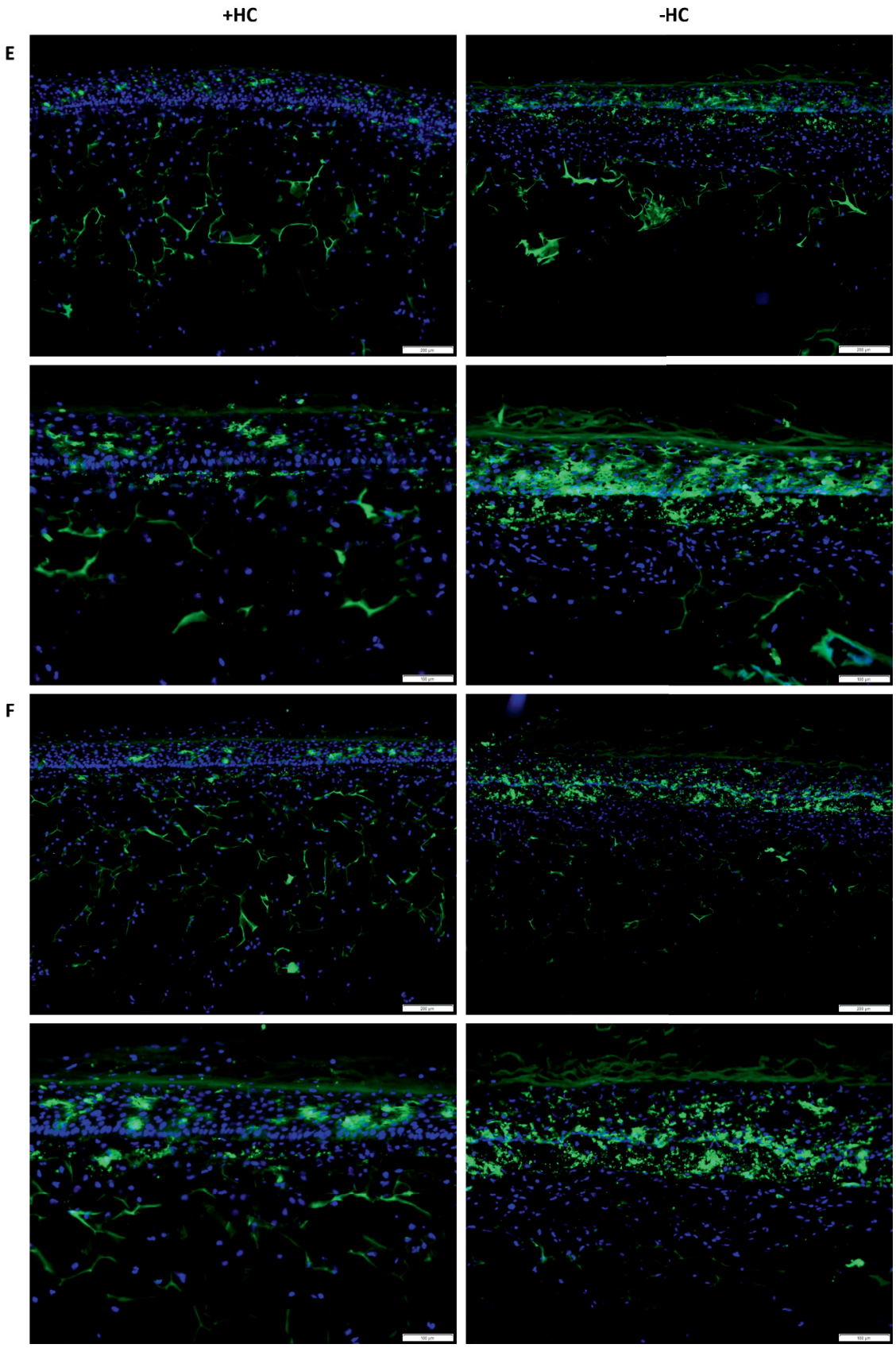
+HC
-HC
E
F

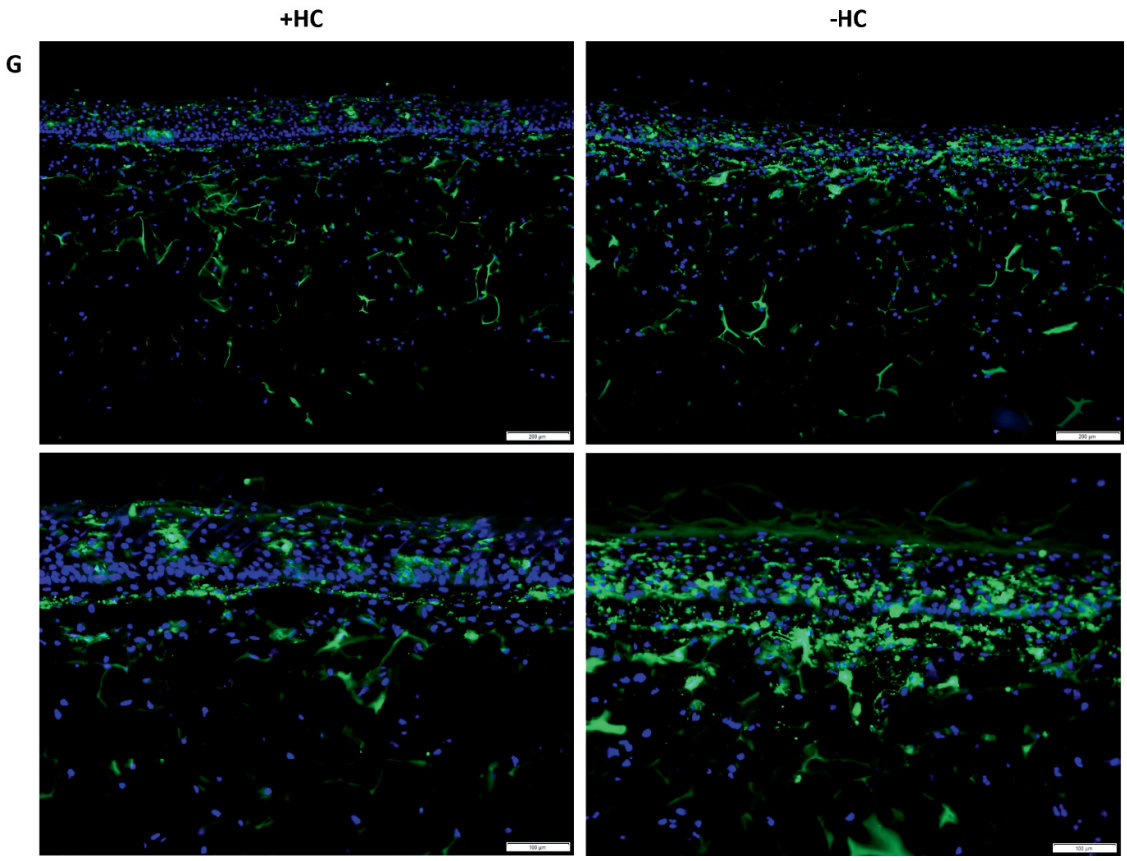

Figure 27: Effect of DNCB and $NiSO_4$ treatment on CD1a expression in standard Phenion® Full-Thickness skin models with integrated 5 % FCS-differentiated MUTZ-LCs, cultured with and without hydrocortisone (HC).
Representative microscopic images of frozen sections of standard skin models on ALI day twelve with an immunofluorescence staining for CD1a, which is expressed by MUTZ-LCs. A comparison of Phenion® Full-Thickness standard skin models cultured with HC (left side) and without HC (right side) during ALI culture. Skin models without integrated MUTZ-LCs (A) and untreated skin models with integrated MUTZ-LCs (B), which were differentiated for seven days with 5 % FCS. In addition, skin models with integrated MUTZ-LCs were treated for 20 h with Acetone -vehicle control for DNCB- (C), 0.01 % DNCB (D), PBS -vehicle control for $NiSO_4$- (E), 0.1 mM $NiSO_4$ (F) and 0.5 mM $NiSO_4$ (G). CD1a is depicted in green (FITC) and the nuclei in blue (DAPI). Green, fluorescent signals in the lower part of dermis were false-positive ones, emitted by the matrix. Scale bars represent 200 µm in the upper images and 100 µm in the lower images of each condition.

4.6 Viability of untreated and treated Phenion® Full-Thickness skin models with integrated MUTZ-LCs

A TUNEL assay was conducted to assess the DNA fragmentation and identify apoptotic cells in untreated and treated skin models (Figure 28). The green, fluorescent signal, which can be associated with cells, were apoptotic cells (positive signals). Green signals in the lower part of the images were emitted by the matrix structure and were false-positive ones. In addition, the cells were stained with PI to label all cells and to visualize

the epidermal boundary. In the negative control sample, where the TUNEL mix was omitted, no positive signals were detected (Figure 28A). In contrast, the positive control, which was incubated with DNase I prior to the TUNEL assay, exhibited a significant number of positive signals (Figure 28B). In untreated as well as Acetone- and DNCB-treated skin models only a few positive signals (apoptotic cells) could be detected, regardless of whether they were cultured with or without HC (Figure 28C-H). These signals were predominantly observed in the stratum corneum. Additional samples showing similar results, e.g., $NiSO_4$-treated skin models, are depicted in the appendix (Supplemental Figure 2).

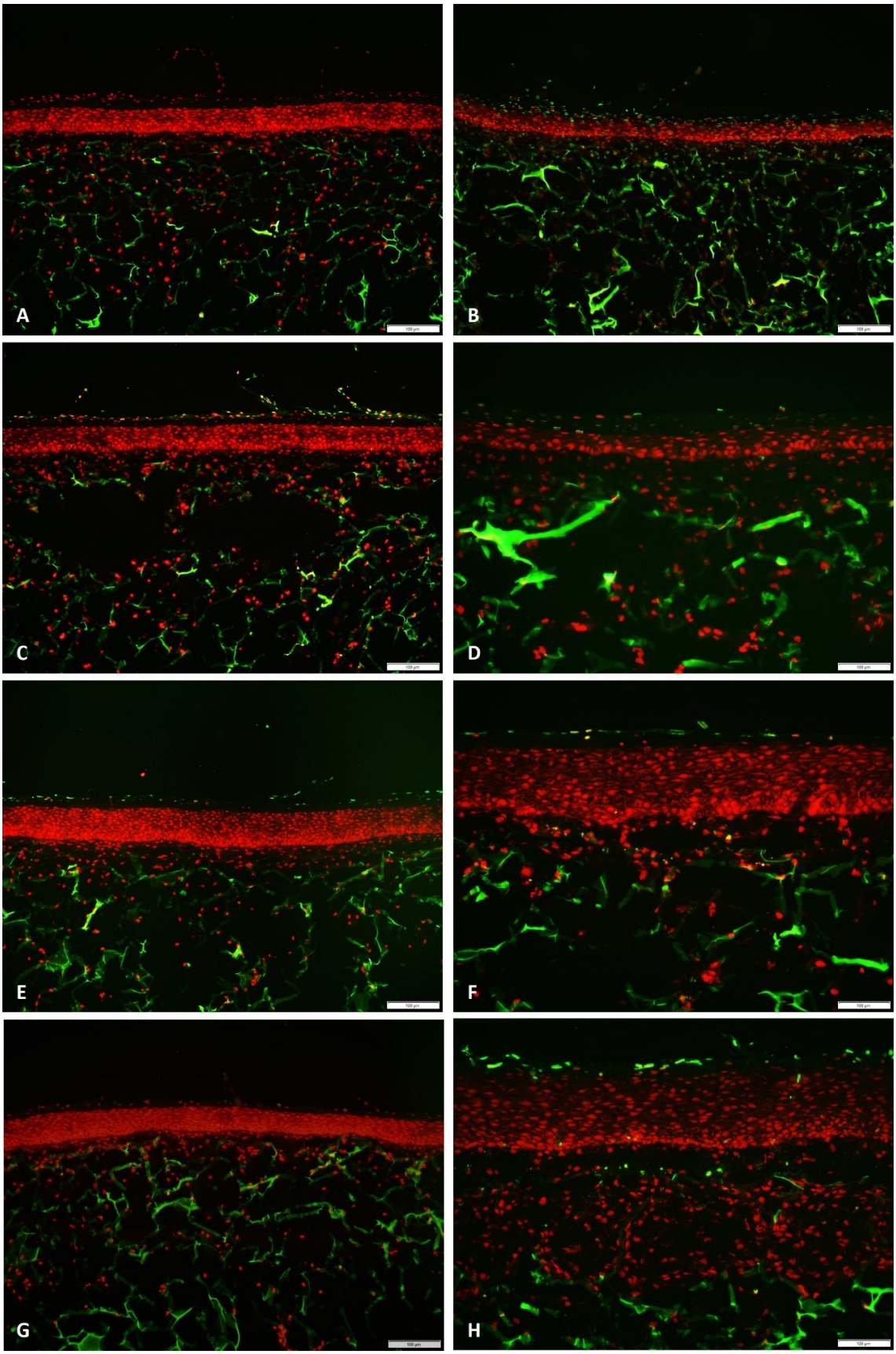

Figure 28: Effect of DNCB treatment and hydrocortisone (HC) on cell viability within Phenion® Full-Thickness standard skin models without or with integrated 5 % FCS-differentiated MUTZ-LCs. Representative microscopic images of frozen sections of Phenion® Full-Thickness standard skin models on ALI day twelve after conducting a TUNEL assay. Apoptotic cells emitted a green fluorescence signal. A comparison of Phenion® Full-Thickness standard skin models cultured with HC (C, E, G) and without HC

(D, F, H) during ALI culture. Skin models without integrated MUTZ-LCs (C, D) and skin models with integrated MUTZ-LCs (E-H), which were differentiated for seven days with 5 % FCS. In addition to the untreated control (A-D), skin models were treated for 20 h with Acetone -vehicle control for DNCB- (E, F) and 0.01 % DNCB (G, H). Moreover, cells were stained with PI. Green, fluorescent signals in the lower part of dermis were false-positive ones, emitted by the matrix. Scale bars represent 100 µm.

4.7 Effect of MUTZ-LC integration and sensitizer exposure on the Phenion® Full-Thickness skin model differentiation

Furthermore, it was analyzed whether HC in the culture medium as well as the exposure to sensitizers had a significant impact on the epidermal thickness of the Phenion® FT skin models. First, the epidermis of skin models without integrated LCs (e/-LCs), which served as controls, were studied. For each culture condition, with HC (+HC), five days without HC (-5dHC) and completely without HC (-HC), the box plots overlapped, and the median lines were inside of all other boxes (Figure 29). Here, the epidermal thickness ranged from around 20 µm to 190 µm. The other skin model culture conditions also had a wide range of epidermal thicknesses, e/-LCs/-5dHC with 70 µm to 193 µm and e/-LCs/-HC with 45 µm to 200 µm, while the mean was approximately 100 µm and the median around 120 µm. The mean and median of e/-LCs/-5dHC and e/-LCs/-HC were about 130 µm, thus, around 30 µm higher than the ones of the e/-LCs/+HC.

The epidermal thickness of e/+LCs showed a wide spread of data values (+HC with 32 µm to 234 µm and three outliers above 220 µm; -HC 70 µm to 180 µm), especially of the skin models -5d HC (52 µm to 112 µm). The mean and median of e/+LCs/+HC and /-5dHC were around 130 µm and the ones of /-HC 15 µm lower. Epidermal thicknesses of e/-LCs/-HC had the smallest data range.

Comparing the e/-LCs with /+LCs within the same culture condition, the epidermal thicknesses were quite similar. However, a few differences could be detected: The mean of e/-LCs/-HC was 25 µm and the median 5 µm lower than the e/+LCs/-HC ones. The e/+LCs/-5dHC had a wider distribution of measured epidermal thicknesses than e/-LCs/-5dHC. Still, the mean and median were comparable. Overall, the e/-LCs/+HC were thinner than the e/+LCs/+HC, but with similar mean and median.

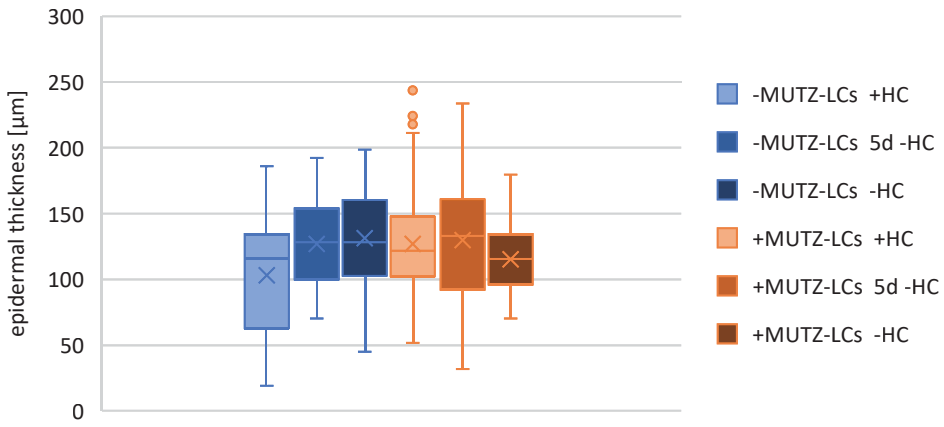

Figure 29: Effect of MUTZ-LC integration into the Phenion® Full-Thickness skin models, cultured with hydrocortisone (HC), 5 days without and completely without HC, on the epidermal thickness. Depicted is the distribution of the epidermal thickness of Phenion® Full-Thickness skin models without (blue colors) and with MUTZ-LCs (orange colors). MUTZ-LCs were differentiated for seven days in 5 % FCS medium before being integrated into the skin models. The skin models were cultured for 12 days in ALI phase with HC (bright colors), 5 days without HC (middle bright colors) and completely without HC (dark colors). Epidermal thickness was measured on hematoxylin-eosin-stained frozen sections of skin models with ImageJ. If possible, eleven equidistant parallel lines, which were drawn perpendicular to the dermo-epidermal junction, were measured for each skin model. The cross of the box plots presents the mean, the line inside the boxes the median, the upper whisker the upper 25 % and the lower whisker the lower 25 % of data values. Outliners are depicted in points, above or below the whiskers. Data points from the culture conditions with and without HC were from five skin model batches, with two skin models for each condition in one batch. The data from the culture condition five days without HC were from three skin batches, also with two skin models for each condition in one batch.

After treating the e/+LCs/+HC, /-5dHC or /-HC with Acetone (Ac) and DNCB, respectively, both median and mean values of epidermal thickness varied between 109 µm and 141 µm (Figure 30). All measured epidermal thicknesses showed a wide variability from 19 µm to 225 µm. Moreover, the boxes of all conditions overlapped. However, not all median lines lay inside the boxes of the other samples: the median of e/+LCs/+HC/Ac were outside the box of the e/+LCs/-HC/Ac or /DNCB. In addition, the median of e/+LCs/+HC/DNCB was outside the box of /-HC/Ac. The mean of the e/+LCs/+HC had the highest mean values, followed by the /-5dHC. The e/+LCs/-HC revealed the lowest data variability, but also the lowest mean values compared to the other culture conditions.

Comparing Acetone-treated with DNCB-treated skin models for each culture condition, some slight differences could be detected: The median of e/+LCs/+HC/DNCB was 13 µm smaller than the one of /Ac. The median of the epidermal thickness of e/+LCs/+HC/DNCB was only around 5 µm smaller, but the overall data value spread was

larger than observed with /Ac. The median of e/+LCs/-HC/DNCB was only 5 µm higher than the one of /Ac.

Thus, the thickest epithelia were observed in the skin models cultured with HC and treated with Ac, followed by +HC/DNCB, -5dHC/Ac, -5dHC/DNCB, -HC/DNCB and -HC/Ac.

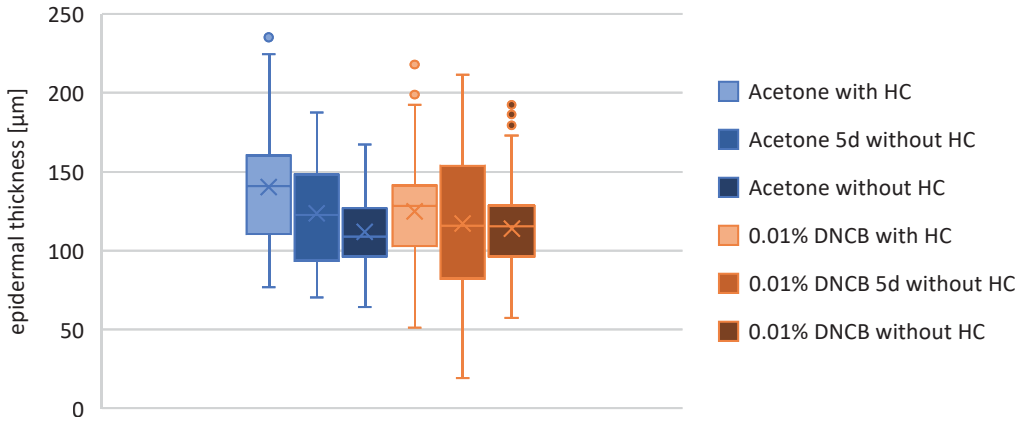

Figure 30: Effect of DNCB treatment on the epidermal thickness of Phenion® Full-Thickness skin models with integrated MUTZ-LCs, cultured with hydrocortisone (HC), 5 days without and completely without HC.
Depicted is the distribution of the epidermal thickness of Phenion® Full-Thickness skin models with integrated MUTZ-LCs and treated for 20 h with Acetone (blue colors), vehicle control for DNCB, and with 0.01 % DNCB (orange colors). MUTZ-LCs were differentiated for seven days in 5 % FCS medium before being integrated into the skin models. The skin models were cultured for 12 days in ALI phase with HC (bright colors), 5 days without HC (middle bright colors) and completely without HC (dark colors). Epidermal thickness was measured on hematoxylin-eosin-stained frozen sections of skin models with ImageJ. If possible, eleven equidistant parallel lines, which were drawn perpendicular to the dermo-epidermal junction, were measured for each skin model. The cross of the box plots presents the mean, the line inside the boxes the median, the upper whisker the upper 25 % and the lower whisker the lower 25 % of data values. Outliners are depicted in points, above or below the whiskers. Data points from the culture conditions with and without HC were from five skin model batches, with two skin models for each condition in one batch. The data from the culture condition five days without HC were from three skin batches, also with two skin models for each condition in one batch.

The epidermal thickness of e/+LCs/PBS and /$NiSO_4$-treated varied between 19 µm and 218 µm (Figure 31). All boxes of PBS- and $NiSO_4$-treated skin models overlapped. However, not all medians lay within the overlap of the boxes: The medians of e/+LCs/+HC/PBS and /0.1 mM $NiSO_4$ were outside the box of -HC/0.5 mM $NiSO_4$. Moreover, the median of e/+LCs/-5dHC/0.1 mM $NiSO_4$-treated skin models, lay outside of the following boxes: /-HC/PBS, /+HC/ 0.1 mM $NiSO_4$, /-5dHC/0.5 mM $NiSO_4$ as well as /-HC/0.5 mM $NiSO_4$-treated skin models. The median of e/+LCs/+HC/0.5 mM $NiSO_4$ was slightly outside the box of /+HC/0.1 mM $NiSO_4$. The e/+LCs/-5dHC/0.5 mM $NiSO_4$

and /-HC/0.5 mM $NiSO_4$ had a median, which lay outside the box of all /PBS and /0.1mM $NiSO_4$. The median of the epidermal thickness in e/+LCs/+HC/PBS was 6 µm higher than the ones of /-5dHC/PBS and /-HC/PBS (115 µm). When treating the skin models with 0.1 mM $NiSO_4$, the highest median was found in /-5dHC (128 µm), followed by a 6 µm lower median in /+HC and /-HC ones (103 µm). Treating the skin models with 0.5 mM $NiSO_4$, the highest median of epidermal thickness was found with 109 µm in the /-5dHC, followed by the /-HC ones (106 µm) and the /+HC (96 µm).

Comparing the epidermal thickness of PBS-, 0.1 mM and 0.5 mM $NiSO_4$-treated skin models for each culture condition, several differences could be determined: Culturing the skin models with HC, the median in e/+LCs/+HC/PBS and /0.1 mM $NiSO_4$ were comparable, but the median in /0.5 mM $NiSO_4$ was smaller by at least 25 µm. For e/+LCs/-5dHC, the median in /0.1 mM $NiSO_4$ was 13 µm higher than /PBS, which in turn was nearly 20 µm higher than /0.5 mM $NiSO_4$. The median of the epidermal thickness in e/+LCs/-HC/PBS was 13 µm higher than /0.1 mM $NiSO_4$ and /0.5 mM $NiSO_4$.

Thus, except for e/+LCs/-HC, the epidermis of /0.5 mM $NiSO_4$ were slightly thinner than the other treated skin models. Regardless of the treatment, the smallest data distributions were found in the /-HC ones.

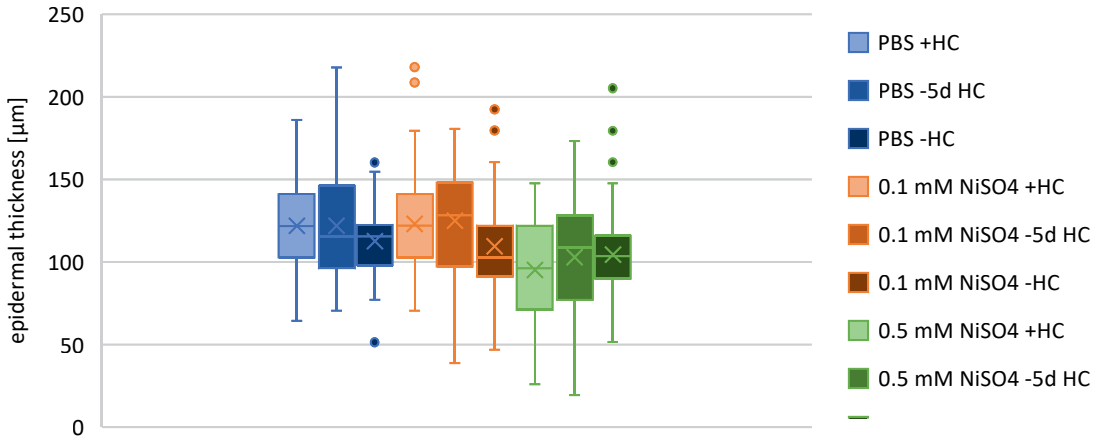

Figure 31: Effect of $NiSO_4$ treatment on the epidermal thickness of Phenion® Full-Thickness skin models with integrated MUTZ-LCs, cultured with hydrocortisone (HC), 5 days without and completely without HC.
Depicted is the distribution of the epidermal thickness of Phenion® Full-Thickness skin models with integrated MUTZ-LCs and treated for 20 h with PBS (blue colors), vehicle control for $NiSO_4$, and with 0.1 mM $NiSO_4$ (orange colors) as well as 0.5 mM $NiSO_4$ (green colors). MUTZ-LCs were differentiated for seven days in 5 % FCS medium before being integrated into the skin models. The skin models were cultured for 12 days in ALI phase with HC (bright colors), 5 days without HC (middle bright colors) and

completely without HC (dark colors). Epidermal thickness was measured on hematoxylin-eosin-stained frozen sections of skin models with ImageJ. If possible, eleven equidistant parallel lines, which were drawn perpendicular to the dermo-epidermal junction, were measured for each skin model. The cross of the box plots presents the mean, the line inside the boxes the median, the upper whisker the upper 25 % and the lower whisker the lower 25 % of data values. Outliners are depicted in points, above or below the whiskers. Data points from the culture conditions with and without HC were from five skin model batches, with two skin models for each condition in one batch. The data from the culture condition five days without HC were from three skin batches, also with two skin models for each condition in one batch.

Overall, the epidermal thickness of untreated as well as treated skin models without and with MUTZ-LCs had a wide spread of data, independent of the treatment and culture condition. The medians ranged from 96 µm to 141 µm.

4.8 Effect of $NiSO_4$-treated s Phenion® Full-Thickness kin models on RNA expression

In order to identify further read-out parameters to characterize the sensitizing potential of a chemical, a NGS was performed for a first set of samples. For that, PBS- and $NiSO_4$-treated skin models with integrated 5% FCS-differentiated MUTZ-LCs were analyzed, cultured with or without HC during the ALI phase. The exposure with 0.1 mM and 0.5 mM $NiSO_4$ was chosen, as the CD1a immunofluorescence staining of $NiSO_4$-treated skin models showed nearly half of the fluorescent signals in the dermis (same samples as in Figure 27E-G). The dermal CD1a-positive cells indicated a MUTZ-LC migration from the epidermis into the dermis upon exposure with a sensitizer. As LC migration is a key component of the allergic contact dermatitis elicitation, observing an apparently similar effect in the 3D skin model might be an indicator for LC activation. Hence, these skin models appear to be well-suited for a more in-depth analysis of their gene expression profile, intended to identify prominent genes involved in the elicitation process. Following the 20 hours exposure time with $NiSO_4$, the epidermis was enzymatically separated from the dermis before isolating the RNA. Thus, any regulated genes could be assigned to the epidermis or dermis, enabling a more precise evaluation.

The first two principal components (PCs) explain with ~94 % the majority of the variance (scree plot in Supplemental Figure 3). Consequently, the first two components were used for the analysis. The principal component analysis (Figure 32) clearly separates the

dermis and epidermis samples as well as the HC culture condition of the skin models (with and without HC).

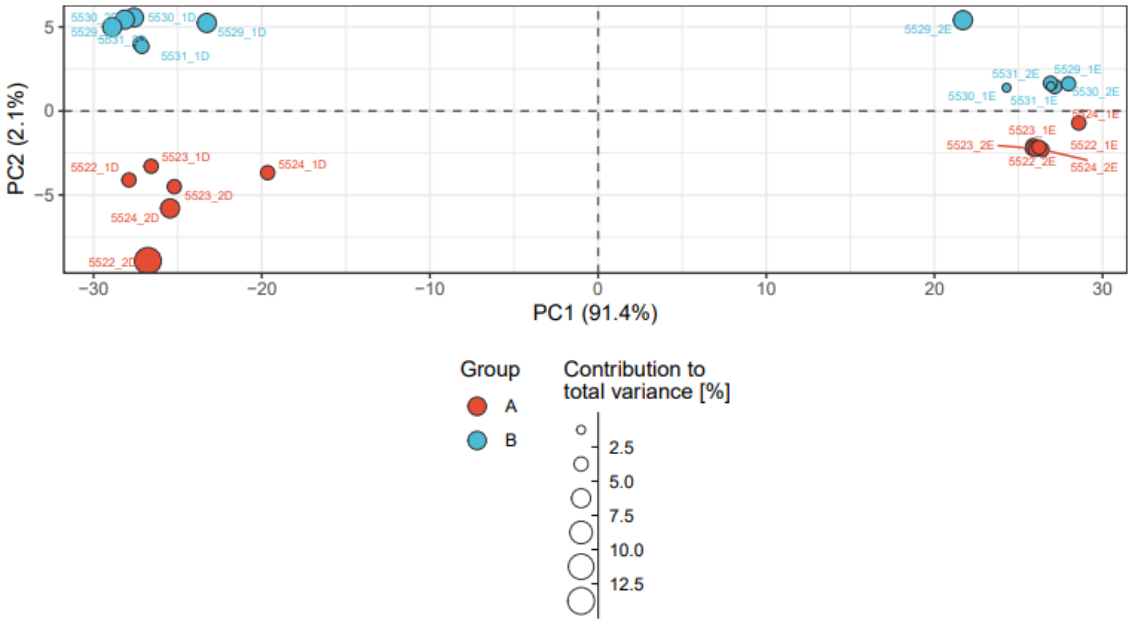

Figure 32: Principal component 1 (PC1) vs. PC2 of the $NiSO_4$-treated Phenion® Full-Thickness skin models integrated with MUTZ-LCs, cultured with or without hydrocortisone (HC) during ALI phase.
Depicted is the principal component analysis (PCA) of the epidermis and dermis samples (#_1/2E and _1/2D) of Phenion® Full-Thickness skin models with integrated 5% FCS-differentiated MUTZ-LCs. The skin models were treated with PBS (#5522, 5529), 0.1 mM $NiSO_4$ (#5523, 5530) or 0.5 mM $NiSO_4$ (#5524, 5531). In addition, the skin models were cultured with HC (red) or without HC (blue) during ALI phase. The PCA of the first two PCs clearly separates the dermis and epidermis samples (left and right side) as well as the culture condition of the skin models, with HC in red and without HC in blue (upper and lower part).

Applicable for the following NGS results, differential gene expression was determined by comparing the genes transcribed within one experimental group with the gene expression profile in the PBS-treated tissues (negative control). Thus, the identified regulated genes are the genes, which are regulated compared to the negative control. Only the genes with a p value below 0.05 were included in the analysis, which is a commonly used threshold (Koch et al., 2018). The p value serves as a statistical indicator, assessing the likelihood of observing differences in gene expression. All results below the threshold of 0.05 were considered statistically significant. Thus, on the basis of the gene expressions in PBS-treated samples, the genes which were up- or downregulated by $NiSO_4$ treatment

of the tissue models could be identified. Differences in gene expressions were documented as log2 fold changes.

The overview heat map of regulated genes of each sample shows more differentially regulated genes in the dermis than in the epidermis (Figure 33). In addition, more regulated genes were found in the samples which were cultured without HC compared to skin models cultured with HC. This result was independent of the chosen $NiSO_4$ concentration. The circle graphs of the samples show the exact numbers of regulated genes and the distribution of up- and downregulated genes (Figure 34). Around 60 % of the detected genes in both epidermis and dermis after $NiSO_4$-treatment were downregulated. This was also the case for $NiSO_4$-treated epidermis, cultured without HC (e/+LCs/-HC/$NiSO_4$). However, the numbers of up- and downregulated genes in $NiSO_4$-treated dermis, cultured without HC (d/+LCs/-HC/$NiSO_4$), were more balanced compared to the other samples, while there were slightly more up- than downregulated genes in the d/+LCs/+HC/0.1 mM $NiSO_4$.

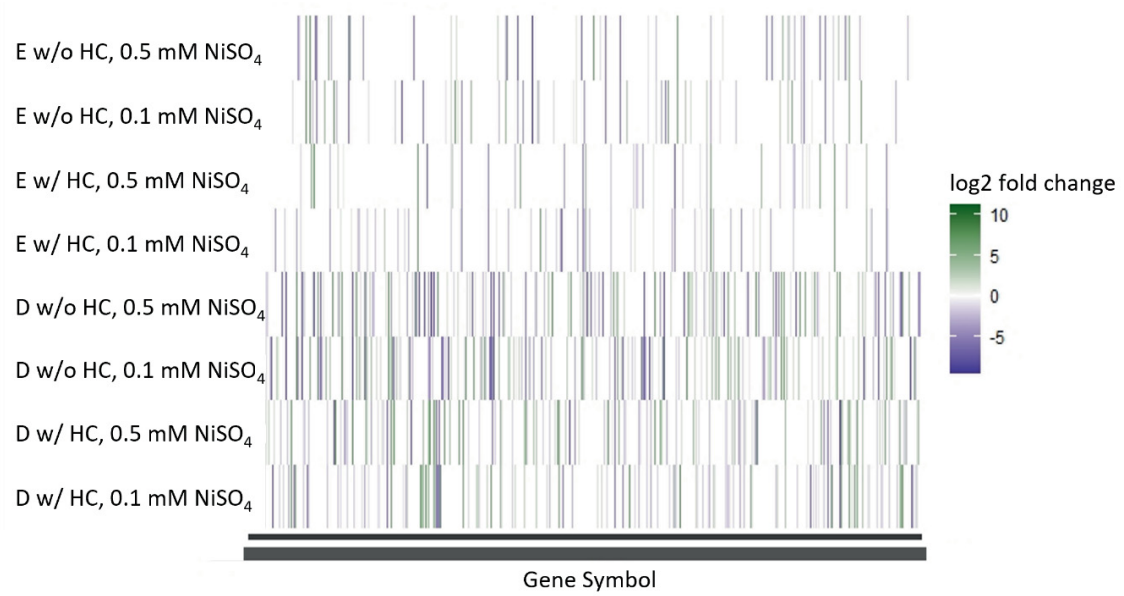

Figure 33: Comparison of regulated genes of $NiSO_4$-treated Phenion® Full-Thickness epidermis and dermis.
Heat map of up- (green) and downregulated genes (purple) in epidermis (E) and dermis (D) tissue samples of Phenion® Full-Thickness skin models with integrated 5% FCS-differentiated MUTZ-LCs (two skin models for each treatment), which were enzymatically separated. The skin models were treated after eleven days of ALI culture for 20 h with 0.1 mM or 0.5 mM $NiSO_4$. Skin models were either cultured in ALI medium supplemented with HC (w/ HC) or without HC (w/o HC). Presented are genes, which were regulated based on the gene expression of the vehicle control (PBS-treated skin models) and had a p value below 0.05.

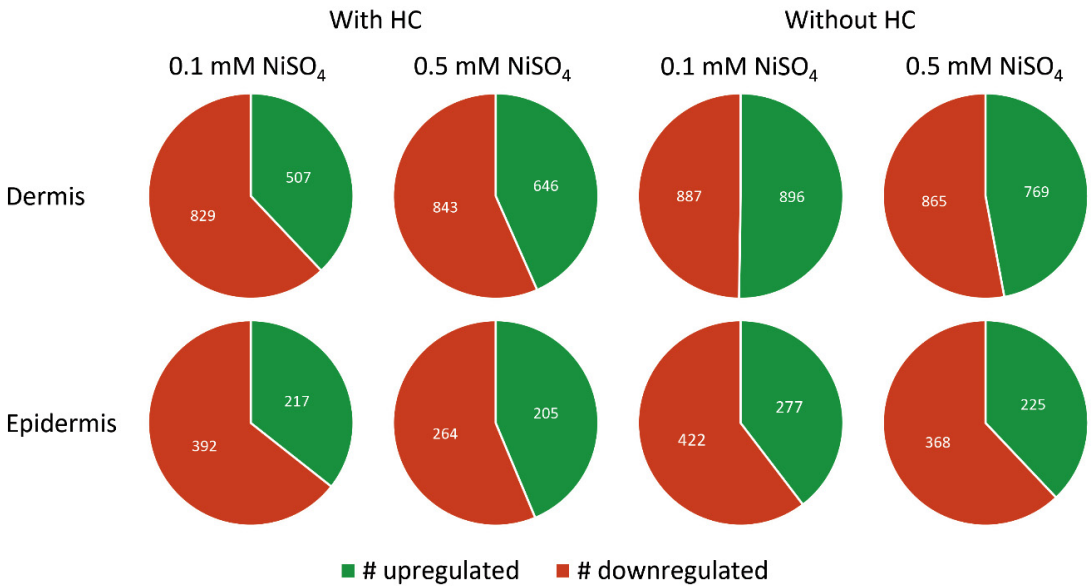

Figure 34: Effect of $NiSO_4$ treatment of Phenion® Full-Thickness dermis and epidermis, cultured with or without hydrocortisone (HC), on the distribution of up- and downregulated genes.
Depicted are the distribution of up- (green) and downregulated genes (red) from the dermis and epidermis of Phenion® Full-Thickness skin models with integrated 5% FCS-differentiated MUTZ-LCs. The skin models were treated for 20 h with 0.1 mM or 0.5 mM $NiSO_4$. Skin models were either cultured for eleven days in ALI phase with HC (left side) or without HC (right side) before being treated with $NiSO_4$ for 20 h. The exact numbers of regulated genes, determined with a NGS analysis are depicted in the corresponding sections. Each condition was from two skin models (one batch). Presented are genes, which were differentially regulated compared to the vehicle control (PBS-treated skin models) and had a p value below 0.05.

The distribution of x-fold gene expression is presented in Figure 35. All samples had a wide spread of data, from -10 to 12 log2 fold change. Moreover, all boxes overlapped, and all median lines were inside the boxes of all other samples. The medians of all samples were between -1 and -2 log2 fold change, except for d/+LCs/-HC/0.1 mM $NiSO_4$ with around 0.5 log2 fold change. The box sized varied, the three largest ones, comparable in size, were from the e/+LCs/-HC/0.1 mM and /0.5 mM $NiSO_4$ as well as from the d/+LCs/-HC/0.5 mM $NiSO_4$. Boxes, slightly smaller than the largest ones, were from the d/+LCs/-HC/0.1 mM and /0.5 mM $NiSO_4$. Next smaller boxes were from e/+LCs/+HC/ 0.5 mM $NiSO_4$-treated and d/+LCs/+HC/0.1 mM $NiSO_4$. E/+LCs/+HC/0.1 mM $NiSO_4$ had the smallest box, but similar to the other box plots with long whiskers.

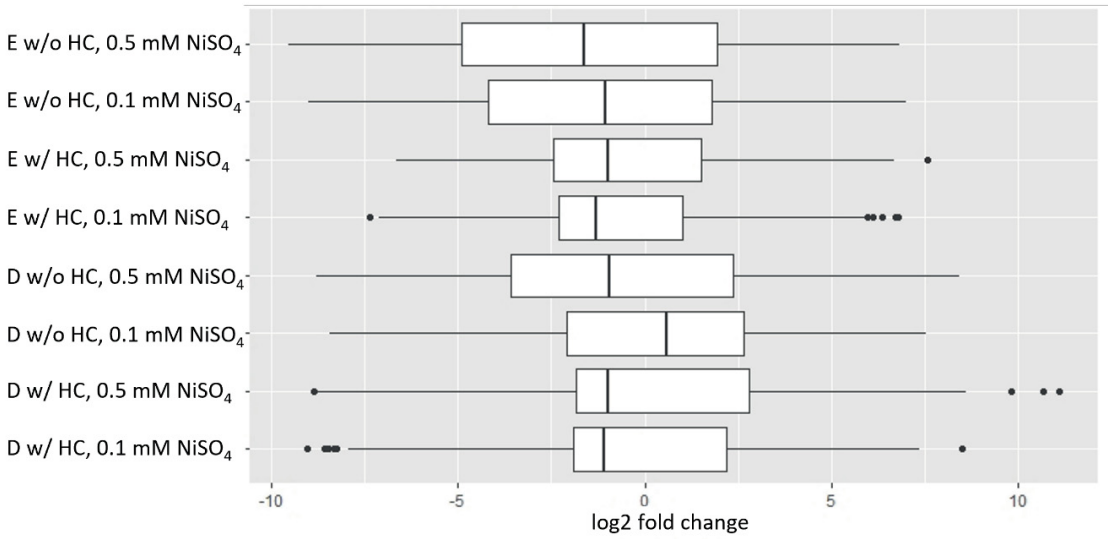

Figure 35: Distribution of the log2 fold change values of genes in epidermis and dermis, regulated by the $NiSO_4$ treatment of Phenion® Full-Thickness skin models, cultured with or without hydrocortisone (HC).
Boxplots of the log2 fold change values of all genes in epidermis and dermis, which were regulated after treating the Phenion® Full-Thickness skin models (with integrated 5% FCS-differentiated MUTZ-LCs) for 20 h with 0.1 mM and 0.5 mM $NiSO_4$. The skin models were cultured with or without HC during ALI phase. After the treatment, the epidermis was enzymatically separated from the dermis and a NGS analysis of the samples was performed. The epidermis and dermis with the same culture condition and treatment were from the same skin models, two for each condition. The log2 fold change of the genes were calculated relative to the PBS-treated samples, the vehicle control for $NiSO_4$. Only the genes with a p value below 0.05 were analyzed.

Next, a process analysis was performed with the regulated genes of $NiSO_4$-treated skin models to study their involvement in biological processes. This analysis was performed with the data analysis bank Gene Ontology (Ashburner et al., 2000; Gene Ontology Consortium, 2021). The processes, which were addresed by the regulated genes, are depicted in Figure 36. They can be divided into four topics, among others, which are relevant for this project. For one, several biological processes can be assigned/allocated the metabolism, e.g., response to chemical stimulus or metal ion binding. Another topic is the immune system including, e.g., responses to growth factor stimulus and the regulation of immune system processes. Additional processes, only addressed by $NiSO_4$-treated and HC-free cultured samples, were, e.g., responses to cytokines or regulation of chemotaxis. Also belonging to the immune system, but due to its´ possible importance for the skin sensitization assay listed as an own group, are all reactions corresponding to migration, e.g., cell motility, regulation of locomotion, regulation of cell projection

organization. Moreover, some of the regulated processes could be grouped under the topic "Differentiation/Development", e.g., multicellular organism development.

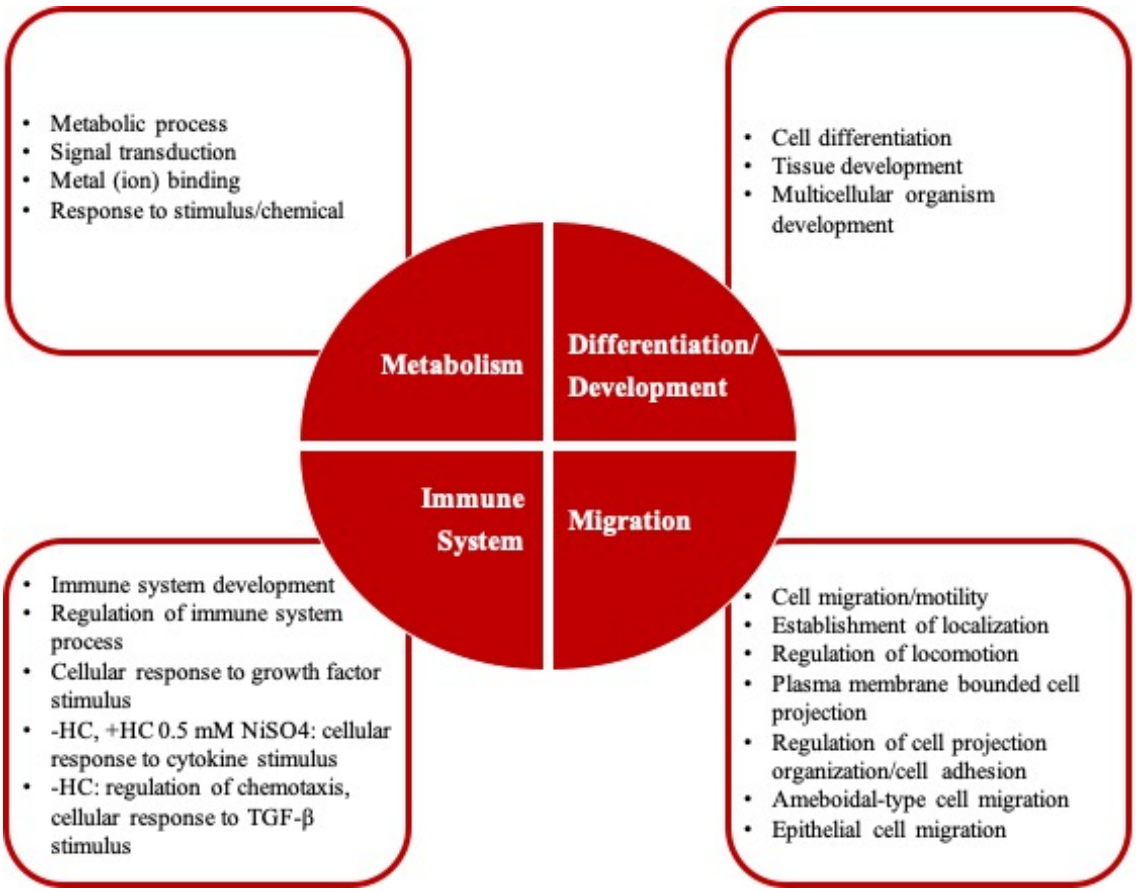

Figure 36: Regulated biological processes in Phenion® Full-Thickness skin models following $NiSO_4$ treatment.
Overview of addressed biological processes by the genes, which were up-or downregulated after treating the Phenion® Full-Thickness skin models (with integrated 5% FCS-differentiated MUTZ-LCs) for 20 h with 0.1 mM and 0.5 mM $NiSO_4$. The processes, relevant for this thesis, were grouped in four main topics: metabolism, differentiation/development, migration and immune system. In the boxes next to each topic are exemplary addressed biological processes listed. The analysis was performed with Gene Ontology (Ashburner et al., 2000; Gene Ontology Consortium, 2021).

In addition, the genes that were regulated in the epidermis and dermis following treatment with both $NiSO_4$ concentrations were compared to known genes associated with the immune system process and migration process. The lists of known genes were sourced from Gene Ontology (GO) knowledgebase (Ashburner et al., 2000; Gene Ontology Consortium, 2021). Immune system and migration process genes were selected due to their integral roles in the skin´s immune reactions after sensitizer exposure. The listed

matches (Table 4) represent the regulated genes in the samples of this project that correspond to known genes associated with the immune system and migration process.

In this comparison, 23 genes which have been demonstrated to play a role in the human immune system (Gene Ontology; Ashburner et al., 2000; Gene Ontology Consortium, 2021) were found in the epidermis of 0.1 mM and 0.5 mM $NiSO_4$-treated skin models cultured with HC (e/+LCs/-HC/0.1 mM $NiSO_4$ or /0.5 mM $NiSO_4$). In contrast, after treating the HC-free cultured skin models with $NiSO_4$, 41 genes of the immune system process were regulated. Only the genes *LGALS7* and *PTN* were regulated in both culture conditions. While 74 immune system process genes were regulated in $NiSO_4$-treated and HC-cultured dermis (d/+LCs/+HC/$NiSO_4$), 66 immune system process genes were regulated in the culture condition without HC. Here, two immune system process genes, *LAMP3* and *ITGB6*, were regulated in all dermis samples.

At least 26 regulated migration genes were found in e/+LCs/+HC/$NiSO_4$, additional 6 genes were regulated in the culture condition without HC. Both conditions had the following genes in common: *PTN*, *HAS2*, *SDCBP*, *DDR2* and *TMSB4X*. In the d/+LCs/+HC/$NiSO_4$ 38 genes were regulated, known to play a role in migration processes. In contrast, 29 genes related to cell migration processes were found in d/+LCs/-HC/$NiSO_4$. The migration gene *OGT* was regulated in all dermis samples.

The highest number of regulated immune process and migration genes were detected in the e/+LCs/-HC/0.1 mM $NiSO_4$. In contrast, the highest number of dermal regulated immune process and migration genes were found in d/+LCs/+HC/0.1 mM $NiSO_4$.

Table 4: Regulated genes by $NiSO_4$ treatment of Phenion® Full-Thickness skin models, known to play a role in the immune system process and migration.

Listed are genes, which were regulated after treating the Phenion® Full-Thickness skin models (with integrated 5% FCS-differentiated MUTZ-LCs) for 20 h with 0.1 mM and 0.5 mM $NiSO_4$. Skin models were cultured with or without hydrocortisone (HC) during ALI phase. After the treatment, the epidermis was enzymatically separated from the dermis. The regulated genes, determined with a NGS RNA analysis, were compared to known genes, which play a role in the immune system process (left side) or in the migration (right side), and the matches are listed for each treatment and culture condition. The known genes were sourced from Gene Ontology (GO) knowledgebase (Ashburner et al., 2000; Gene Ontology Consortium, 2021).

Regulated Immune System Process Genes				**Regulated Migration Genes**			
With HC +$NiSO_4$		**Without HC +$NiSO_4$**		**With HC +$NiSO_4$**		**Without HC +$NiSO_4$**	
Epidermis	**Dermis**	**Epidermis**	**Dermis**	**Epidermis**	**Dermis**	**Epidermis**	**Dermis**
ACTG1	*ABCB9*	*ADK*	*ACP5*	*ACTG1*	*ADAM15*	*APOD*	*ACP5*
ADAM10	*ACTR2*	*APOD*	*ALOX5*	*ADAM10*	*ADAM8*	*COL1A1*	*BMP2*
ADD1	*ADAM15*	*BLM*	*AP3B1*	*AKAP12*	*AMOTL2*	*CXCL10*	*CTSH*
C1QA	*ADAM8*	*CFD*	*ARG1*	*CD9*	*BEX4*	*DDR2*	*DDRGK1*
CD86	*AHR*	*COL3A1*	*CARD9*	*DDR2*	*CD81*	*EMILIN1*	*DYSF*
CD9	*ANK1*	*COLEC12*	*CD36*	*FGF1*	*CDH1*	*FGF2*	*EPHA4*
EPHB4	*ARRB2*	*CXCL10*	*CD86*	*GAS6*	*CLDN1*	*FGF7*	*F2RL1*
GAS6	*BAP1*	*EIF2AK2*	*CEACAM1*	*GPSM3*	*CLDN4*	*GREM1*	*FGF22*
GPSM3	*CADM1*	*EMILIN1*	*CFP*	*HAS2*	*EPHB2*	*HAS2*	*FGR*
IFNGR1	*CD81*	*ERMAP*	*CTSC*	*NTN1*	*EPPK1*	*JAM2*	*GRB7*
IL4I1	*CEBPA*	*FCGRT*	*CTSH*	*PFN1*	*ITGA2*	*LDLRAD4*	*IFITM1*
LGALS7	*CHD7*	*FLVCR1*	*CXADR*	*PFN2*	*KRT5*	*MMP2*	*OGT*
LST1	*CTSL*	*GREM1*	*CYLD*	*PTN*	*LDLRAD4*	*MMP3*	*PTGER3*
LTBR	*DEFB1*	*HMGN2*	*DLG1*	*SDCBP*	*MAPK8*	*OSGIN1*	*RNF41*
PNMA1	*DHX36*	*IFI44L*	*DYSF*	*SLAMF8*	*MARVELD3*	*PDGFRB*	*SDCBP*

Regulated Immune System Process Genes				**Regulated Migration Genes**			
With HC +$NiSO_4$		**Without HC +$NiSO_4$**		**With HC +$NiSO_4$**		**Without HC +$NiSO_4$**	
Epidermis	**Dermis**	**Epidermis**	**Dermis**	**Epidermis**	**Dermis**	**Epidermis**	**Dermis**
PRNP	*EIF6*	*IFIT1*	*EDNRB*	*SLIT2*	*MIEN1*	*PTN*	*SEMA3F*
PSMB8	*EPHB2*	*IFIT3*	*EIF2B1*	*SNAI2*	*MMP9*	*RARRES2*	*SEMA4B*
PTN	*FGFR3*	*IGFBP2*	*F2RL1*	*TMSB4X*	*NOD2*	*SDCBP*	*SINHCAF*
SLAMF8	*GAPDH*	*IL6*	*FGR*	*WNT5B*	*OGT*	*SFRP2*	*STK39*
SLC25A5	*GFUS*	*ITGA7*	*FOXL1*		*PLD2*	*STC1*	*SWAP70*
SLIT2	*H2BC21*	*JAM2*	*FRK*		*PTP4A1*	*STK39*	
SNAI2	*HCST*	*LGALS1*	*GATA3*		*PYCARD*	*TBX5*	
TYROBP	*HDAC7*	*LGALS7*	*GBP2*		*RBBP7*	*THY1*	
	IRF5	*LOX*	*GPLD1*		*RCC2*	*TMSB4X*	
	ITGA2	*MASP1*	*HES1*		*RHOC*	*TWIST2*	
	ITGAM	*MFAP4*	*HSPA1B*		*SEMA4A*		
	ITGB6	*MMP2*	*IFITM1*		*SEMA6C*		
	JAML	*NFE2L1*	*IFNK*		*SEMA6D*		
	JUND	*PTGDS*	*IL18R1*		*STK4*		
	KRT1	*PTN*	*IRAK2*		*WNT4*		
	LAMP3	*PTX3*	*ITGB6*				
	LCP1	*RARRES2*	*JAK1*				
	LGALS7	*SOX13*	*LACC1*				
	LY6D	*SSC5D*	*LAMP3*				
	MARCO	*STK39*	*LCN2*				
	MMP9	*THY1*	*LIG4*				
	MYC	*TMEM176A*	*MAP4K2*				

Regulated Immune System Process Genes				**Regulated Migration Genes**			
With HC +$NiSO_4$		**Without HC +$NiSO_4$**		**With HC +$NiSO_4$**		**Without HC +$NiSO_4$**	
Epidermis	**Dermis**	**Epidermis**	**Dermis**	**Epidermis**	**Dermis**	**Epidermis**	**Dermis**
	NCAPH2	*TMEM176B*	*MKRN2*				
	NFKBIL1	*TWIST1*	*MR1*				
	NOD2	*TWIST2*	*MX1*				
	PAXIP1	*UBA5*	*MX2*				
	PELI1		*NDRG1*				
	PLD2		*NLRP10*				
	PMAIP1		*PIK3CG*				
	POLB		*PMS2*				
	POLR3B		*PRKCH*				
	POLR3F		*PRKCZ*				
	PTMS		*PTGER3*				
	PTPN2		*PTPN6*				
	PYCARD		*RAB20*				
	RAB5B		*RNF41*				
	RNF135		*RPS14*				
	RNF187		*SHLD1*				
	RNF19B		*STAT1*				
	S100A8		*STK39*				
	SEMA4A		*STXBP3*				
	SENP1		*STXBP4*				
	SLC39A7		*SWAP70*				
	SLPI		*TCEA1*				

Regulated Immune System Process Genes				**Regulated Migration Genes**			
With HC +$NiSO_4$		**Without HC +$NiSO_4$**		**With HC +$NiSO_4$**		**Without HC +$NiSO_4$**	
Epidermis	**Dermis**	**Epidermis**	**Dermis**	**Epidermis**	**Dermis**	**Epidermis**	**Dermis**
	SP1		*TFRC*				
	SP110		*TLR1*				
	TEC		*TLR3*				
	TNFAIP3		*WFDC12*				
	TNFRSF9		*ZBTB16*				
	TRIM11						
	TRIM26						
	TRIM62						
	TYK2						
	UFL1						
	WNT4						
	XRCC5						
	ZDHHC5						

5. Discussion

Nearly 20 % of the European population suffer from an allergic contact dermatitis (ACD) (Diepgen et al., 2016). Due to continued exposure to an allergic chemical, some individuals, particularly health professionals, chemical industry workers, and beauticians/hairdressers, find themselves no longer able to perform their jobs (Rodriguez et al., 2022). ACD can occur not only in occupational settings but also in everyday life due to exposure to various allergens. There are more than 4,000 low-molecular allergens (Chittiboyina et al., 2015). These allergens can be found in numerous sources, including but not limited to jewelry (e.g., nickel), cosmetic products (e.g., fragrances, hair dyes) and plants (e.g., poison ivy) (Treadwell, 2020; Uter et al., 2020). Hence, ACD has a significant impact on industry productivity and healthcare costs (Cvetkovski et al., 2005). Therefore, it is not surprising that a lot of research is performed to better understand and eventually prevent ACD. The number of PubMed-indexed publications on “allergic contact dermatitis” has significantly increased over the last decades, from 89 in 1980 to 678 in 2023 (Figure 37). This underlines the growing scientific interest and importance of the ACD research.

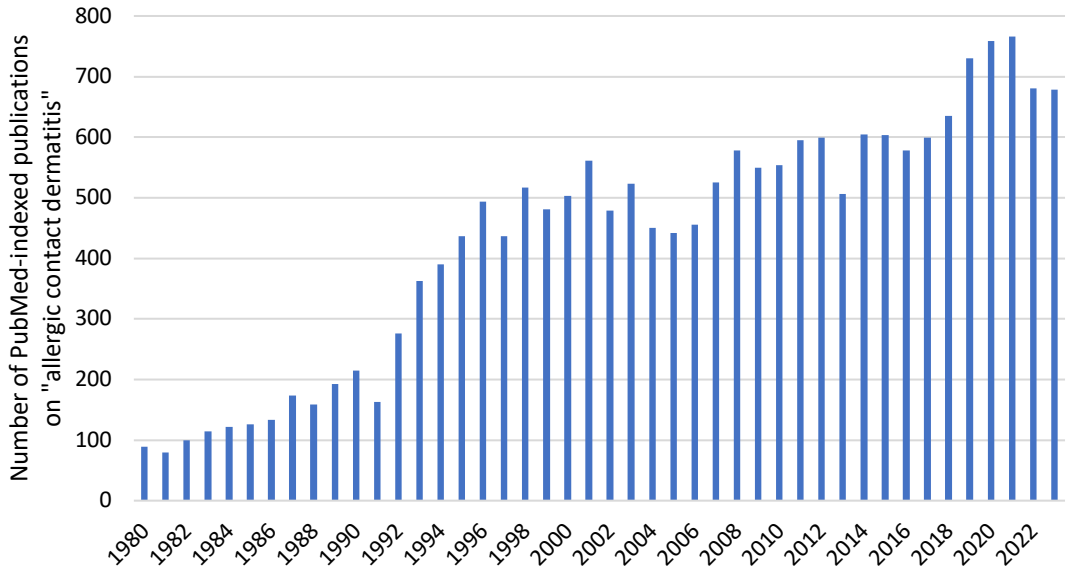

Figure 37: Research growth in allergic contact dermatitis.
Annual number of PubMed-indexed publications on “allergic contact dermatitis” from 1980 to 2023. The rise in publication volume highlights the increasing scientific relevance, as allergic contact dermatitis is a significant public health concern due to its impact on the quality of life. [number of PubMed-indexed publications, PubMed, derived in November 2024]

The organization for economic co-operation and development (OECD) summarized the cellular reactions of the adverse outcome pathway (AOP) for "skin sensitization initiated by covalent binding to proteins" (OECD No. 168, 2014). The four key events of the AOP are: 1. haptenization of the chemicals, 2. the inflammatory responses of keratinocytes, 3. the activation of dendritic cells and 4. the T cell activation (OECD No. 168, 2014). Moreover, the OECD validates alternative *in vitro* methods, or new approach methodologies (NAMs), which assess the sensitizing potential of a chemical. However, until now, all OECD-accepted methods address only one key event of the AOP. Consequently, several NAMs need to be combined for a defined approach to get reliable findings, which is described in the OECD TG 497 (2023). The aim of this study is to develop an immunocompetent skin model with Langerhans cells (LCs), which would combine the first three key events in one assay. Such a model would be more *in vivo* like and thus enhance the prediction of the assessed potential or even potency of a chemical. Furthermore, the applicability domain would be extended, as, e.g., creams, ointments, viscous formulations could be applied on the dry surface of the skin models, which is not possible with cells in suspension culture. A few research groups have already published first results in generating an immunocompetent skin model (e.g., Kosten et al., 2015; Bock et al., 2018). Until now, every one of them had disadvantages, which will be addressed in the following chapters, and not one has yet been authorized by OECD.

Moreover, this work also addresses the increasing demand for the reduction of animal-derived products. The shift to animal-free methods was initiated by Russel and Burch´s ethical guidelines (1959). Nowadays, several journals have restrictions for using animal-derived products. For example, ALTEX "require[s] authors to discuss […the use of animal-derived products], […] and indicate whether such materials could/shall be replaced in future studies" (author's instructions published by ALTEX).

The present work shows important steps in the development of an immunocompetent skin model, while also improving the reproducibility of protocols and reducing the use of animal-derived products.

5.1 Optimization of the MUTZ-LC differentiation protocol

The use of native LCs for *in vitro* studies is constrained by factors such as limited supply, donor variabilities and standardization (Santegoets et al., 2008). As an alternative, the acute myeloid leukemia cell line MUTZ-3 was chosen as a LC surrogate. MUTZ-3 cells can be differentiated into MUTZ-LCs upon exposure to a cytokine cocktail. Santegoets et al. (2008) compared the ability to differentiate into functional dendritic cells based on protein expression of several cell lines, THP-1, KG-1, HL-60, Monomac-6, U-937, K562 and MUTZ-3 cells. They concluded that from all tested cell lines, differentiated MUTZ-LCs are the most suitable dendritic cell surrogates. Several MUTZ-LC differentiation protocols have already been published, which vary in differentiation time and medium supplements (e.g., Masterson et al., 2002; Santegoets et al., 2006; Nelissen et al., 2009; Kosten et al., 2015; Ruben et al., 2015; Groell et al., 2018; Bock et al., 2018). Hence, one aim of this study was to select the best-suited MUTZ-LC differentiation medium.

To address this, the expression of specific proteins known to be characteristic for LCs was analyzed using flow cytometry. One typical LC marker is CD1a, one of the four family 1 CD1 proteins, which presents microbial lipid and glycolipid antigens to T cells (Melián et al., 1996). Another specific LC marker is CD207, which is involved in the formation of the LC-typical Birbeck granules (Valladeau et al., 2000). The expression of CD34, a hematopoietic stem cell marker, and CD14 have been reported to become lost during differentiation (Masterson et al., 2002). CD14 plays a crucial role in the recognition, binding and uptake of bacterial lipopolysaccharides (Wright et al., 1990). In addition, the expression level of HLA-DR was studied, an MHC class II molecule presenting antigens to T cells (Puré et al., 1990). Dendritic cells express the costimulatory factors CD80 (B7-1) and CD86 (B7-2), which can bind to the CD28 receptor family on T cells, resulting in the activation of T cells (Slavik et al., 1999). Another marker for the maturation of LCs is CD54 (Sheikh and Jones, 2008). CD54 and CD86 are already used as sensitization markers in OECD-approved *in vitro* test methods, e.g., in the h-CLAT and the U-Sens assays (OECD TG 442E, 2023). However, in the present project nearly every MUTZ-LC was already positive for CD54, CD86 and HLA-DR. Consequently, other specific markers were added to the marker panel to test whether the differentiated MUTZ-LCs were in an immature or mature state: CD18, CD40, CD44, CD83, CD184, and CCR7. The functions of these proteins will be discussed in the corresponding chapters.

It is important to phenotypically analyze the MUTZ-LCs, as they need to exhibit an immature state to enable a stimulation by a sensitizing chemical. Subsequently, the differentiated MUTZ-LCs were subjected to treatment with known sensitizers to assess their potential to undergo maturation, which is a prerequisite for their utilization in a skin sensitization assay.

5.1.1 Comparison of the analyzed MUTZ-3 cell phenotype with data from literature

It was important to analyze the original cell population, the undifferentiated MUTZ-3 cells, before starting the differentiation, as all following experiments were based on these cells. The morphology of the MUTZ-3 cells was comparable to the published microscopic images from the DSMZ MUTZ-3 cell culture data. Moreover, this was also the case for the analyzed protein expression profiles. The LC-typical marker CD1a was not expressed by any MUTZ-3 cell, which was also documented by Masterson et al. (2002), Larsson et al. (2006) and Rasaiyaah et al. (2009). CD207, a protein responsible for the formation of the LC Birbeck granules (Valladeau et al., 2000), was also not expressed. About 20 % of the MUTZ-3 cells were positive for CD14, a percentage comparable to data which have been published by several authors (DSMZ cell culture data; Masterson et al., 2002; Larsson et al., 2006), but twice as high than documented by Rasaiyaah et al. (2009). CD14 is known to bind bacterial lipopolysaccharides (Wright et al., 1990). Not every MUTZ-3 cell was positive for CD14, as different subpopulations can be found in MUTZ-3 cell culture, which has been described by Santegoets et al. (2008). Another typical marker for MUTZ-3 cells is CD34, its measured expression (about 25 %) was nearly two-times lower as documented by Masterson et al. (2002) and slightly higher than the published data from DSMZ (cell culture data) as well as two times higher than determined by Rasaiyaah et al. (2009). The intermediate numbers of MUTZ-3 cells positive for CD86 and the high numbers of HLA-DR-positive cells were comparable to Rasaiyaah et al. (2009), while the CD40 expression was three-times lower in this study. The observed differences of the marker expressions between this study and the published data can have several causes. For instance, the culture, including choice of medium and temperature, as well as handling of MUTZ-3 cells, e.g., cell passage and cryopreservation methods, might influence the expression profiles (Hirsch and Schildknecht, 2019). In addition, there are a lot of possible variations for flow cytometry, which might explain the differences between research groups: antibodies from different suppliers or with different

fluorochromes, staining protocol (e.g., time, temperature), hardware configuration and instrumental setups (e.g., flow rate, gating strategy) (Easthope, 2022).

To sum it up, the overall expression profile of the used MUTZ-3 cells resembles the data found in the literature. Thus, the purchased MUTZ-3 cells were suitable for the use in further experiments.

5.1.2 Granulocyte-macrophage colony-stimulating factor increases the yield of CD1a- and CD207-positive MUTZ-LCs

This work was initially based on a study conducted earlier at Henkel (bachelor thesis, Cox, 2016). In this study, the MUTZ-3 cells were differentiated into MUTZ-LCs within seven days in culture medium supplemented with 20 % fetal calf serum (FCS), 10 % 5637-conditioned medium (5637CM), TGF-β and TNF-α (5TT). However, most of the published differentiation media are enriched with granulocyte-macrophage colony-stimulating factor (GM-CSF) (Masterson et al., 2002; Larsson et al., 2006; Santegoets et al., 2006; Rasaiyaah et al., 2009; Nelissen et al., 2009; Kosten et al., 2015; Ruben et al., 2015; Groell et al., 2018; Bock et al., 2018). GM-CSF is known to play an important role in dendritic cell differentiation (Inaba et al., 1992). Consequently, the 5TT differentiation medium, as previously described, was augmented with the addition of GM-CSF (5TTG medium) to assess the impact on the MUTZ-LC differentiation process. Furthermore, the present study investigated the most suitable duration for differentiation by evaluating the outcomes at different time points (one, two or three weeks). A comparative analysis was conducted between the two differentiation media (5TT and 5TTG).

While differentiating the MUTZ-3 cells into MUTZ-LCs, the morphology of the cells changed in both differentiation media. The MUTZ-LCs were bigger than the MUTZ-3 cells and cluster-like formations could be observed, which was also described by Riedl et al. (2000). In addition, more dead cells and debris were found, which was also confirmed by flow cytometry. This finding will be further discussed in chapter 5.1.6. The MUTZ-LCs formed small cytoplasmic protrusions, which was also described by Santegoets et al. (2008). These cytoplasmic protrusions might be the precursor of the LC-typical long dendritic processes (Swetman et al., 2002).

Besides the morphology of the cells, the expression profile of the surface proteins also changed during differentiation. For one, the characteristic *de novo* expression of the LC-typical marker CD207 and CD1a was observed in both differentiation media, as described by, e.g., Masterson et al. (2002), Larsson et al. (2006), Santegoets et al. (2006), Rasaiyaah et al. (2009), Nelissen et al. (2009), Kosten et al. (2015), Ruben et al. (2015), Groell et al. (2018), and Bock et al. (2018). The medium supplement GM-CSF further increased the expression of CD1a and CD207 by at least two-fold. The successful differentiation of MUTZ-3 cells into MUTZ-LCs was indicated by the high expression of the LC-characteristic markers CD1a and CD207, which showed an increasing trend during the first two weeks of differentiation. Furthermore, only when adding GM-CSF to the differentiation medium, the CD14 expression was lost after two weeks, which confirms the results published by Masterson et al. (2002) and Larsson et al. (2006). The MHC class II molecule, HLA-DR, presents antigens to T cells (Puré et al., 1990) and is known to be expressed on LCs (Simon et al., 1991; Rizova et al., 1994). Masterson et al. (2002) observed that HLA-DR was upregulated during differentiation. In the present study, the differentiation in 5TTG medium led to an increase from an initial proportion of 65 % HLA-DR-positive MUTZ-3 cells to 90 % HLA-DR-positive MUTZ-LCs after two weeks of differentiation, with expression levels remaining stable between weeks two and three. When the cells were differentiated without GM-CSF, less MUTZ-LCs expressed HLA-DR.

In addition to the previously described markers that are characteristic for MUTZ-3 cells and MUTZ-LCs, CD86, a typical marker for LC maturation, was also analyzed in this study. It is important to verify that the differentiated MUTZ-LCs are in an immature state. Only upon exposure with a sensitizer the MUTZ-LCs should mature, as described for native LCs in the AOP (OECD No. 168, 2014). The CD86 expression was more pronounced in the differentiation media supplemented with GM-CSF (approximately 80 %). CD86 is a maturation marker and functions as a read-out parameter for several OECD-approved *in vitro* skin sensitization methods, e.g., h-CLAT assay and the U-SENS™ (TG 442E, 2023). However, both methods are based on THP-1 cells, another surrogate for dermal LCs. The numbers of CD86-positive MUTZ-LCs were higher than documented by Nelissen et al. (2009), but comparable to the published CD86 histograms by Masterson et al. (2002), which showed that nearly every cell was positive for CD86. In contrast to the h-CLAT assay with THP-1 cells, CD86 seemed to be not suitable as a

maturation marker for MUTZ-LCs, as nearly every cell was already CD86-positive and thus a further increase of positive cells upon exposure with a sensitizing chemical was not likely. This will be further discussed in chapter 5.2. More maturation markers were added to the panel for the next experiments, which are described in the following chapters.

Taken together, supplementing the medium with GM-CSF resulted in a higher yield of successfully differentiated CD1a- and CD207-positive MUTZ-LCs. In addition, the expression levels of the proteins increased during the first two weeks of differentiation, while no significant changes were detected between week two and three, indicating a plateau in marker expression beyond the two-week timeframe. Therefore, the differentiation protocol, used by Cox (2016), was modified by adding the supplement GM-CSF to the medium and prolonging the differentiation from 7 to 14 days.

5.1.3 5637-conditioned medium has no positive effect on MUTZ-LC differentiation

The DSMZ recommends supplementing the culture medium of MUTZ-3 cells with the conditioned medium by 5637 cells (5637CM), a bladder carcinoma cell line, which is known to induce the proliferation of leukemia cell lines (Quentmeier et al., 1997). Quentmeier et al. (1997) listed and quantitated the secreted cytokines by 5637 cells, which also included, e.g., GM-CSF, TNF-α and TGF-β. As 5637CM is enriched with cytokines, which are relevant for LC-differentiation (Inaba et al., 1992; Koch et al., 1990; Borkowski et al., 1997), it could also have a positive effect on LC differentiation. In some of the published differentiation media, it is not clearly described, whether 5637CM is added to the differentiation media (e.g., Masterson et al., 2002; Rasaiyaah et al., 2009). For example, Masterson et al. (2002) described the differentiation as the following: “For the generation of LC-like cells, MUTZ-3 cells were cultured in GM-CSF and TNFα […] for 9 days.”. Thus, the components of the differentiation medium are not clearly defined. Most of the supplements of published differentiation media are completely listed and did not include 5637CM (Santegoets et al., 2006; Larsson et al., 2006; Ouwehand et al., 2008; Nelissen et al., 2009; Ruben et al., 2015; Groell et al., 2018; Bock et al., 2018). However, none of the research groups state the rationale behind removing 5637CM from the differentiation medium, while adding it to the maintenance medium of the MUTZ-3 cell culture. Due to this uncertainty regarding 5637CM, the impact of the conditioned cell medium on the MUTZ-LC differentiation was analyzed. To the author´s knowledge, this

is the first report analyzing the effect of 5637CM on MUTZ-LC differentiation. For that, two differentiation media were tested: with 5637CM (5TTG medium) and without 5637CM (TTG medium).

5637CM did not seem to impact the morphology of MUTZ-LCs. Moreover, the expression profiles of 5TTG- and TTG-differentiated MUTZ-LCs were nearly identical. The morphology of the differentiated MUTZ-LCs was similar in both culture conditions, with similar size and enhanced granularity. Additionally, the characteristic formation of cell cluster could be observed. These findings were consistent with the previous described morphology of the 5TTG-differentiated MUTZ-LCs (chapter 5.1.2). However, compared to the previous marker expression results with 5TTG-differentiated MUTZ-LCs (chapter 5.1.2), the expression of CD1a and CD207 was even more increased. Nearly every MUTZ-LC, differentiated for 14 days in 5TTG and TTG, was positive for these LC-typical markers. Therefore, the yield of CD1a- and CD207-positive cells was higher than the published data, e.g., about 35 % (Larsson et al., 2006), 65 % (Nelissen et al., 2009) and 80 % (Masterson et al., 2002). The loss of CD34 expression as well as the high expression levels of CD86 and HLA-DR were comparable to the previous described results. In addition, the membrane-bound protein CD34 was analyzed. The CD34 expression was lost after one week of differentiation, which was also documented by Masterson et al. (2002). This was expected, as CD34 is a marker for hematopoietic stem cells (Sutherland et al., 1993) and thus should get lost during the differentiation. Simon et al. (1991) showed that human LCs express adhesion molecules, e.g., CD18 and CD54, and that these are important for T cell activation. Similar to the native LCs, the MUTZ-LCs expressed CD18 and CD54. However, the percentage of CD18-positive MUTZ-3 cells was higher than the one of MUTZ-LCs. To the author's knowledge, the CD18 expression has not yet been analyzed on MUTZ cells. The reasons for the decrease in CD18 expression are unknown. Still, CD18 expression could be demonstrated on the MUTZ-LCs, resembling native LCs. CD54 was expressed by nearly every MUTZ-3 cell and MUTZ-LC, which is comparable to the results reported by Masterson et al. (2002). CD40 is another costimulatory marker playing a role in the T cell activation, which is expressed by human LCs (Péguet-Navarro et al., 1995). During MUTZ-LC differentiation the CD40 expression was upregulated and nearly every cell was CD40-positive, similar to native LCs, which was also observed by Masterson et al. (2002). In addition, CD44 was analyzed as another marker in the present study. CD44 is a membrane-bound

adhesion molecule expressed by native LCs (Aiba et al., 1993). Its expression was also detected on nearly every MUTZ-LC, consistent with the published results by Larsson et al. (2006).

It was observed that the expression profiles of the TTG-differentiated MUTZ-LCs differed compared to the preciously described expression levels during the GM-CSF experiments in chapter 5.1.2, despite the utilization of the same differentiation medium. This disparity could potentially result of the use of different antibodies for the analysis. Instead of animal-derived antibodies, recombinant antibodies were used to further increase the reproducibility, as they have higher purity as well as lot-to-lot consistency (product data sheet, Miltenyi Biotec). Moreover, according to the producer, the recombinant antibodies are considered to be more specific than animal-derived ones (product data sheet, Miltenyi Biotec). Therefore, the documented protein expressions with the recombinant antibodies should allow more consistency than the previous ones. Another advantage of the recombinant antibodies is the reduction of animal derived products.

Overall, the results suggest a successful differentiation of MUTZ-3 cells into MUTZ-LCs, supported with an even wider antibody panel than in the previous experiments with GM-CSF. Moreover, 5637CM seems to have no impact on MUTZ-LC differentiation. As a biological product, it is likely that 5637CM has lot-to-lot variabilities, which might influence the MUTZ-LC differentiation when using different lots. Consequently, for the reproducibility of differentiation protocol, 5637CM was excluded from the differentiation medium for all following experiments.

5.1.4 FCS reduction in the differentiation medium accelerates MUTZ-LC differentiation

Apart from the defined cytokines, another undefined cytokine cocktail is FCS, which is still commonly supplemented to the differentiation medium. FCS contains growth factors, adhesion and attachment factors as well as other cytokines, which have a positive impact on cell culture, e.g., cell proliferation and viability (product data sheet, Biochrom). Besides the beneficial effects, FCS has the disadvantage that it is prone to lot-to-lot variations (Baker et al. 2016) and thus might affect the outcome of experiments. In

addition, FCS is generated by slaughtering pregnant cows in an ethical questionable manner (Jochems et al., 2002; McCann and Treasure, 2022). Despite these disadvantages, nearly every published MUTZ-LC differentiation medium contains 20 % FCS (e.g. Santegoets et al., 2006; Nelissen et al., 2009; Kosten et al., 2015; Groell et al., 2018). Moreover, the percentage of this animal-derived product is unusually high compared to other commonly used cell culture media, which are mostly supplemented with 10 % FCS, e.g., THP-1 cells, U-937 cells or SenzaCells (OECD TG 442E, 2023). Consequently, the present study aimed to test if FCS can be excluded, or at least reduced in the differentiation medium. This potential modification of the differentiation medium would further improve the standardization of the protocol and also align with the principles of the 3Rs (Russel and Burch, 1959). Four differentiation media were tested, TTG medium supplemented with 0 %, 5 %, 10 % and 20 % FCS.

After being differentiated for seven days in TTG medium without FCS, nearly all MUTZ-LCs were dead. A MUTZ-LC differentiation completely without FCS and without any alternative supplement to compensate for FCS was not possible. Consequently, the survival of the cells seems to rely on the presence of the components in FCS. Without supplementation of those components, the cells were not able to survive. However, the differentiation with 5 % and 10 % FCS resulted in enough viable cells to perform flow cytometry analysis. After seven days of differentiation in the media supplemented with reduced FCS content (5 % and 10 % FCS), there were more CD1a- and CD207-positive MUTZ-LCs than in 20 % FCS enriched medium. The numbers were comparable to the CD1a and CD207 expression after 14 days of differentiation in fully 20 % FCS-supplemented medium. Moreover, the typical loss of CD14 expression occurred one week earlier in the FCS reduced media than in the original medium. The expression levels of all other markers were similar to the already discussed ones in the previous chapter: A high number of MUTZ-LCs expressed CD40, CD44, CD54, CD86 and HLA-DR, while the expression of CD34 was lost within the first week of differentiation. The LC-typical marker, CD1a and CD207, were also documented to be expressed on the MUTZ-LCs differentiated in 5 % and 10 % FCS. This indicates a successful MUTZ-LC differentiation in the presence of FCS, regardless of the FCS content.

The morphology of the MUTZ-LCs was consistent with the results of the 5637CM analysis (chapter 5.1.3). However, MUTZ-LCs, cultured in 5 % FCS- or 10 % FCS-

supplemented medium, already expressed the LC-typical dendritic processes after seven days of differentiation. In contrast, in 20 % FCS enriched medium, the numerous dendritic processes of adherent MUTZ-LCs were not found until two weeks of differentiation.

To sum it up, a reduction of the FCS percentage in the differentiation media from 20 % to 5 % FCS was sufficient for a successful MUTZ-LC differentiation. Since FCS is an undefined cytokine cocktail, the medium with the lowest FCS concentration tested so far (5 % FCS), which still supported the differentiation process, was chosen to continue with during this study. Moreover, the differentiation with the reduced FCS percentage seemed to accelerate the MUTZ-LC differentiation. As a result, the differentiation time could be shortened from 14 to 7 days. Thus, the differentiation process required a shorter duration compared to the protocols published by Ouwehand et al. (2010) and Bock et al. (2018). Notably, Nelissen et al. (2009) and Groell et al. (2018) also reported a differentiation for seven days. In addition, the reduction of the FCS percentage improved the standardization of the differentiation protocol and contributed to the demand for less animal-derived products. From an economic standpoint, the optimized differentiation protocol was even more cost-effective compared to original method. Thus, the enhanced efficiency also optimizes budget utilization.

5.1.5 Ultroser G is not a suitable FCS alternative for MUTZ-LC differentiation

The present study showed that the FCS content of the differentiation medium could be reduced by 75 % without apparent loss of cell function. To further improve the standardization, it would have been ideal to completely remove the FCS from the medium. However, the previous results have shown that a differentiation without FCS resulted in a high cell death rate. Therefore, Ultroser G, a commercially available serum-free alternative to FCS, was tested to possibly prevent the negative effect on cell viability. Ultroser G has a semi-defined composition, which ensures a batch-to-batch reproducibility, and a five-times higher bioactivity than FCS (product data sheet, Pall BioSepra). Unfortunately, the supplier did not disclose its composition. The differentiation medium was supplemented with 4 % Ultroser G which should be equally biologically active as 20 % FCS (originally used FCS concentration). To determine the degree of MUTZ-LC differentiation, the morphological and physiological properties of

the cells were analyzed in 4 % Ultroser G- and the 5 % FCS-supplemented media (the optimized protocol).

The morphologies of the MUTZ-LCs differed. In contrast to the numerous and long dendritic processes exhibited by 5 % FCS-differentiated MUTZ-LCs, only a few 4 % Ultroser G-differentiated MUTZ-LCs adhered to the bottom of the culture dishes and formed small dendritic processes. Consequently, the differentiation in Ultroser G-supplemented medium resulted in a less LC characteristic morphology than the differentiation with 5 % FCS. This finding was confirmed by analyzing the expression of typical marker proteins. Less than half of the LC-characteristic CD1a- and CD207-positive MUTZ-LCs were found in 4 % Ultroser G-supplemented medium compared to the 5 % FCS-containing medium. Another indicator that not all cells in 4 % Ultroser G enriched medium were differentiated is the detection of a significant number of CD14- and CD34-positive cells, which are typical for undifferentiated MUTZ-3 cells (product data sheet, DSMZ). Moreover, the antigen presenting molecule HLA-DR and the costimulatory factor CD40 were more expressed on 5 % FCS-differentiated MUTZ-LCs than on 4 % Ultroser G-differentiated cells. Besides CD86, which was also analyzed in the previous experiments, the other costimulatory factor CD80 was analyzed as well. Both membrane-bound proteins are expressed on LCs and bind to the CD28 receptor family on T cells resulting in T cell activation (Slavik et al., 1999). While the CD86 expression was comparable, the CD80 expression was more pronounced in MUTZ-LCs differentiated in 5 % FCS-supplemented medium. All these results suggest that Ultroser G is less suitable for MUTZ-LC differentiation than FCS. The only marker in favor of the differentiation with the FCS substitute is CD18. There were more CD18-positive cells in 4 % Ultroser G-differentiated than in 5 % FCS-differentiated MUTZ-LCs. CD18 is expressed on LCs and plays a role in the T cell activation (Simon et al., 1991). Hence, a higher expression of CD18 might indicate a more LC-like differentiation. However, the marker was also detected on 5 % FCS-differentiated MUTZ-LCs, although at a slightly lower rate.

Overall, the differentiation of MUTZ-LCs supplemented with Ultroser G has a more than 50 % lower yield of differentiated MUTZ-LCs than the differentiation with 5 % FCS. One reason for this observation might be that Ultroser G has been developed and tested specifically for adherent cell types (product data sheet, Pall BioSepra), but not for LCs which are generally cultured under non-adherent conditions. Nevertheless, it is still

possible that both differentiation media generated functional MUTZ-LCs capable of maturing upon exposure to a sensitizer. Hence, MUTZ-LCs differentiated in the presence of 5 % FCS and 4 % Ultroser G were treated with sensitizers to assess their potential reaction. This will be discussed in the chapter 5.2.

Moreover, the validation of FCS alternatives such as Ultroser G to replace FCS completely in cell culture aligns with the 3Rs (Russel and Burch, 1959) by reducing the dependency on animal-derived products. It represents the growing demand towards completely animal-free, sustainable and reproducible methods. However, despite the advantages of using animal-free products, the present study demonstrates the importance of testing the alternatives before replacing animal-derived medium supplements. Not every animal-free alternative is suitable for every cell culture condition. Some studies suggest adding growth factors to the FCS-free culture medium improves cell viability and cell growth (Deangelis et al., 2013; Ghasemi et al., 2019; Alghadeer et al., 2024). Further studies would be needed to assess if the addition of growth factors could also be sufficient for a serum-free differentiation of MUTZ-3 cells into MUTZ-LCs.

5.1.6 Differentiating MUTZ-3 cells into MUTZ-LCs results in less viable cells

Regardless of the supplements, a decrease in cell number were observed in every differentiation media. To the author's knowledge, this aspect had not yet been discussed critically in any paper. However, it is important to quantify the basis of cellular viability before performing further experiments, as the viability of the cells can influence the phenotype and thus the way the cells react. Bohets et al. (1994) showed that FCS affects the cytotoxicity of chemicals, meaning a higher FCS content resulted in a lower cell toxicity. The authors documented that a lower concentration of FCS had a negative impact on cell viability, respectively. Consequently, the base line of cellular viability can impact the results of cell experiments. Cell viability is an important factor for this present study too, as the MUTZ-LCs are foreseen to function as LC surrogates to validate the sensitization potential of a chemical. For example, in the h-CLAT assay, at least 90 % of the THP-1 cells must be viable, otherwise the assay is not valid (OECD TG 442E, 2023).

The viability of the MUTZ-LC culture decreased from about 90 % at the beginning of the differentiation culture to approximately 50 % after seven days of culture. Only when

differentiating the cells with Ultroser G a slightly higher cell viability (about 60 %) was detected compared to the FCS-supplemented differentiation media. This indicates a better baseline of cellular viability in the media enriched with the FCS alternative, which is favorable. However, the numbers of viable CD1a- and CD207-positive cells were lower in the Ultroser G than in the FCS-supplemented differentiation medium. For this project, achieving successful MUTZ-LC differentiation is prioritized over high cell yield, as it is more crucial to obtain MUTZ-LCs in the required differentiated state than a larger quantity with compromised differentiation.

The overall documented decrease in cell number could have several reasons. For one, it might be the result of a proliferation arrest, which was demonstrated by Masterson al. (2002). However, it is rather unlikely that this is the only reason. Otherwise, the number of MUTZ-LCs should be comparable to the initial cell number before starting of differentiation. Santegoets et al. (2006) observed that the MUTZ-3 population consists of three sub-populations and showed that only CD14-positive cells could be differentiated into CD207-positive MUTZ-LCs. In contrast to the present study, Santegoets et al. (2006) initiated the differentiation culture with the individual subpopulations after cell sorting. Thus, the presence of cells from the other subpopulations might have an effect on the CD14-positive MUTZ-3 cells in the present study. Approximately 20 % of the MUTZ-LCs were positive for CD14. It could be possible that the CD14-positive cells are first proliferating, more than doubling their numbers, before changing into a proliferation arrest. The other MUTZ-3 sub-populations might have died resulting in the high numbers of debris in the differentiation medium. However, more analyses must be conducted to elucidate the mechanisms behind the apparent decline in cell number.

Furthermore, the numbers of viable cells are important for planning experimental setups. To generate the desired numbers of viable MUTZ-LCs for further experiments, one has to start with approximately twice the number of MUTZ-3 cells. Nevertheless, the decisive factor is that the MUTZ-LCs, which are present after differentiation, have the desired LC-phenotype and respond properly upon exposure to a sensitizer in a way which is comparable to native LCs. This was analyzed as well and will be discussed in the following chapter.

5.2 5 % FCS-differentiated MUTZ-LCs show LC-characteristic reactions upon exposure with a known sensitizer

After optimizing the differentiation protocol regarding the yield of LC-typical cells, standardization, speed and cost-effectiveness, the immunocompetence of the MUTZ-LCs had to be verified. It is important that the MUTZ-LCs are in a differentiated, but immature state and can still mature upon exposure with a sensitizer. This is a prerequisite for their intended role in an immunocompetent skin model to assess the sensitizing potential of chemicals. To test their immunocompetence, MUTZ-LCs were treated with two sensitizers, which are part of the OECD proficiency chemicals: 2,4-dinitrochlorobenzene (DNCB) was chosen as an example for an extreme sensitizer and imidazolidinyl urea (I. Urea) as a weak sensitizer to evaluate whether the potency of the chemical has also an impact on the cell reaction. The reaction upon sensitizer treatment were studied in MUTZ-LCs, which were differentiated for seven days in TTG medium supplemented with 5 % FCS (optimized differentiation protocol) or with 4 % Ultroser G. 4 % Ultroser G-differentiated MUTZ-LCs were still tested for functionality, despite the lower yield of CD1a- and CD207-positive cells, as the use of the FCS substitute would further increase the reproducibility compared the FCS-supplemented medium. In addition to the previous tested marker, CD83 was analyzed as well, due to its role in the maturation process of LCs, which will be discussed in the following chapter.

Overall, DNCB exposure induced LC-characteristic reactions in the MUTZ-LCs but only when they were differentiated in medium supplemented with 5 % FCS. However, no change in the maturation markers CD54 and CD86 could be detected, which are characteristic for THP-1 cells and thus are employed as read-out parameters in the h-CLAT assay (OECD 442E, 2023), but an increase in CD83 expression, another marker for matured LCs (Zhou and Tedder, 1995). The treatment with I. Urea did not induce an increase of the CD83 expression. Nevertheless, I. Urea might have still induced a reaction of the MUTZ-LCs, which have to be studied by analyzing further parameters.

5.2.1 DNCB treatment increases CD83 expression in 5 % FCS-differentiated MUTZ-LCs

The DNCB treatment resulted in visible changes in the cell morphology of 5 % FCS-differentiated MUTZ-LCs. Compared to the untreated MUTZ-LCs and the vehicle control, nearly no adherent MUTZ-LCs exhibiting dendritic processes were observed after the cells were treated with DNCB. This cellular reaction upon sensitizer exposure is similar to the one of native LCs. After LC maturation following a chemical stimulus in native skin, the MUTZ-LCs retract their dendritic processes and detach from the keratinocytes in order to migrate into the dermis, which has been well characterized in mice models (Deckers et al., 2018). To the author's knowledge, the retraction of the dendrites has not yet been published in the culture of MUTZ-LCs. In contrast to the differentiation with 5 % FCS, there was nearly no formation of dendritic processes observed in the controls of 4 % Ultroser G-differentiated MUTZ-LCs. Thus, no characteristic detachment of the cells could be observed upon sensitizer treatment.

In addition, in both differentiation media were more dead cells observed after treating the cells with DNCB solutions in two different concentrations, except for the lower DNCB concentration in 5 % FCS-containing medium. The flow cytometric analysis confirmed the decrease in cell viability of DNCB-treated cells. This was exactly the desired effect on cell viability, as DNCB was used in a concentration resulting in about 25 % cell toxicity, except for the lower DNCB concentration in 5 % FCS-supplemented medium. The DNCB concentration causing a 25 % decrease in cell viability was determined with a dose finding assay, based on the h-CLAT assay (OECD TG 442E, 2023). By using a concentration that induces 25 % cell toxicity, a balance should be achieved between conducting a valid sensitization assessment and minimizing the potential interference from excessive cytotoxicity. This level of cell toxicity allows the analysis of the chemical´s sensitizing potential without overwhelming the cells with excessive cell toxicity. (OECD TG 442E, 2023)

Furthermore, after DNCB exposure, no relevant changes in the expression of the analyzed proteins were detected, except for CD83. CD83 is a known maturation marker, which plays an important role in an effective immune response (Zhou and Tedder, 1995; Aerts-Toegaert et al., 2007). Cao et al. (2005) have shown that CD83 is preformed and intracellular present in immature LCs, enabling a rapidly induction upon LC maturation.

The immunoglobulin protein CD83 has been documented to promote the expression of other maturation markers such as CD86 and MHC class II (Tze et al., 2011). Additionally, CD83 has been reported to modulate T cell responses and contributing to immunoregulation, as it promotes the development and function of regulatory T cells (Doebbeler et al., 2018). Thus, CD83-mediated LC interactions with regulatory T cells can help to regulate immune balance and suppress excessive immune responses. In the present study, an at least three-fold increase in CD83 expression was documented after DNCB treatment, but only on 5 % FCS-differentiated MUTZ-LCs. The expression of the other LC-typical maturation markers remained unchanged. The majority of 5 % FCS-differentiated MUTZ-LCs was already positive for CD54 and CD86. Neither a change in the numbers of positive cells, nor in the mean fluorescence intensity (MFI) was detected. Both markers are typical read-out parameters for activated THP-1 cells, used to characterize the sensitizing potential of chemicals in several OECD-accepted methods, e.g., in the h-CLAT assay (OECD TG 442E, 2023). One could argument, that a different cell line is used in the h-CLAT assay, as MUTZ-3 cells and THP-1 cells have different phenotypes. For example, in contrast to the high expression on the MUTZ-3 cells, nearly no THP-1 cell is positive for CD54 or CD86 without sensitizer exposure (Azam et al., 2006). Thus, an increase in the numbers of CD54- and CD86-positive THP-1 cells is possible, but not for MUTZ-LCs. Ruben et al. (2015) also showed nearly identical CD86 histograms of untreated and matured MUTZ-LCs, which were treated with a cytokine cocktail. In contrast, Santegoets et al. (2008) documented a slight increase in the MFI emitted from CD54- and especially from CD86-positive MUTZ-LCs after stimulating the cells with a cytokine cocktail. The CD54 and CD86 histograms of immature and matured MUTZ-LCs from Masterson et al. (2002) showed a slight increase in the MFI. Therefore, on the one hand, the apparently missing CD54 and CD86 induction might indicate that the MUTZ-LCs in this project already matured during the differentiation and were not in an immature state any longer. On the other hand, an increase in the expression of the costimulatory molecule CD83 was detected after DNCB stimulation. Therefore, the MUTZ-LCs, but only when differentiated in medium supplemented with 5 % FCS, reacted upon sensitizer treatment indicating an immune reaction, even if not consistent with every published expression profile. Moreover, this is the analyzed reaction in cell suspension. The MUTZ-LCs were foreseen to be integrated into the Phenion® Full-Thickness (FT) skin model, where the cell-cell contact to keratinocytes and potentially fibroblasts could influence the cellular reaction of the MUTZ-LCs after sensitizer

exposure. Apart from that, these results further confirmed that Ultroser G is not a suitable FCS substitute for the differentiation of MUTZ-LCs, at least for the aim of this project to generate an immunocompetent skin model.

5.2.2 Imidazolidinyl urea treatment has no impact on the analyzed protein expression profile of MUTZ-LCs

Besides DNCB, the MUTZ-LCs differentiated in medium supplemented with 5 % FCS or 4 % Ultroser G were also treated with I. Urea. Similar to the DNCB treatment, there were more dead cells in both differentiation media after exposure with I. Urea, as the chemical was also used in a concentration corresponding to cell toxicity of around 25 %, as described in the h-CLAT assay (OECD TG 442E, 2023). However, there was no difference detected regarding the morphology of the cells. In contrast to the DNCB treatment, there were still adherent 5 %FCS-differentiated MUTZ-LCs with dendritic processes after I. Urea treatment. Thus, the lack of retracting dendritic processes suggests that I. Urea treatment did not result in MUTZ-LC maturation. Furthermore, this was confirmed by the measured expression levels of the maturation markers, e.g., CD54, CD83 and CD86, which did not markedly change after I. Urea treatment.

Taken together, the MUTZ-LC treatment with I. Urea did not result in any detectable morphological changes, nor did it modify the analyzed marker expressions, regardless of the used differentiation medium. Based on local lymph node assay data, I. Urea has only a weak sensitizing potency compared to the extreme one of DNCB (OECD TG 429 or 442A, 2010). Hence, I. Urea might not be strong enough to activate the MUTZ-LCs in a measurable or observable way as the DNCB treatment.

5.3 Successful integration of MUTZ-LCs into the Phenion® Full-Thickness skin model

The protocol applied to differentiate MUTZ-3 cells into MUTZ-LCs was successfully optimized. The standardization and reproducibility were enhanced by reducing the

amount of animal-derived products. Moreover, the yield of successfully differentiated CD1a- and CD207-positive MUTZ-LCs could be enhanced compared to the literature (Masterson et al., 2002; Larsson et al., 2006; Nelissen et al., 2009). In addition, the cellular reactions were analyzed after exposure with a sensitizer. Next, the differentiated, immature MUTZ-LCs had to be integrated into the Phenion® FT skin model. The Phenion® FT skin model consists of primary human keratinocytes and fibroblasts isolated from skin biopsies. Furthermore, the model comprises a fully differentiated epidermis with all layers seen in native human skin, including a functional skin barrier, and a dermal compartment characterized by a plethora of extracellular matrix proteins deposited by the fibroblasts embedded in the dermis (Mewes et al. 2007; Ackermann et al. 2010). Its xenobiotic metabolic competence has been demonstrated in a study published by Wiegand et al. (2014).

Different seeding protocols of MUTZ-LCs and keratinocytes on the dermis model had been tested. One complication was that the MUTZ-LCs are suspension cells and the keratinocytes adhesion cells. When seeding both cell types at the same time, the keratinocytes seemed to sediment faster than the MUTZ-LCs. Thus, the keratinocytes were nearly completely adherent before most of the MUTZ-LCs sedimented and reached the dermis. Consequently, the majority of the MUTZ-LCs were not integrated between the keratinocytes. After observing this, the seeding protocol was modified by seeding half of the keratinocytes with the MUTZ-LCs followed by an additional seeding of keratinocytes to confine the MUTZ-LCs to the lower-most cell layers and hence to prevent them from floating. To ensure a successful integration with the optimized seeding protocol, the skin models were analyzed with various staining methods to locate the MUTZ-LCs (chapter 5.3.1 and 5.3.2).

5.3.1 CFSE labeling of MUTZ-LCs is lost in frozen sections of Phenion® Full-Thickness skin models

In order to demonstrate the integration of the MUTZ-LCs into the skin models, the cells were stained with CFSE beforehand, based on a protocol published by Kosten et al. (2015). The cell permeable tracker CFSE is intracellularly cleaved by esterases, resulting in the formation of the fluorescent compound, and covalently binds to all intracellular molecules with amine residues (product data sheet, eBioscience Inc.). Due to the typical

proliferation arrest of the MUTZ-LCs (Masterson et al., 2002) it was expected that the CFSE staining would still detectable after about two weeks of ALI culture. This was confirmed by the enzymatically separated epidermis, which showed green fluorescence signals, emitted by the CFSE-stained MUTZ-LCs. The CFSE-stained MUTZ-LCs were more cumulated and not as sporadic and scattered as in Kosten et al. (2015). These aggregates might be the effect of the already observed cluster-formations of the MUTZ-LCs in the suspension culture. Hence, the integration of the MUTZ-LCs had been confirmed.

Still, with the plan view of a separated epidermis it was not possible to specify in which epidermal layer the MUTZ-LCs were located. To achieve that, frozen sections of the skin models were made. However, no fluorescence signals were observed. Thus, it seemed that the CFSE staining was lost after freezing the skin models at -80 °C and cutting the frozen sections. However, this was not observed by Lönnqvist et al. (2019), who could verify the location of CFSE-stained keratinocytes in frozen skin sections. Further research must be performed to analyze, why the CFSE staining was apparently lost in this study. Consequently, at least for this study, CFSE was not a suitable staining method for locating the MUTZ-LCs in frozen sections. Hence, the CFSE staining was not performed any longer for the following experiments.

5.3.2 MUTZ-LCs are integrated in all epidermal layers of Phenion® Full-Thickness skin models

Instead of the CFSE staining of the MUTZ-LCs, an immunofluorescence staining for CD1a was performed on the frozen sections of the skin models. As CD1a was expressed by nearly every MUTZ-LC at the end of their differentiation culture and is known to be selectively expressed by epidermal and dermal LCs (Furue et al., 1992), it is the ideal marker to locate the MUTZ-LCs. The MUTZ-LCs were found in all epidermal layers, but especially in the stratum spinosum, similar to the native human skin (Breathnach, 1964). Regardless of the MUTZ-LC differentiation protocol (original vs. optimized) applied before seeding into the skin models, the cells formed long dendritic processes in the skin model like the native LCs in the human skin (Chu and Jaffe, 1994). Therefore, MUTZ-LCs differentiated with the optimized protocols (5 % FCS, seven days of differentiation) were suited for the integration into the skin model and were used for all following

experiments. Only a few positive signals were found in the dermis, but they were so small that they were likely to be cell fractures. In addition, the collagen matrix of Phenion® FT skin models elicit bright autofluorescent signals at the same excitation wavelength chosen for the detection of the anti-CD1a antibodies. This unspecific staining of the matrix is a known problem of cross-linked collagen (Sherlock et al., 2018). Still, the false-positive signals could be distinguished from the CD1a-stained MUTZ-LCs, as the matrix signals were in the lower section of the dermis and more linear as well as longer than the ones emitted by the MUTZ-LCs. Accordingly, a distinction of the positive and false-positive signals was possible.

Compared to the immunofluorescence staining of the skin models published by Kosten et al. (2015), more signals were found in the epidermis of the Phenion® FT skin model with integrated MUTZ-LCs. Moreover, there were less signals in the dermis than showed by Kosten et al. (2015), where several MUTZ-LCs seemed to have migrated into the dermis. CD1a staining as reported by Bock et al. (2018) showed similar results. There were fewer positive signals in the epidermis compared to the skin model with integrated MUTZ-LCs of the present study. Kosten et al. (2015) and Bock et al. (2018) applied the same numbers of seeded MUTZ-LCs as used in the present project. Therefore, the integration of the MUTZ-LCs seemed to be more efficient in the Phenion® FT skin model. Moreover, the MUTZ-LCs seemed to have more and longer dendritic processes compared to the literature (Kosten et al., 2015; Bock et al., 2018).

Beside the standard version, Phenion® has also a LONG-LIFE model, among several others. The LONG-LIFE version can be longer cultured enabling with 50 days a four-times longer experimental test phase than the standard skin model, which is interesting for special applications, e.g., for repeated applications of chemicals. Thus, it was also tested whether the MUTZ-LCs can be integrated into the Phenion® FT LONG-LIFE skin model. This was successfully done with the same modified seeding protocol. However, for the establishment of an immunocompetent skin model, the experiments were performed with the Phenion® FT standard skin model, as it is faster produced and more cost-effective than the LONG-LIFE version.

Overall, the CD1a immunofluorescence staining showed a successfully integration of the MUTZ-LCs into the Phenion® FT standard and LONG-LIFE skin models.

5.3.3 Integration of MUTZ-LCs has no impact on Phenion® Full-Thickness skin model differentiation

In order to demonstrate that the MUTZ-LCs are indeed stably integrated into the epidermis of the Phenion® FT skin model, different histological analyses had been conducted. A first analysis revealed that no structural differences were observed between standard and LONG-LIFE Phenion® FT skin models without and with integrated MUTZ-LCs. The integration of the MUTZ-LCs seemed to have no impact on the correct differentiation of the epidermal layers. Moreover, adding this new cell line to the keratinocytes resulted in an overall slightly thicker epidermis compared to the skin models without integrated MUTZ-LCs. However, the epidermal thicknesses varied over a wide range of values between different tissue batches and even between tissues within one production batch, regardless of the MUTZ-LC integration. This observation is supported by the documentations of the Phenion® FT skin model production lots over more than a decade (statement from Lars Vierkotten, manager of the Phenion® FT skin model production, 2022). Nevertheless, it is not unrealistic that an additional seeding of one million cells per skin model might result in a somewhat thicker epidermis. This could be considered as a further indicator of a successful MUTZ-LC integration.

Compared to the structure of the frozen sections of the reconstructed human skin model with integrated MUTZ-LCs published by Bock et al. (2018), the Phenion® FT skin model seems to be better differentiated, e.g., the starum basale and stratum spinosum can be clearly identified based on the specific cellular characteristics and thus appear more *in vivo* like. The epidermis of the FT skin equivalent with integrated MUTZ-LC from Kosten et al. (2015) looks quite similar compared to the structure of the Phenion® FT skin model, but the dermis of the Phenion® FT skin model seems to be better differentiated with an extracellular matrix formed/secreted by the dermal fibroblasts.

Overall, the tissue architecture of the skin models, standard and LONG-LIFE versions, was not affected by the integration of the MUTZ-LCs. Only the epidermal thickness was slightly bigger when the additional cell type was seeded. Furthermore, it was not possible to identify the MUTZ-LCs in the hematoxylin-eosin (HE) staining of frozen tissue sections.

5.4 Analysis of the immunocompetence of the Phenion® Full-Thickness skin model with integrated MUTZ-LCs

After having successfully integrated the MUTZ-LCs into the Phenion® FT skin model, the immunocompetence of the skin models was analyzed. For that, the skin models were treated with DNCB, an extreme sensitizer, and $NiSO_4$, a strong sensitizer. Both chemicals are part of the OECD proficiency chemicals list (OECD TG 442E, 2023). First, suitable concentrations of the sensitizers had to be determined with a dose finding assay. In a next step, the structure of the skin model and the localization of the MUTZ-LCs were analyzed after exposure to the sensitizers. Moreover, to find suitable read-out parameters, the gene expression pattern of the immunocompetent skin models under different experimental conditions was analyzed with the Next Generation Sequencing (NGS) method.

5.4.1 Discrepancy of the determined sensitizer cytotoxicity between MTT assay, tissue architecture and literature

A dose finding assay was performed to determine the optimal concentration of the sensitizers, which is the highest concentration that could be topically applied without significant tissue damage. For the dose finding assay, the concentration range was set based on literature. Kosten et al. (2015) used, e.g., 10 mM $NiSO_4$ and Bock et al. (2018) 0.07 % DNCB in their experiments.

When treating the Phenion® FT skin models with DNCB solutions of the indicated concentrations, the tissue viability was apparently similar to that of the untreated skin models, as determined with the MTT viability assay. However, the histological analysis of the tissues showed a clear disturbance in the structure of the treated skin models (e.g., thinner epidermis and unorganized stratum basale), indicating tissue damage and consequently decreased viability. The discrepancy between the MTT results and the structure of the skin models could result from the fact, that the reduction of the tetrazolium salts is not only performed by mitochondrial reductases, but also by cellular reductases (Berridge and Tan, 1993). Thus, for example, high cellular NADH concentrations can affect the results of the MTT assay resulting in false-positive results, as NADH is an electron donor for the MTT assay (Berridge and Tan, 1993; Liu et al., 1997; Berridge et al., 2005). However, if this mechanism is also responsible for the observed high MTT

reduction rate in otherwise damaged Phenion® FT skin models remains open. In previous studies it was confirmed that only the keratinocytes located in the stratum basale and the lower stratum spinosum are still physiologically competent for MTT reduction reactions (Melyanti, diploma thesis, 2008).

Consequently, the concentrations of the sensitizers were determined with the observed skin model structure of the HE-stained frozen sections. It should be emphasized, that the determined concentrations of $NiSO_4$ and DNCB of the present study are only a fraction of the used concentrations by Kosten et al. (2015) and Bock et al. (2018). This is unusual, as the Phenion® FT skin model has a well-established skin barrier, which should rather increase the suitable concentration of the sensitizer. In this study DNCB was used in a seventh concentration of the used DNCB concentration by Bock et al (2018) and the concentration of $NiSO_4$ was even 20- and 100-times lower than applied by Kosten et al. (2015). Neither Kosten et al. (2015) nor Bock et al. (2018) showed microscopic images of treated skin models. Bock et al. (2018) only referred to the results of Kosten et al. (2015) showing that DNCB concentrations up to 0.1 % result in minimal cell toxicity of treated epidermis models. Ouwehand et al. (2011) observed no detrimental structural changes of skin equivalents treated with up to 19 mM $NiSO_4$. In comparison, when treating the Phenion® FT skin models with 10 mM $NiSO_4$, the epidermis of the skin models was lost during the washing steps of the MTT assay. The published skin equivalents and the Phenion® FT skin model differ in structure. The Phenion® FT skin model for example is based on a matrix, while most of the published models are generated with collagen gels (Ouwehand et al., 2011; Kosten et al., 2015; Bock et al., 2018). This difference could have an impact on the induced cytotoxicity of the sensitizers.

In general, further experiments and comparison of different skin equivalents used by other research groups had to be performed to identify the reasons for the different cytotoxicity of DNCB and $NiSO_4$ treatment. The inaccurate results of the MTT assay show the importance to analyze the tissue architecture of the skin models with HE-stained frozen sections.

5.4.2 Hydrocortisone impacts the MUTZ-LC migration in Phenion® Full-Thickness skin models upon sensitizer exposure

The LCs in the native skin start to migrate into the dermis after an exposure with a sensitizer. Thus, to observe a possible migration of the MUTZ-LCs in the Phenion® FT skin models of the present study, the location of the CD1a-immunofluorescence stained MUTZ-LCs of untreated and treated skin models were compared. The first experiments of treating the Phenion® FT skin models with the determined sensitizer concentrations did not result in a migration of MUTZ-LCs. However, when treating the MUTZ-LCs in suspension culture with DNCB, they showed a LC-typical response by retracting their dendritic processes, which is a crucial step before they are able to migrate into the dermis (Deckers et al., 2018). On the one hand, the cells might react differently once they are integrated into the skin model and have contact to other cell types. On the other hand, it was possible that a medium supplement might interfere with the immune reaction of the cells. One medium supplement, which had been added to the ALI culture medium since the beginning of Phenion®, is hydrocortisone (HC). While HC has a known positive effect on the proliferation of keratinocytes (Rheinwald and Green, 1975), it turned out that HC seemed to suppress the immune reaction of the MUTZ-LCs. The sensitizer treatment of the Phenion® FT skin models cultured without HC resulted in CD1a-positive signals in the dermis. The CD1a-stained MUTZ-LCs in the dermis of DNCB- or $NiSO_4$-treated MUTZ-LCs were more spherical and seemed to have no dendritic processes compared to the epidermal MUTZ-LCs. The different morphology is typical for migrated LCs, which have to change their size and form to be able to find a way between the keratinocytes and fibroblasts (Deckers et al., 2018).

In addition, a TUNEL assay was performed to analyze whether the cells were viable, as it labels DNA strand breaks, which are typically generated during apoptosis (product data sheet, Roche). With this assay it could be verified that the MUTZ-LCs, especially the dermal ones, were viable and not only fragments. There were only a few positive signals found, regardless of the treatment and culture condition of the Phenion® FT skin moels. Hence, the CD1a-positive MUTZ-LCs seemed to be viable, as well as the overall viability of the skin models.

All these results suggest a successful migration of the MUTZ-LCs after sensitizer exposure, but only when the skin models were cultured without HC. Kosten et al. (2015)

and Bock et al. (2018) both use the same HC concentration in their skin model culture medium as usually used in the Phenion® ALI culture medium. However, they still monitored a migration of the MUTZ-LCs in the skin models. Hence, there might be other factors influencing the migration of the MUTZ-LCs. One possible factor might be the architecture of the skin models. The Phenion® FT skin model is based on a bioartificial collagen matrix in which the fibroblasts are cultivated. In contrast, the skin model from Kosten et al. (2015) and Bock et al. (2018) are based on a collagen hydrogel. Further experiments have to be performed to test whether the structure of the Phenion® collagen matrix impedes the migration of the MUTZ-LCs compared to the hydrogel counterpart.

5.4.3 Impact of hydrocortisone and sensitizer treatment on the Phenion® Full-Thickness skin model architecture

The skin models without or with integrated MUTZ-LCs, cultured with or without HC, showed well developed and differentiated skin layers. Consequently, HC seemed to have no impact on the correct differentiation of the Phenion® FT skin models. In addition, the effect on the epidermal thickness was analyzed. The medians of the epidermal thickness ranged from about 95 µm to 140 µm and thus showed a wide distribution, which is typical for the Phenion® FT skin models (statement Lars Vierkotten, Manager of the Skin Model Production at Henkel AG & Co. KGaA, 2022).

Comparing the epidermal thicknesses of the skin models cultured in three culture conditions (with HC, 5 days without HC and without HC during ALI culture), regardless of the treatment, only slight differences could be detected: The medians of the HC-cultured ones were slightly higher than the ones cultured without HC. However, the epidermal thicknesses of the HC-free cultured skin models had the smallest data distribution. Therefore, the epidermal thicknesses of the HC-free cultured skin models were more homologous than the ones cultured with HC. This is an important factor for the reproducibility of the experiments. Still, it has to be verified whether the culture without HC during the ALI phase of the Phenion® FT skin models indeed results in a slightly thinner, but more homologous epidermis compared to the ones cultured with HC. It is also possible that these differences might result because of the biological variation of the skin model batches.

The DNCB-treatment of the skin models had no impact on the epidermal thickness. Besides the architecture of the skin models, this indicates that the sensitizer treatment did not affect the structure of the skin models. Hence, the DNCB concentration did not seem to be too high. This was also observed after treating the skin models with 0.1 mM $NiSO_4$. The higher $NiSO_4$ concentration, 0.5 mM, resulted in a slight decreased epidermal thickness compared to the control. This might indicate that the treatment with 0.5 mM $NiSO_4$ could have a negative impact on the epidermal structure and thus be too high for treating the skin models. It is crucial that the skin models are still viable after the sensitizer treatment, as the skin equivalent is foreseen to serve as a model to analyze the immune reaction upon a sensitizer exposure and not the cellular reactions upon a damaged skin. Further experiments have to be performed to decide if 0.5 mM $NiSO_4$ should be removed from the sensitizer panel.

5.4.4 Sensitizer treatment of Phenion® Full-Thickness skin models regulates typical immune system process and migration genes

To identify other read-out parameters besides the migration of the MUTZ-LCs, an RNA sequencing with NGS was performed by Life & Brain GmbH. This was the first time that such a sequencing was performed with a Phenion® FT skin model. Hence, an initial selection of samples was chosen, where the immunofluorescence staining of the frozen sections showed an apparent migration of the MUTZ-LCs after $NiSO_4$ treatment (Figure 27) when the skin models were cultured without HC. In addition, the vehicle control, PBS-treated skin models, were analyzed. Hereby, two culture conditions, with and without HC, were compared to study the effect of HC on gene regulation.

The first two principal components described the majority of the variance. The principal component analysis (PCA) showed a clear separation of the regulated genes of the epidermis and dermis. Moreover, the culture condition with or without HC during ALI phase were also distinguishable, even if the differences were not as pronounced as the epidermis vs. dermis samples. Thus, the PCA showed four separated groups with a small variance within a group. This indicates that the samples within those groups share a similar gene expression profile, while being different from the samples of the other groups (e.g., culture with and without HC). Hence, certain gene expressions are associated with

the epidermis and dermis as well as the culture condition with and without HC, potentially reflecting biologically relevant differences. However, the treatments of the skin models could not be allocated to a distinguishable group, indicating that there were no discernible differences in the overall gene expression profile associated with the treatments.

The detected log2 fold changes of the regulated genes ranged from nearly -10 to about +10. This means that the genes were decreased or increased by approximately 1,000-times. These gene regulations are very high, e.g., compared to the maximum detected 6 log2 fold changes of the GARD assay (Forreryd et al., 2014). Thus, $NiSO_4$ treatment seemed to induce strong responses in the cells of the Phenion® FT skin models, which is good for future interpretations. For example, it could be possible that a weaker sensitizer results in lower fold changes of the relevant genes. This would enable a categorization of the sensitizer potency based on the log2 fold change, similar to the prediction of the sensitizer potency in the GARD assay (OECD TG 442E, 2023).

Moreover, it was tested what kind of pathways were addressed by the regulated genes in the Phenion® FT skin models. The pathways, which were relevant for this project, were assigned to four topics: metabolism, differentiation/development, immune system, and migration. Several processes were related to the metabolism, which might reflect the cellular reaction upon contact with $NiSO_4$. “Metal binding” could be directly linked to nickel. However, this had to be validated with other experiments, e.g., the detection of nickel in the skin model. Besides that, pathways were regulated, which can be assigned to the differentiation and development of the skin model. Especially interesting for this project were the regulated pathways of the immune system and more specific of the migration. Some of the regulated pathways can be assigned to the cellular reactions of LCs after sensitizer treatment, e.g., “cellular responses to growth factor stimulus”, which is a central step of immune system reactions. The treated Phenion® FT skin models of the present study, which were cultured without HC, had even more LC-typical regulated pathways, e.g., “cellular response to TGF-ß stimulus” (Thomas et al., 2001). Further, pathways of HC-free and treated skin models even addressed the “regulation of chemotaxis”, which is crucial for the migration of LCs (Koch et al., 2006). One example for chemotaxis is the C-X-C motif chemokine ligand 12 (CXCL12), which is expressed by fibroblasts (Quan et al., 2015). The corresponding receptor is C-X-C motif chemokine receptor 4 (CXCR4), which is expressed on LCs, is induced upon sensitizer exposure

(Kabashima et al., 2007). Due to this gradient the LCs migrate from the epidermis into the dermis (Kabashima et al., 2007). These findings further confirm the observed migration of the MUTZ-LCs, but only when the skin models were cultured without HC. Pathways, which are assigned to the topic migration, were regulated in all treated skin models. When the LCs mature upon sensitizer exposure, a lot of cellular responses take place. For one, the LC-typical dendritic processes have to get retracted to enable the migration through the keratinocyte layers into the dermis (Deckers et al., 2018). In the present study, the pathway "regulation of cellular projection organization and cell adhesion" was also addressed by the $NiSO_4$-treated skin models. All the regulated pathways suggest that the skin models with integrated MUTZ-LCs were immunocompetent and reacted to the sensitizer treatment.

A comparison of the regulated genes with genes that are known to play a role in the immune system and in migration processes, provided by the gene data bank Gene Ontology (Ashburner et al., 2000; Gene Ontology Consortium, 2021), showed several matches. This indicated that the skin models initiated an immune response after being treated with a sensitizer. When comparing the regulated genes in the $NiSO_4$-treated Phenion® FT skin models with the migration genes from Gene Ontology, five genes matched in every epidermis of the treated skin models (± HC): *PTN*, *HAS2*, *SDCBP*, *DDR2* and *TMSB4X*. *PTN* is the gene for the heparin-binding growth factor pleiotrophin (PTN). This growth factor induces, e.g., the migration of glioblastoma migration (Lu et al., 2005). Moreover, PTN induces the expression of inflammatory cytokines like TNF-α and IL-1β (Achour et al., 2008). These cytokines are involved in the migration of LCs (Cumberbatch et al., 2003). To the author's knowledge it had not yet been studied if PTN has also an impact on the migration of LCs from the epidermis into the dermis. To validate that, further experiments have to be performed, e.g., an enzyme-linked immunosorbent assay (ELISA). Hyaluronan synthase *2* (*HAS2*) is also regulated in the $NiSO_4$-treated epidermis of the Phenion® FT skin models. HAS2 synthesize hyaluronic acid (HA), which is a component of the extracellular matrix and mostly produced by dermal fibroblasts (Tzellos et al., 2011). This might indicate that the enzymatically separation of the epidermis and dermis was not perfectly done. Additional research has to be performed to analyze how many fibroblasts are still attached to the epidermis after the separation. However, Mummert et al. (2002) also showed that dendritic cells express mRNAs for HAS and that HA polymers on the surface of dendritic cells may be important for the

migration to the afferent lymphatics. So, it has to be further validated, if the dendritic cells or the possible contamination with fibroblasts are responsible for the *HAS2* regulation. Syndecan binding protein (SDCBP) is a syntenin protein and also regulated in all treated epidermal samples from Phenion® FT skin models. Koo et al. (2002) reported that syntenin promotes the migration of human breast and gastric cancer cell lines. Another regulated gene, which is known to be involved in tumor cell migration, is discoidin domain receptor tyrosine kinase 2 (*DDR2*) (Xie et al., 2015). However, DDR2 is also reported to be mainly expressed by fibroblasts and not keratinocytes (Cario, 2018), which might further indicate a contamination of the epidermis samples with dermal keratinocytes. Thymosin beta 4 X-linked (*TMSB4X*) encodes an actin sequestering protein, which has been shown to be involved in cell migration (Sribenja et al., 2013). As *SDCBP*, *DDR2* as well as *TMSB4X* were regulated in the epidermis of the skin model, they might also play a role in the migration of the LCs. This has to be verified with follow-up experiments.

When comparing the regulated genes in the dermis of $NiSO_4$-treated Phenion® FT skin models (± HC) with known migration genes from Gene Ontology, the gene *OGT* is regulated in every sample. *OGT* encodes the O-linked N-acetylglucosamine (GlcNAc) transferase, which, e.g., promotes the migration of the cancer cell line NSCLC (Non-small-cell-lung-lancer) (Ge et al., 2021). Like the previous addressed migration genes it still needs to be analyzed whether the GlcNAc transferase also has an effect on the migration of LCs in the human skin.

The comparison of the regulated genes in the epidermis with the immune system genes from Gene Ontology, the genes *LGALS7* and *PTN* were regulated in every treated skin model (± HC). *LGALS7* encodes the protein galectin 7, which is produced by epidermal keratinocytes and has an immunomodulatory effect on LCs (Umayahara et al., 2017). Besides promoting cell migration (Lu et al., 2005), PTN has also been reported to play a role in the immune system, e.g., by inducing the expression of inflammatory cytokines (Achour et al., 2008).

In the dermis samples of the treated skin models (± HC), two genes, *ITGB6* and *LAMP3*, were regulated, which matched with the immune system genes from Gene Ontology. *ITGB6* encodes the protein integrin subunit beta 6. It forms with the subunit αv the

integrin αvβ6, which activates TGF-β (Koivisto et al., 2018). TGF-β regulates the immune responses, while affecting the proliferation, differentiation, survival, and migration of immune cells (Li et al., 2006). The lysosomal associated membrane protein 3 (*LAMP3*) is induced upon maturation of dendritic cells (de Saint-Vis et al., 1998).

Overall, these regulated genes of $NiSO_4$-treated skin models compared to the controls clearly show that an immune response occurred in the skin equivalent. Several typical genes were regulated, which indicate the migration of LCs after sensitizer exposure. Characteristic immune system and migration genes were also regulated in skin models cultured with HC. This finding is contradicting the results of the CD1a-immunofluorescence staining of the frozen skin model sections (refer to Figure 27), which only showed a clear migration of MUTZ-LCs in HC-free cultured Phenion® FT skin models after $NiSO_4$ treatment. Hence, it could be the case that the MUTZ-LCs need more time to start migrating, when the skin models were cultured with HC compared to the culture without HC. Another possibility is that HC has a positive effect on the robustness of the skin model architecture. As a result, the MUTZ-LCs might not be able to actively migrate into the dermis, but still exhibit typical immune responses. These hypotheses have to be tested with further experiments.

All in all, the first run of NGS analysis was successful, enabling a new method to analyze experiments with Phenion® FT skin models. The sequencing has to be repeated with a higher number of samples and skin model batches. In addition, further research has to be performed to validate the regulated genes on protein basis, which are characteristic for the immune system and migrated cells.

6. Outlook

The research on generating skin models with integrated MUTZ-LCs to characterize the sensitization potential of chemicals has shown promising results, e.g., a successful integration of MUTZ-LCs into the Phenion® FT skin model. These immunocompetent skin models could provide valuable insights in the cosmetical and clinical research (e.g., dermatological, pharmaceutical), as they reflect the native skin architecture as well as metabolism. Moreover, such a skin model would be the first method that addresses the key event 1, 2 and 3 from the AOP which is a prerequisite to function as a stand-alone method for the toxicological risk assessment (OECD TG 497, 2023). Apart from serving as a prediction model to assess the prediction of the potential or potency of a chemical, the applicability domain of the Phenion® FT skin models could be extended to test even formulations (e.g., creams or ointments) due to its dry surface that closely resembles the native barrier of the human skin. These reproducible skin models would serve as an ethical alternative for animal tests, thus aligning with the 3Rs (Russel and Burch, 1959) and growing demand for animal-free methods. Still, besides offering several advantages and a higher complexity than 2D cell cultures, such immunocompetent skin models with integrated MUTZ-LCs also have their limitations. One disadvantage is their limited availability, as they can only be bought from specialized manufacturers. This also applies to the epidermis models that are used for the TG 431/439 test guidelines (OECD, 2019/2021). Another aspect are the high costs of the 3D skin models which is significantly higher than the costs of simpler 2D cell cultures due to complexity of the skin models and high manual workload. Despite these economic disadvantages, the higher costs could be justified if the predictivity of the skin model exceeds that of conventional methods. One could also argue that the skin models do not express every structure that can be found in the native skin, e.g., blood vessels or lymph nodes. However, the described immunocompetent skin model is characterized by a high complexity and *in vivo* relevance, which sets it apart from other available methods. Thus, further development of this skin model into a predictive method would already present a significant advance in ACD testing. A potential approach to increase the complexity by linking the skin model to other organs could be the organ-on-a-chip technology. First promising results were published by Tao et al. (2023) and Brandmair et al. (2024), showing that the Phenion® FT skin model seems to be stable in a microfluid system (skin-liver-thyroid Chip 3 and

skin-liver Chip 2 model) and had comparable chemical penetration to the native skin. It has to be noted that it might also be possible to directly integrate additional components into the skin model, but the effort and complexity would likely exceed the scientific and economic benefit.

Overall, immunocompetent skin models with integrated MUTZ-LCs represent an important step forward in dermatological, cosmetical and immunological research. This shift from traditional 2D cell suspension to 3D culture enables a more *in vivo* like environment.

After showing successful MUTZ-LC integration into the Phenion® FT skin models and gaining first insights into the immunocompetence of the skin models in the present study, several important points remain to be explored to further advance this field. One of them is a comprehensive verification of the immunocompetence of the skin models. Moreover, the robustness of the skin model production with integrated MUTZ-LCs needs to be analyzed through numerous inter- and intra-laboratory experiments. The immunocompetent skin models must match defined quality parameters and follow a standardized generation process/protocol. Furthermore, read-out parameters have to be identified in order to develop a new and OECD-accepted method to predict the sensitization potential of chemicals. Additionally, once the read-out parameters have been identified, a validation study with different chemicals needs to be performed to characterize the performance data. The next crucial step to further improve the method would be the incorporation of the sensitizer potency assessment. This would significantly enhance its utility in chemical safety assessment and regulatory decision making.

Moving forward, one of the first steps is to scale up the experiments with a broader range of sensitizers. While the initial sensitizer treatments show promising results, a more comprehensive panel of sensitizers would be needed to establish the models´ predictive capacity across chemicals. After testing and verifying the reliability of the skin model to identify the sensitization potential of the known proficiency chemicals (OECD TG 442E, 2023), new chemicals which are not yet categorized should be analyzed as the next step. The results should then be verified with OECD-approved methods.

For the analysis of the immunocompetence of the skin models several additional methods could be taken into consideration:

To deepen the understanding of the molecular responses to the sensitizers treatment, NGS should be incorporated in the validation process. Thus, potential read-out parameters could be identified and their gene expression level be analyzed to assess the sensitization potential. Moreover, it will also contribute to a more mechanistic understanding of the immune response to sensitizers. However, there are also more cost-effective methods to analyze gene expression level after identifying and aligning on a panel of read-out parameters, e.g., polymerase chain reaction (PCR). In addition, it would be easier to use the migration of MUTZ-LCs or the expression of specific proteins as read-out parameters instead of the time-consuming gene expression analysis of skin models.

Another approach could be the expansion of the validation process to include an ELISA in order to analyze the cytokine profile. This will further support the skin model's reliability and understanding. Cytokines play a central role in immune responses and their secretion could provide valuable insights if the chemical treatment results in sensitizing immune reactions.

Moreover, a successful differentiation of MUTZ-3 cells into MUTZ-LCs has been crucial in generating immunocompetent skin models. Further analyzing the cellular reaction of MUTZ-LCs upon sensitizer treatment in a controlled 2D environment, might provide a more comprehensive understanding of their responses to sensitizers. This approach may also lead to the discovery of more read-out parameters to characterize the sensitization potential of a chemical, which could be leveraged as well for the Phenion® FT skin models with integrated MUTZ-LCs.

Besides its importance in assessing new chemicals for risk assessment, the immunocompetent skin model with integrated MUTZ-LCs also could also demonstrate clinical relevance. For one, the model might further increase the understanding of immune reactions in the skin, as it is more *in vivo* like than other OECD-accepted test methods. Another advantage is the potential to enable personalized medicine for immune dysfunctions of the skin, e.g., allergic contact dermatitis. When using patients-specific cells, the immunocompetent skin model would ensure targeted therapies that address

specifically the patient's disease (e.g., biomarkers). This approach could lead to an improved clinical outcome for the patients. However, the integration protocol of patient-specific cells into the Phenion® FT skin model might differ to the established MUTZ-LC integration protocol in the present study. These personalized immunocompetent Phenion® FT skin models would also need to be validated first.

In conclusion, the continuous advancement of the immunocompetent skin model for sensitization testing offers significant improvement for the field of chemical safety assessment with animal-free methods. Moreover, the immunocompetent skin model shows also potential for other research fields, e.g., personalized medicine. By addressing the aspects mentioned above, the understanding and reliability of the so far established immunocompetent Phenion® FT skin model would be enhanced. This comprehensive approach will drive the development of alternative methods, or new approach methodologies (NAMs), while ensuring the safety of chemicals and products for human health.

7. References

Achour A, M'bika JP, Baudouin F, Caruelle D, Courty J. Pleiotrophin induces expression of inflammatory cytokines in peripheral blood mononuclear cells (2008). Biochimie. 90(11-12):1791-5. doi: 10.1016/j.biochi.2008.04.010.

Ackermann K, Borgia SL, Korting HC, Mewes KR, Schäfer-Korting M. (2010). The Phenion full-thickness skin model for percutaneous absorption testing. Skin Pharmacol Physiol. 23(2):105-12. doi: 10.1159/000265681.

Aerts-Toegaert C, Heirman C, Tuyaerts S, Corthals J, Aerts JL, Bonehill A, Thielemans K, Breckpot K (2007). CD83 expression on dendritic cells and T cells: correlation with effective immune responses. Eur J Immunol. 37(3):686-95. doi: 10.1002/eji.200636535.

Aiba S, Nakagawa S, Ozawa H, Miyake K, Yagita H, Tagami H (1993). Up-regulation of alpha 4 integrin on activated Langerhans cells: analysis of adhesion molecules on Langerhans cells relating to their migration from skin to draining lymph nodes. J Invest Dermatol. 100(2):143-7. doi: 10.1111/1523-1747.ep12462783.

Akhtar A (2015). The flaws and human harms of animal experimentation. Camb Q Healthc Ethics. 24(4):407-19. doi: 10.1017/S0963180115000079.

Alghadeer A, Patni AP, Li Z, Lim YC, Mathieu J, Ruohola-Baker H (2024). Protocol for generating three-dimensional induced early ameloblasts using serum-free media and growth factors. STAR Protoc.5(2):103100. doi: 10.1016/j.xpro.2024.103100.

Ashburner M, Ball CA, Blake JA, Botstein D, Butler H, Cherry JM, Davis AP, Dolinski K, Dwight SS, Eppig JT, Harris MA, Hill DP, Issel-Tarver L, Kasarskis A, Lewis S, Matese JC, Richardson JE, Ringwald M, Rubin GM, Sherlock G (2000). Gene ontology: tool for the unification of biology. The Gene Ontology Consortium. Nat Genet. (1):25-9. doi: 10.1038/75556.

Azam P, Peiffer JL, Chamousset D, Tissier MH, Bonnet PA, Vian L, Fabre I, Ourlin JC (2006). The cytokine-dependent MUTZ-3 cell line as an in vitro model for the screening of contact sensitizers. Toxicol Appl Pharmacol. 1;212(1):14-23. doi: 10.1016/j.taap.2005.06.018.

Baker M (2016). Reproducibility: Respect your cells! Nature. 537(7620):433-5. doi: 10.1038/537433a.

Berridge MV, Herst PM, Tan AS (2005). Tetrazolium dyes as tools in cell biology: new insights into their cellular reduction. Biotechnol Annu Rev. 11:127-52. doi: 10.1016/S1387-2656(05)11004-7.

Berridge MV, Tan AS (1993). Characterization of the cellular reduction of 3-(4,5-dimethylthiazol-2-yl)-2,5-diphenyltetrazolium bromide (MTT): subcellular localization, substrate dependence, and involvement of mitochondrial electron transport in MTT reduction. Arch Biochem Biophys. 303(2):474-82. doi: 10.1006/abbi.1993.1311.

Birbeck MS, Breathnach AS, Everall JD (1961). An Electron Microscope Study of Basal Melanocytes and High-Level Clear Cells (Langerhans cells) in Vitiligo. J Invest Dermatol. 37:51-64. doi: 10.1038/jid.1961.80.

Bock S, Said A, Müller G, Schäfer-Korting M, Zoschke C, Weindl G (2018). Characterization of reconstructed human skin containing Langerhans cells to monitor molecular events in skin sensitization. Toxicol In Vitro. 46:77-85. doi: 10.1016/j.tiv.2017.09.019.

Bohets HH, Nouwen EJ, De Broe ME, Dierickx PJ (1994). Effects of foetal calf serum on cell viability, cytotoxicity and detoxification in the two kidney-derived cell lines LLC-PK1 and MDCK. Toxicol In Vitro. 8(4):559-61. doi: 10.1016/0887-2333(94)90016-7.

Borkowski TA, Letterio JJ, Mackall CL, Saitoh A, Wang XJ, Roop DR, Gress RE, Udey MC (1997). A role for TGFbeta1 in langerhans cell biology. Further characterization of the epidermal Langerhans cell defect in TGFbeta1 null mice. J Clin Invest. 100(3):575-81. doi: 10.1172/JCI119567.

Böttcher P (2019). Integration of Immune Competent Cells into the Phenion® Full-Thickness Skin Model. Master Thesis, University of Göttingen.

Böttcher P, Steinmeyer L, Stark H, Breitkreutz J, Mewes KR (2024). Integration of MUTZ-Langerhans cells into a 3D full-thickness skin equivalent and influences of serum reduction and undefined medium supplements on differentiation. Toxicol In Vitro. 102:105948. doi: 10.1016/j.tiv.2024.105948

Bouroncle BA (1967). Preservation of human normal and leukemic cells with dimethyl sulfoxide at -80 degrees C. Cryobiology. 3(6):445-55. doi: 10.1016/s0011-2240(67)80154-8.

Brandmair K, Tao TP, Gerlach S, Przibilla J, Schepky A, Marx U, Hewitt NJ, Kühnl J, Maschmeyer I (2024). Suitability of different reconstructed human skin models in the skin and liver Chip2 microphysiological model to investigate the kinetics and first-pass skin metabolism of the hair dye, 4-amino-2-hydroxytoluene. J Appl Toxicol. 44(3):333-343. doi: 10.1002/jat.4542.

Breathnach AS (1964). Observations on cytoplasmic organelles in Langerhans cells of human epidemris. J Anat. 98(Pt 2):265-70. PMID: 14154427.

Cao W, Lee SH, Lu J (2005). CD83 is preformed inside monocytes, macrophages and dendritic cells, but it is only stably expressed on activated dendritic cells. Biochem J. 1;385(Pt 1):85-93. doi: 10.1042/BJ20040741.

Cario M (2018). DDR1 and DDR2 in skin. Cell Adh Migr. 12(4):386-393. doi: 10.1080/19336918.2018.1485618.

Chan JK (2014). The wonderful colors of the hematoxylin-eosin stain in diagnostic surgical pathology. Int J Surg Pathol. 22(1):12-32. doi: 10.1177/1066896913517939.

Chen X, Thibeault S (2013). Effect of DMSO concentration, cell density and needle gauge on the viability of cryopreserved cells in three dimensional hyaluronan hydrogel. Annu Int Conf IEEE Eng Med Biol Soc. 2013:6228-31. doi: 10.1109/EMBC.2013.6610976.

Chittiboyina AG, Avonto C, Rua D, Khan IA (2015). Alternative testing methods for skin sensitization: NMR spectroscopy for probing the reactivity and classification of potential skin sensitizers. Chem Res Toxicol. 28(9):1704-14. doi: 10.1021/acs.chemrestox.5b00098.

Chu T, Jaffe R (1994). The normal Langerhans cell and the LCH cell. Br J Cancer Suppl. 23:S4-10. PMID: 7521202.

Cichorek M, Wachulska M, Stasiewicz A, Tymińska A (2013). Skin melanocytes: biology and development. Postepy Dermatol Alergol. 30(1):30-41. doi: 10.5114/pdia.2013.33376.

Cumberbatch M, Bhushan M, Dearman RJ, Kimber I, Griffiths CE (2003). IL-1beta-induced Langerhans' cell migration and TNF-alpha production in human skin: regulation by lactoferrin. Clin Exp Immunol. 132(2):352-9. doi: 10.1046/j.1365-2249.2003.02146.x.

Cottrez F, Boitel E, Auriault C, Aeby P, Groux H (2015). Genes specifically modulated in sensitized skins allow the detection of sensitizers in a reconstructed human skin model. Development of the SENS-IS assay. Toxicol In Vitro. 29(4):787-802. doi: 10.1016/j.tiv.2015.02.012.

Cottrez F, Boitel E, Ourlin JC, Peiffer JL, Fabre I, Henaoui IS, Mari B, Vallauri A, Paquet A, Barbry P, Auriault C, Aeby P, Groux H (2016). SENS-IS, a 3D reconstituted epidermis based model for quantifying chemical sensitization potency: Reproducibility and predictivity results from an inter-laboratory study. Toxicol In Vitro. 32:248-60. doi: 10.1016/j.tiv.2016.01.007.

Cox K (2016). Integration von immunkompetenten Zellen in ein 3D-Vollhautmodell. Bachelor Thesis, Hochschule Furtwangen University, Furtwangen.

Cvetkovski RS, Rothman KJ, Olsen J, Mathiesen B, Iversen L, Johansen JD, Agner T (2005). Relation between diagnoses on severity, sick leave and loss of job among patients with occupational hand eczema. Br J Dermatol. 152(1):93-8. doi: 10.1111/j.1365-2133.2005.06415.x.

Deangelis T, Quong A, Morrione A, Baserga R (2013). Growth of v-src-transformed cells in serum-free medium through the induction of growth factors. J Cell Physiol. 228(7):1482-6. doi: 10.1002/jcp.24303.

De Libero G, Mori L (2005). Recognition of lipid antigens by T cells. Nat Rev Immunol. 5(6):485-96. doi: 10.1038/nri1631.

De Saint-Vis B, Vincent J, Vandenabeele S, Vanbervliet B, Pin JJ, Aït-Yahia S, Patel S, Mattei MG, Banchereau J, Zurawski S, Davoust J, Caux C, Lebecque S (1998). A novel lysosome-associated membrane glycoprotein, DC-LAMP, induced upon DC maturation, is transiently expressed in MHC class II compartment. Immunity. 9(3):325-36. doi: 10.1016/s1074-7613(00)80615-9.

Deckers J, Hammad H, Hoste E (2018). Langerhans Cells: Sensing the Environment in Health and Disease. Front Immunol. 9:93. doi: 10.3389/fimmu.2018.00093.

Diepgen TL, Ofenloch RF, Bruze M, Bertuccio P, Cazzaniga S, Coenraads PJ, Elsner P, Goncalo M, Svensson Å, Naldi L (2016). Prevalence of contact allergy in the general population in different European regions. Br J Dermatol. 174(2):319-29. doi: 10.1111/bjd.14167.

Doebbeler M, Koenig C, Krzyzak L, Seitz C, Wild A, Ulas T, Baßler K, Kopelyanskiy D, Butterhof A, Kuhnt C, Kreiser S, Stich L, Zinser E, Knippertz I, Wirtz S, Riegel C, Hoffmann P, Edinger M, Nitschke L, Winkler T, Schultze JL, Steinkasserer A, Lechmann M (2018). CD83 expression is essential for Treg cell differentiation and stability. JCI Insight. 3(11):e99712. doi: 10.1172/jci.insight.99712.

Dos Santos GG, Reinders J, Ouwehand K, Rustemeyer T, Scheper RJ, Gibbs S (2009). Progress on the development of human in vitro dendritic cell based assays for assessment of the sensitizing potential of a compound. Toxicol Appl Pharmacol. 236(3):372-82. doi: 10.1016/j.taap.2009.02.004.

Easthope E (2022). How to generate more reproducible flow cytometry data. https://www.biocompare.com/Editorial-Articles/586043-How-to-Generate-More-Reproducible-Flow-Cytometry-Data/.

European Parliament and Council of the European Union. Regulation (EC) No 1223/2009 of the European Parliament and of the Council of 30 November 2009 on cosmetic products. Off J Eur Union. 2009; L342:59-209. Available from https://eur-lex.europa.eu/eli/reg/2009/1223/oj.

Facy V, Flouret V, Régnier M, Schmidt R (2005). Reactivity of Langerhans cells in human reconstructed epidermis to known allergens and UV radiation. Toxicol In Vitro. 19(6):787-95. doi: 10.1016/j.tiv.2005.03.018.

Fithian E, Kung P, Goldstein G, Rubenfeld M, Fenoglio C, Edelson R (1981). Reactivity of Langerhans cells with hybridoma antibody. Proc Natl Acad Sci U S A. 78(4):2541-4. doi: 10.1073/pnas.78.4.2541.

Forreryd A, Johansson H, Albrekt AS, Lindstedt M (2014). Evaluation of high throughput gene expression platforms using a genomic biomarker signature for prediction of skin sensitization. BMC Genomics. 15(1):379. doi: 10.1186/1471-2164-15-379.

Fritsch (2003). Dermatologie Venerologie: Grundlagen, Klinik, Atlas. Springer Berlin Heidelberg, 2nd Edition.

Fuchs E, Raghavan S (2002). Getting under the skin of epidermal morphogenesis. Nat Rev Genet. 3(3):199-209. doi: 10.1038/nrg758.

Furue M, Nindl M, Kawabe K, Nakamura K, Ishibashi Y, Sagawa K (1992). Epitope mapping of CD1a, CD1b, and CD1c antigens in human skin: differential localization on Langerhans cells, keratinocytes, and basement membrane zone. J Invest Dermatol. 99(5):23S-26S. doi: 10.1111/1523-1747.ep12668273.

Gao Y, Tannenbaum A, Chen H, Torres M, Yoshida E, Yang X, Wang Y, Curran W, Liu T (2013). Automated skin segmentation in ultrasonic evaluation of skin toxicity in breast cancer radiotherapy. Ultrasound Med Biol. 39(11):2166-75. doi: 10.1016/j.ultrasmedbio.2013.04.006.

Ge X, Peng X, Li M, Ji F, Chen J, Zhang D (2021). OGT regulated O-GlcNacylation promotes migration and invasion by activating IL-6/STAT3 signaling in NSCLC cells. Pathol Res Pract. 225:153580. doi: 10.1016/j.prp.2021.153580.

Gene Ontology Consortium (2021). The Gene Ontology resource: enriching a GOld mine. Nucleic Acids Res. 49(D1):D325-D334. doi: 10.1093/nar/gkaa1113.

Ghasemi N, Bandehpour M, Ranjbari J (2019). Optimization of Key Factors in Serum Free Medium for Production of Human Recombinant GM-CSF Using Response Surface Methodology. Iran J Pharm Res. 18(Suppl1):146-156. doi: 10.22037/ijpr.2020.112322.13681.

Ginhoux F, Tacke F, Angeli V, Bogunovic M, Loubeau M, Dai XM, Stanley ER, Randolph GJ, Merad M (2006). Langerhans cells arise from monocytes in vivo. Nat Immunol. 7(3):265-73. doi: 10.1038/ni1307.

Groell F, Jordan O, Borchard G (2018). In vitro models for immunogenicity prediction of therapeutic proteins. Eur J Pharm Biopharm. 130:128-142. doi: 10.1016/j.ejpb.2018.06.008.

Halata Z, Grim M, Bauman KI (2003). Friedrich Sigmund Merkel and his "Merkel cell", morphology, development, and physiology: review and new results. Anat Rec A Discov Mol Cell Evol Biol. 271(1):225-39. doi: 10.1002/ar.a.10029.

Hirsch C, Schildknecht S (2019). *In Vitro* Research Reproducibility: Keeping Up High Standards. Front Pharmacol. 10:1484. doi: 10.3389/fphar.2019.01484.

Inaba K, Inaba M, Romani N, Aya H, Deguchi M, Ikehara S, Muramatsu S, Steinman RM (1992). Generation of large numbers of dendritic cells from mouse bone marrow cultures supplemented with granulocyte/macrophage colony-stimulating factor. J Exp Med. 176(6):1693-702. doi: 10.1084/jem.176.6.1693.

Jochems CE, van der Valk JB, Stafleu FR, Baumans V (2002). The use of fetal bovine serum: ethical or scientific problem? Altern Lab Anim. 30(2):219-27. doi: 10.1177/026119290203000208.

Jubin K, Martin Y, Lawrence-Watt DJ, Sharpe JR (2011). A fully autologous co-culture system utilising non-irradiated autologous fibroblasts to support the expansion of human keratinocytes for clinical use. Cytotechnology. 63(6):655-62. doi: 10.1007/s10616-011-9382-5.

Kabashima K, Shiraishi N, Sugita K, Mori T, Onoue A, Kobayashi M, Sakabe J, Yoshiki R, Tamamura H, Fujii N, Inaba K, Tokura Y (2007). CXCL12-CXCR4 engagement is required for migration of cutaneous dendritic cells. Am J Pathol. 171(4):1249-57. doi: 10.2353/ajpath.2007.070225.

Kalboussi H, Kacem I, Aroui H, El Maalel O, Maoua M, Brahem A, El Guedri S, Chatti S, Ghariani N, Mrizak N (2019). Impact of Allergic Contact Dermatitis on the Quality of Life and Work Productivity. Dermatol Res Pract. 2019:3797536. doi: 10.1155/2019/3797536.

Kanitakis J, Morelon E, Petruzzo P, Badet L, Dubernard JM (2011). Self-renewal capacity of human epidermal Langerhans cells: observations made on a composite tissue allograft. Exp Dermatol. 20(2):145-6. doi: 10.1111/j.1600-0625.2010.01146.x.

Kaplan DH, Igyártó BZ, Gaspari AA (2012). Early immune events in the induction of allergic contact dermatitis. Nat Rev Immunol. 12(2):114-24. doi: 10.1038/nri3150.

Kashem SW, Haniffa M, Kaplan DH (2017). Antigen-Presenting Cells in the Skin. Annu Rev Immunol. 35:469-499. doi: 10.1146/annurev-immunol-051116-052215.

Koch CM, Chiu SF, Akbarpour M, Bharat A, Ridge KM, Bartom ET, Winter DR (2018). A Beginner's Guide to Analysis of RNA Sequencing Data. Am J Respir Cell Mol Biol. 59(2):145-157. doi: 10.1165/rcmb.2017-0430TR.

Koch F, Heufler C, Kämpgen E, Schneeweiss D, Böck G, Schuler G (1990). Tumor necrosis factor alpha maintains the viability of murine epidermal Langerhans cells in culture, but in contrast to granulocyte/macrophage colony-stimulating factor, without inducing their functional maturation. J Exp Med. 171(1):159-71. doi: 10.1084/jem.171.1.159.

Koch S, Kohl K, Klein E, von Bubnoff D, Bieber T (2006). Skin homing of Langerhans cell precursors: adhesion, chemotaxis, and migration. J Allergy Clin Immunol. 117(1):163-8. doi: 10.1016/j.jaci.2005.10.003.

Koivisto L, Bi J, Häkkinen L, Larjava H (2018). Integrin αvβ6: Structure, function and role in health and disease. Int J Biochem Cell Biol. 99:186-196. doi: 10.1016/j.biocel.2018.04.013.

Koo TH, Lee JJ, Kim EM, Kim KW, Kim HD, Lee JH (2002). Syntenin is overexpressed and promotes cell migration in metastatic human breast and gastric cancer cell lines. Oncogene. 21(26):4080-8. doi: 10.1038/sj.onc.1205514.

Kosten IJ, Spiekstra SW, de Gruijl TD, Gibbs S (2015). MUTZ-3 derived Langerhans cells in human skin equivalents show differential migration and phenotypic plasticity after allergen or irritant exposure. Toxicol Appl Pharmacol. 287(1):35-42. doi: 10.1016/j.taap.2015.05.017.

Kubo A, Nagao K, Yokouchi M, Sasaki H, Amagai M (2009). External antigen uptake by Langerhans cells with reorganization of epidermal tight junction barriers. J Exp Med. 206(13):2937-46. doi: 10.1084/jem.20091527.

Langerhans, P (1868). Ueber die Nerven der menschlichen Haut. Archiv f. pathol. Anat. 44:325–337. doi: 10.1007/BF01959006

Larsson K, Lindstedt M, Borrebaeck CA (2006). Functional and transcriptional profiling of MUTZ-3, a myeloid cell line acting as a model for dendritic cells. Immunology. 117(2):156-66. doi: 10.1111/j.1365-2567.2005.02274.x.

Lee J, Lee P, Wu X (2017). Molecular and cytoskeletal regulations in epidermal development. Semin Cell Dev Biol. 69:18-25. doi: 10.1016/j.semcdb.2017.05.018.

Li MO, Wan YY, Sanjabi S, Robertson AK, Flavell RA (2006). Transforming growth factor-beta regulation of immune responses. Annu Rev Immunol. 24:99-146. doi: 10.1146/annurev.immunol.24.021605.090737.

Lin CL, Suri RM, Rahdon RA, Austyn JM, Roake JA (1998). Dendritic cell chemotaxis and transendothelial migration are induced by distinct chemokines and are regulated on maturation. Eur J Immunol. 28(12):4114-22. doi: 10.1002/(SICI)1521-4141(199812)28:12<4114::AID-IMMU4114>3.0.CO;2-C.

Liu Y, Peterson DA, Kimura H, Schubert D (1997). Mechanism of cellular 3-(4,5-dimethylthiazol-2-yl)-2,5-diphenyltetrazolium bromide (MTT) reduction. J Neurochem. 69(2):581-93. doi: 10.1046/j.1471-4159.1997.69020581.x.

Lönnqvist S, Junker JPE, Sedell M, Nyman E, Kratz G (2019). Tracking keratinocytes and melanocytes using carboxyfluorescein hydroxysuccinimidyl ester staining. PLoS One. 14(8):e0221878. doi: 10.1371/journal.pone.0221878.

Lu KV, Jong KA, Kim GY, Singh J, Dia EQ, Yoshimoto K, Wang MY, Cloughesy TF, Nelson SF, Mischel PS (2005). Differential induction of glioblastoma migration and growth by two forms of pleiotrophin. J Biol Chem. 280(29):26953-64. doi: 10.1074/jbc.M502614200.

Masterson AJ, Sombroek CC, De Gruijl TD, Graus YM, van der Vliet HJ, Lougheed SM, van den Eertwegh AJ, Pinedo HM, Scheper RJ (2002). MUTZ-3, a human cell line model for the cytokine-induced differentiation of dendritic cells from CD34+ precursors. Blood. 100(2):701-3. doi: 10.1182/blood.v100.2.701.

McCann TJ, Treasure C (2022). Addressing Animal Welfare Issues in Fetal Blood Collection for Fetal Bovine Serum Production. Altern Lab Anim. 50(5):365-368. doi: 10.1177/02611929221117992.

Mehta AB, Nadkarni NJ, Patil SP, Godse KV, Gautam M, Agarwal S (2016). Topical corticosteroids in dermatology. Indian J Dermatol Venereol Leprol. 82(4):371-8. doi: 10.4103/0378-6323.178903.

Melián A, Beckman EM, Porcelli SA, Brenner MB (1996). Antigen presentation by CD1 and MHC-encoded class I-like molecules. Curr Opin Immunol. 8(1):82-8. doi: 10.1016/s0952-7915(96)80109-9.

Melyanti (2008). Zur Relevanz biochemischer Vitalitätsassays in dreidimesionalen Gewebemodellen der Haut. Diploma Thesis, FH Aachen – Univeristy of Applied Sciences, Jürlich.

Merad M, Manz MG, Karsunky H, Wagers A, Peters W, Charo I, Weissman IL, Cyster JG, Engleman EG (2002). Langerhans cells renew in the skin throughout life under steady-state conditions. Nat Immunol. 3(12):1135-41. doi: 10.1038/ni852.

Mewes KR (2020). The Phenion Full-Thickness Skin Models: variants, barrier function, and in vitro testing. Euro Cosmetics. 11/12, 14-18.

Mewes KR, Raus M, Bernd A, Zöller NN, Sättler A, Graf R (2007). Elastin expression in a newly developed full-thickness skin equivalent. Skin Pharmacol Physiol. 20(2):85-95. doi: 10.1159/000097655.

Mosmann T (1983). Rapid colorimetric assay for cellular growth and survival: application to proliferation and cytotoxicity assays. J Immunol Methods. 65(1-2):55-63. doi: 10.1016/0022-1759(83)90303-4.

Mummert ME, Mummert D, Edelbaum D, Hui F, Matsue H, Takashima A (2002). Synthesis and surface expression of hyaluronan by dendritic cells and its potential role in antigen presentation. J Immunol. 169(8):4322-31. doi: 10.4049/jimmunol.169.8.4322.

Murphy GF, Bhan AK, Sato S, Mihm MC Jr, Harrist TJ (1981). A new immunologic marker for human Langerhans cells. N Engl J Med. 304(13):791-2. doi: 10.1056/NEJM198103263041320.

Nelissen I, Selderslaghs I, Heuvel RV, Witters H, Verheyen GR, Schoeters G (2009). MUTZ-3-derived dendritic cells as an in vitro alternative model to CD34+ progenitor-derived dendritic cells for testing of chemical sensitizers. Toxicol In Vitro. 23(8):1477-81. doi: 10.1016/j.tiv.2009.08.022.

Nguyen AV, Soulika AM (2019). The Dynamics of the Skin's Immune System. Int J Mol Sci. 20(8):1811. doi: 10.3390/ijms20081811.

Nishibu A, Ward BR, Jester JV, Ploegh HL, Boes M, Takashima A (2006). Behavioral responses of epidermal Langerhans cells in situ to local pathological stimuli. J Invest Dermatol. 126(4):787-96. doi: 10.1038/sj.jid.5700107.

OECD (2014). Test No. 168: The Adverse Outcome Pathway for Skin Sensitisation Initiated by Covalent Binding to Proteins. OECD Series on Testing and Assessment, OECD Publishing, Paris. doi: 10.1787/9789264221444-en.

OECD (2022). Test No. 406: Skin Sensitisation, OECD Guidelines for the Testing of Chemicals, Section 4, OECD Publishing, Paris. doi: 10.1787/9789264070660-en.

OECD (2019). Test No. 431: In vitro skin corrosion: reconstructed human epidermis (RHE) test method, OECD Guidelines for the Testing of Chemicals, Section 4, OECD Publishing, Paris. doi: 10.1787/9789264264618-en.

OECD (2010). Test No. 429: Skin sensitization: Local Lymph Node Assay. OECD Publishing, Paris. https://doi.org/10.1787/9789264071100-en.

OECD (2021). Test No. 439: In Vitro Skin Irritation: Reconstructed Human Epidermis Test Method, OECD Guidelines for the Testing of Chemicals, Section 4, OECD Publishing, Paris. doi: 10.1787/9789264242845-en.

OECD (2010). Test No. 442A: Skin Sensitization: Local Lymph Node Assay: DA, OECD Guidelines for the Testing of Chemicals, Section 4, OECD Publishing, Paris. doi: 10.1787/9789264090972-en.

OECD (2018). Test No. 442B: Skin Sensitization: Local Lymph Node Assay: BrdU-ELISA or –FCM, OECD Guidelines for the Testing of Chemicals, Section 4, OECD Publishing, Paris. doi: 10.1787/9789264090996-en.

OECD (2023). Test No. 442C: In Chemico Skin Sensitisation: Assays addressing the Adverse Outcome Pathway key event on covalent binding to proteins. OECD Guidelines for the Testing of Chemicals, Section 4. OECD Publishing, Paris. doi: 10.1787/9789264229709-en.

OECD (2022). Test No. 442D: In Vitro Skin Sensitisation: ARE-Nrf2 Luciferase Test Method. OECD Guidelines for the Testing of Chemicals, Section 4. OECD Publishing, Paris. doi: 10.1787/9789264229822-en.

OECD (2023). Test No. 442E: In Vitro Skin Sensitisation: In Vitro Skin Sensitisation assays addressing the Key Event on activation of dendritic cells on the Adverse Outcome Pathway for Skin Sensitisation. OECD Guidelines for the Testing of Chemicals, Section 4. OECD Publishing, Paris. doi: 10.1787/9789264264359-en.

OECD (2023). Guideline No. 497: Defined Approaches on Skin Sensitisation, OECD Guidelines for the Testing of Chemicals, Section 4, Éditions OECD, Paris. doi: 10.1787/b92879a4-en.

Otsuka M, Egawa G, Kabashima K (2018). Uncovering the Mysteries of Langerhans Cells, Inflammatory Dendritic Epidermal Cells, and Monocyte-Derived Langerhans Cell-Like Cells in the Epidermis. Front Immunol. 9:1768. doi: 10.3389/fimmu.2018.01768.

Ouwehand K, Oosterhoff D, Breetveld M, Scheper RJ, de Gruijl TD, Gibbs S (2011). Irritant-induced migration of Langerhans cells coincides with an IL-10-dependent switch to a macrophage-like phenotype. J Invest Dermatol. 131(2):418-25. doi: 10.1038/jid.2010.336.

Ouwehand K, Santegoets SJ, Bruynzeel DP, Scheper RJ, de Gruijl TD, Gibbs S (2008). CXCL12 is essential for migration of activated Langerhans cells from epidermis to dermis. Eur J Immunol. 38(11):3050-9. doi: 10.1002/eji.200838384.

Ouwehand K, Spiekstra SW, Reinders J, Scheper RJ, de Gruijl TD, Gibbs S (2010). Comparison of a novel CXCL12/CCL5 dependent migration assay with CXCL8 secretion and CD86 expression for distinguishing sensitizers from non-sensitizers using MUTZ-3 Langerhans cells. Toxicol In Vitro. 24(2):578-85. doi: 10.1016/j.tiv.2009.10.014.

Péguet-Navarro J, Dalbiez-Gauthier C, Rattis FM, Van Kooten C, Banchereau J, Schmitt D (1995). Functional expression of CD40 antigen on human epidermal Langerhans cells. J Immunol. 155(9):4241-7. PMID: 7594581.

Peiser M, Tralau T, Heidler J, Api AM, Arts JH, Basketter DA, English J, Diepgen TL, Fuhlbrigge RC, Gaspari AA, Johansen JD, Karlberg AT, Kimber I, Lepoittevin JP, Liebsch M, Maibach HI, Martin SF, Merk HF, Platzek T, Rustemeyer T, Schnuch A, Vandebriel RJ, White IR, Luch A (2012). Allergic contact dermatitis: epidemiology, molecular mechanisms, in vitro methods and regulatory aspects. Current knowledge assembled at an international workshop at BfR, Germany. Cell Mol Life Sci. 69(5):763-81. doi: 10.1007/s00018-011-0846-8.

Puré E, Inaba K, Crowley MT, Tardelli L, Witmer-Pack MD, Ruberti G, Fathman G, Steinman RM (1990). Antigen processing by epidermal Langerhans cells correlates with the level of biosynthesis of major histocompatibility complex class II molecules and expression of invariant chain. J Exp Med. 172(5):1459-69. doi: 10.1084/jem.172.5.1459.

Quan C, Cho MK, Shao Y, Mianecki LE, Liao E, Perry D, Quan T (2015). Dermal fibroblast expression of stromal cell-derived factor-1 (SDF-1) promotes epidermal keratinocyte proliferation in normal and diseased skin. Protein Cell. 6(12):890-903. doi: 10.1007/s13238-015-0198-5.

Quentmeier H, Zaborski M, Drexler HG (1997). The human bladder carcinoma cell line 5637 constitutively secretes functional cytokines. Leuk Res. 21(4):343-50. doi: 10.1016/s0145-2126(96)00132-4.

Rasaiyaah J, Noursadeghi M, Kellam P, Chain B (2009). Transcriptional and functional defects of dendritic cells derived from the MUTZ-3 leukaemia line. Immunology. 127(3):429-41. doi: 10.1111/j.1365-2567.2008.03018.x.

Reisinger K, Blatz V, Brinkmann J, Downs TR, Fischer A, Henkler F, Hoffmann S, Krul C, Liebsch M, Luch A, Pirow R, Reus AA, Schulz M, Pfuhler S (2018). Validation of the 3D Skin Comet assay using full thickness skin models: Transferability and reproducibility. Mutat Res Genet Toxicol Environ Mutagen. 827:27-41. doi: 10.1016/j.mrgentox.2018.01.003.

Rheinwald JG, Green H (1975). Serial cultivation of strains of human epidermal keratinocytes: the formation of keratinizing colonies from single cells. Cell. 6(3):331-43. doi: 10.1016/s0092-8674(75)80001-8.

Riedl E, Stöckl J, Majdic O, Scheinecker C, Knapp W, Strobl H (2000). Ligation of E-cadherin on in vitro-generated immature Langerhans-type dendritic cells inhibits their maturation. Blood. 96(13):4276-84. doi: 10.1182/blood.V96.13.4276

Rizova H, Carayon P, Michel L, Barbier A, Lacheretz F, Dubertret L (1994). Internalization of surface HLA-DR molecules by human epidermal Langerhans cells: analysis by flow cytometry and confocal microscopy. Cell Biol Toxicol. 10(5-6):367-73. doi: 10.1007/BF00755784.

Rodriguez O, Brod BA, James WD (2022). Impact of trends in new and emerging contact allergens. Int J Womens Dermatol. 8(1):e006. doi: 10.1097/JW9.0000000000000006.

Rodrigues Neves C, Gibbs S (2021). Progress on Reconstructed Human Skin Models for Allergy Research and Identifying Contact Sensitizers. Curr Top Microbiol Immunol. 430:103-129. doi: 10.1007/82_2018_88.

Romani N, Koide S, Crowley M, Witmer-Pack M, Livingstone AM, Fathman CG, Inaba K, Steinman RM (1989). Presentation of exogenous protein antigens by dendritic cells to T cell clones. Intact protein is presented best by immature, epidermal Langerhans cells. J Exp Med. 169(3):1169-78. doi: 10.1084/jem.169.3.1169.

Ruben JM, Visser LL, Heinhuis KM, O'Toole T, Bontkes HJ, Westers TM, Ossenkoppele GJ, de Gruijl TD, van de Loosdrecht AA (2015). A Human Cell Line Model for Interferon-α Driven Dendritic Cell Differentiation. PLoS One. 10(8):e0135219. doi: 10.1371/journal.pone.0135219.

Russell WMS, Burch RL (1959). The Principles of Humane Experimental Techniques. London, United Kingdom, Methuen.

Sallusto F, Schaerli P, Loetscher P, Schaniel C, Lenig D, Mackay CR, Qin S, Lanzavecchia A (1998). Rapid and coordinated switch in chemokine receptor expression during dendritic cell maturation. Eur J Immunol. 28(9):2760-9. doi: 10.1002/(SICI)1521-4141(199809)28:09<2760::AID-IMMU2760>3.0.CO;2-N.

Santegoets SJ, Masterson AJ, van der Sluis PC, Lougheed SM, Fluitsma DM, van den Eertwegh AJ, Pinedo HM, Scheper RJ, de Gruijl TD (2006). A CD34(+) human cell line model of myeloid dendritic cell differentiation: evidence for a CD14(+)CD11b(+) Langerhans cell precursor. J Leukoc Biol. 80(6):1337-44. doi: 10.1189/jlb.0206111.

Santegoets SJ, van den Eertwegh AJ, van de Loosdrecht AA, Scheper RJ, de Gruijl TD (2008). Human dendritic cell line models for DC differentiation and clinical DC vaccination studies. J Leukoc Biol. 84(6):1364-73. doi: 10.1189/jlb.0208092.

Sheikh NA, Jones LA (2008). CD54 is a surrogate marker of antigen presenting cell activation. Cancer Immunol Immunother. 57(9):1381-90. doi: 10.1007/s00262-008-0474-9.

Sherlock BE, Harvestine JN, Mitra D, Haudenschild A, Hu J, Athanasiou KA, Leach JK, Marcu L (2018). Nondestructive assessment of collagen hydrogel cross-linking using time-resolved autofluorescence imaging. J Biomed Opt. 23(3):1-9. doi: 10.1117/1.JBO.23.3.036004.

Simon JC, Cruz PD Jr, Tigelaar RE, Sontheimer RD, Bergstresser PR (1991). Adhesion molecules CD11a, CD18, and ICAM-1 on human epidermal Langerhans cells serve a

functional role in the activation of alloreactive T cells. J Invest Dermatol. 96(1):148-51. doi: 10.1111/1523-1747.ep12515946.

Slavik JM, Hutchcroft JE, Bierer BE (1999). CD28/CTLA-4 and CD80/CD86 families: signaling and function. Immunol Res. 19(1):1-24. doi: 10.1007/BF02786473.

Smith Pease CK, Basketter DA, Patlewicz GY (2003). Contact allergy: the role of skin chemistry and metabolism. Clin Exp Dermatol. 28(2):177-83. doi: 10.1046/j.1365-2230.2003.01239.x.

Sribenja S, Wongkham S, Wongkham C, Yao Q, Chen C (2013). Roles and mechanisms of β-thymosins in cell migration and cancer metastasis: an update. Cancer Invest. 31(2):103-10. doi: 10.3109/07357907.2012.756111.

Sutherland DR, Stewart AK, Keating A (1993). CD34 antigen: molecular features and potential clinical applications. Stem Cells. 11 Suppl 3:50-7. doi: 10.1002/stem.5530110914.

Swetman CA, Leverrier Y, Garg R, Gan CH, Ridley AJ, Katz DR, Chain BM (2002). Extension, retraction and contraction in the formation of a dendritic cell dendrite: distinct roles for Rho GTPases. Eur J Immunol. 32(7):2074-83. doi: 10.1002/1521-4141(200207)32:7<2074::AID-IMMU2074>3.0.CO;2-S.

Tao TP, Maschmeyer I, LeCluyse EL, Rogers E, Brandmair K, Gerlach S, Przibilla J, Kern F, Genies C, Jacques C, Najjar A, Schepky A, Marx U, Kühnl J, Hewitt NJ (2023). Development of a microphysiological skin-liver-thyroid Chip3 model and its application to evaluate the effects on thyroid hormones of topically applied cosmetic ingredients under consumer-relevant conditions. Front Pharmacol. 14:1076254. doi: 10.3389/fphar.2023.1076254.

Thomas RM, Belsito DV, Huang C, Chen Lz LZ, Ormsby I, Simmons WJ, Cowin P, Shaw J, Doetschman T, Thorbecke GJ (2001). Appearance of Langerhans cells in the epidermis of Tgfb1(-/-) SCID mice: paracrine and autocrine effects of transforming growth factor-beta 1 and -beta 2(1). J Invest Dermatol. 117(6):1574-80. doi: 10.1046/j.0022-202x.2001.01550.x.

Toebak MJ, Pohlmann PR, Sampat-Sardjoepersad SC, von Blomberg BM, Bruynzeel DP, Scheper RJ, Rustemeyer T, Gibbs S (2006). CXCL8 secretion by dendritic cells

predicts contact allergens from irritants. Toxicol In Vitro. 20(1):117-24. doi: 10.1016/j.tiv.2005.06.039.

Tortora, GJ, Nielsen, M (2020). Principles of Human Anatomy. United States, Wiley, 15th Edition.

Treadwell, P. Allergic Contact Dermatitis (2020). In: Treadwell, P., Smith, M.L., Prendiville, J. (eds) Atlas of Adolescent Dermatology. Springer, Cham. doi: 10.1007/978-3-030-58634-8_12.

Tze LE, Horikawa K, Domaschenz H, Howard DR, Roots CM, Rigby RJ, Way DA, Ohmura-Hoshino M, Ishido S, Andoniou CE, Degli-Esposti MA, Goodnow CC (2011). CD83 increases MHC II and CD86 on dendritic cells by opposing IL-10-driven MARCH1-mediated ubiquitination and degradation. J Exp Med. 208(1):149-65. doi: 10.1084/jem.20092203.

Tzellos TG, Sinopidis X, Kyrgidis A, Vahtsevanos K, Triaridis S, Printza A, Klagas I, Karakiulakis G, Papakonstantinou E (2011). Differential hyaluronan homeostasis and expression of proteoglycans in juvenile and adult human skin. J Dermatol Sci. 61(1):69-72. doi: 10.1016/j.jdermsci.2010.10.010.

Umayahara T, Sakabe JI, Shimauchi T, Tokura Y (2017). Galectin-7 is extracellularly released from epidermal keratinocytes in atopic dermatitis and serves as immunomodulator of Langerhans cells. 86:2. doi: 10.1016/j.jdermsci.2017.02.123

Uter W, Werfel T, Lepoittevin JP, White IR (2020). Contact Allergy-Emerging Allergens and Public Health Impact. Int J Environ Res Public Health. 17(7):2404. doi: 10.3390/ijerph17072404.

Valladeau J, Ravel O, Dezutter-Dambuyant C, Moore K, Kleijmeer M, Liu Y, Duvert-Frances V, Vincent C, Schmitt D, Davoust J, Caux C, Lebecque S, Saeland S (2000). Langerin, a novel C-type lectin specific to Langerhans cells, is an endocytic receptor that induces the formation of Birbeck granules. Immunity. 12(1):71-81. doi: 10.1016/s1074-7613(00)80160-0.

Visscher M, Narendran V (2014). The Ontogeny of Skin. Adv Wound Care (New Rochelle). 3(4):291-303. doi: 10.1089/wound.2013.0467.

Watt FM (1998). Epidermal stem cells: markers, patterning and the control of stem cell fate. Philos Trans R Soc Lond B Biol Sci. 353(1370):831-7. doi: 10.1098/rstb.1998.0247.

Wiegand C, Hewitt NJ, Merk HF, Reisinger K (2014). Dermal xenobiotic metabolism: a comparison between native human skin, four in vitro skin test systems and a liver system. Skin Pharmacol Physiol. 27(5):263-75. doi: 10.1159/000358272.

Wissowzky A (1877). Ueber das Eosin als reagenz auf Hämoglobin und die Bildung von Blutgefässen und Blutkörperchen bei Säugetier und Hühnerembryonen. Archiv für mikroskopische Anatomie. 13:479-496. doi: 10.1007/BF02933947.

Wright SD, Ramos RA, Tobias PS, Ulevitch RJ, Mathison JC (1990). CD14, a receptor for complexes of lipopolysaccharide (LPS) and LPS binding protein. Science. 249(4975):1431-3. doi: 10.1126/science.1698311.

Xie B, Lin W, Ye J, Wang X, Zhang B, Xiong S, Li H, Tan G (2015). DDR2 facilitates hepatocellular carcinoma invasion and metastasis via activating ERK signaling and stabilizing SNAIL1. J Exp Clin Cancer Res. 34(1):101. doi: 10.1186/s13046-015-0218-6.

Yoshida K, Kubo A, Fujita H, Yokouchi M, Ishii K, Kawasaki H, Nomura T, Shimizu H, Kouyama K, Ebihara T, Nagao K, Amagai M (2014). Distinct behavior of human Langerhans cells and inflammatory dendritic epidermal cells at tight junctions in patients with atopic dermatitis. J Allergy Clin Immunol. 134(4):856-64. doi: 10.1016/j.jaci.2014.08.001.

Zhou LJ, Tedder TF (1995). Human blood dendritic cells selectively express CD83, a member of the immunoglobulin superfamily. J Immunol. 154(8):3821-35. PMID: 7706722. doi: 10.4049/jimmunol.154.8.3821.

I. Own Publications

Parts of this PhD thesis has been presented as a poster at the “11th World Congress on Alternatives and Animal Use in the Life Sciences 2021” (Maastricht, The Netherlands, Böttcher et al., 2021) and were recently published in Toxicology In Vitro “Integration of MUTZ-Langerhans cell into a 3D full-thickness skin equivalent and influences of serum reduction and undefined medium supplements on differentiation” (Böttcher et al., 2024).

II. Supplemental Figures

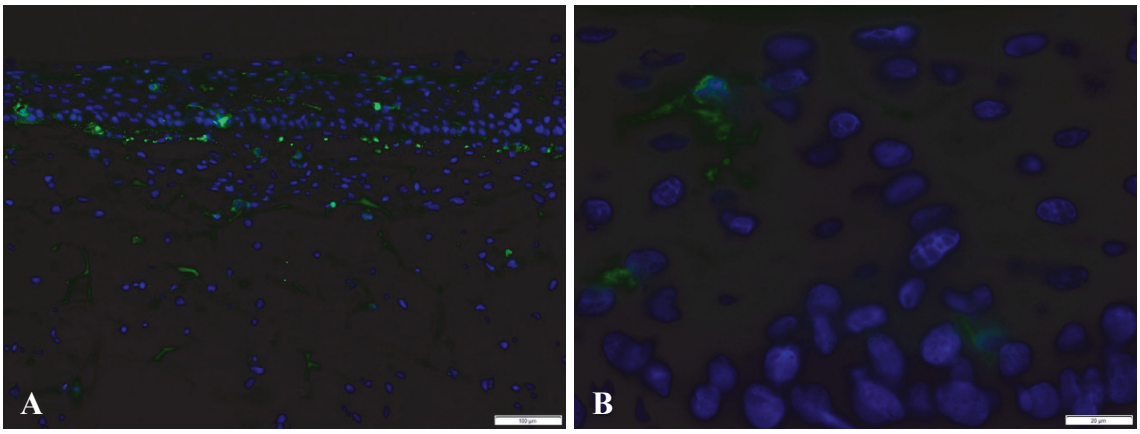

Supplemental Figure 1: CD207 expression in standard Phenion® Full-Thickness skin models with integrated 5 % FCS-differentiated MUTZ-LCs.
Representative microscopic images of frozen sections of Phenion® Full-Thickness standard skin models with integrated 5 % FCS-differentiated MUTZ-LCs. CD207 is depicted in green (FITC) and nuclei in blue (DAPI). (A) Green, fluorescent signals in the lower part of dermis were false-positive ones, emitted by the matrix (A). A magnification of an epidermal CD207-stained MUTZ-LC is depicted to illustrate the morphological features, including the typical dendritic processes (B). Scale bar represents 100 µm (A) and 20 µm (B).

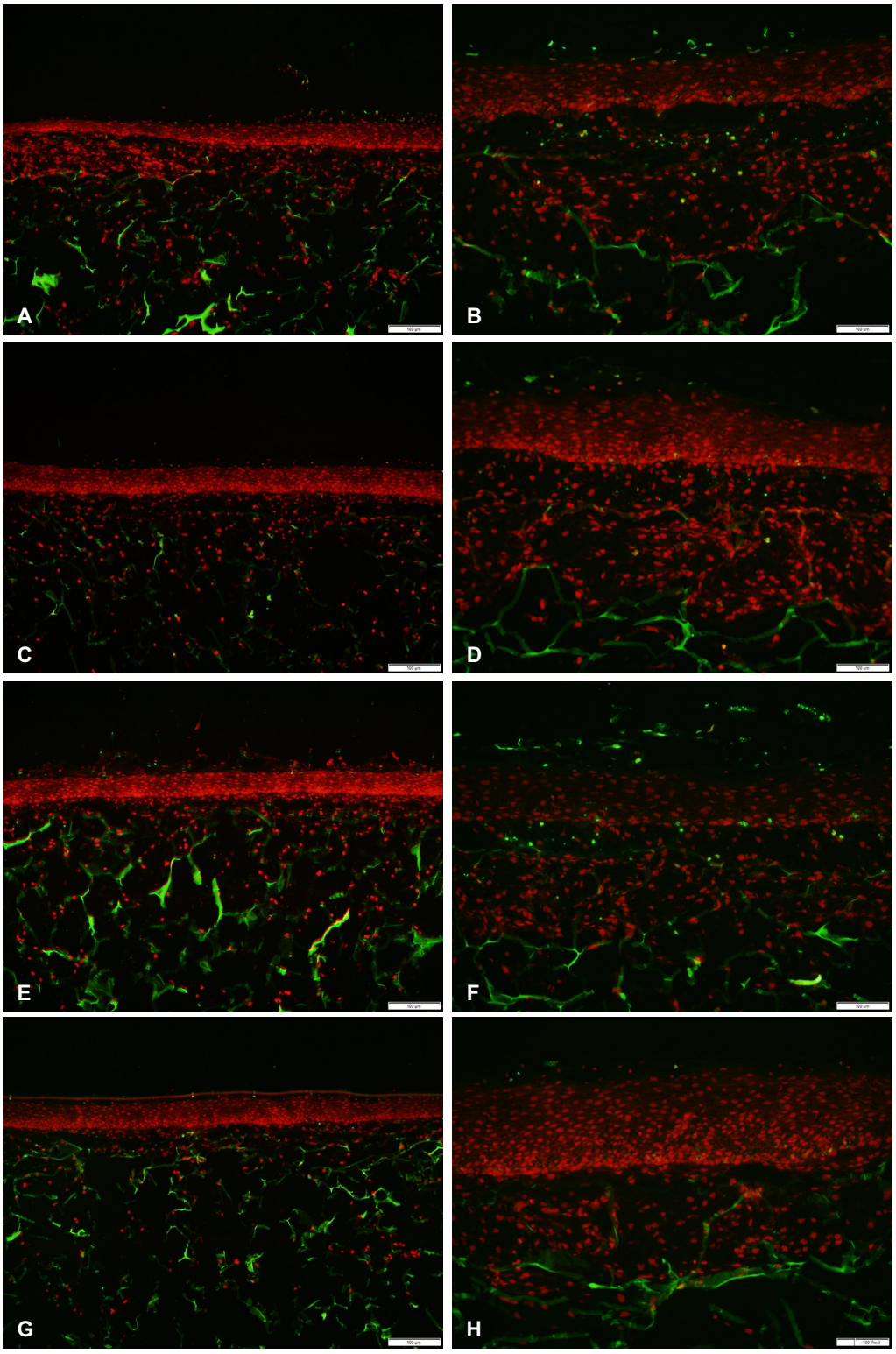

Supplemental Figure 2: Effect of $NiSO_4$ treatment and hydrocortisone (HC) on cell viability within Standard Phenion® Full-Thickness skin models with or without integrated 5 % FCS-differentiated MUTZ-LCs.

Representative microscopic images of frozen sections of standard skin models on ALI day twelve after conducting a TUNEL assay. Apoptotic cells emitted a green fluorescence signal. A comparison of Phenion® Full-Thickness standard skin models cultured with HC (C, E, G) and without HC (D, F, H) during ALI culture. Skin models were integrated with 5 % FCS-differentiated MUTZ-LCs (A-H). Besides untreated skin models (A,B), skin models were also treated for 20 h with PBS -vehicle control for $NiSO_4$- (C, D) and 0.1mM $NiSO_4$ (E, F) as well as 0.5 mM $NiSO_4$ (G, H). In addition, cells were stained with PI. Green, fluorescent signals in the lower part of dermis were false-positive ones, emitted by the matrix. Scale bars represent 100 µm.

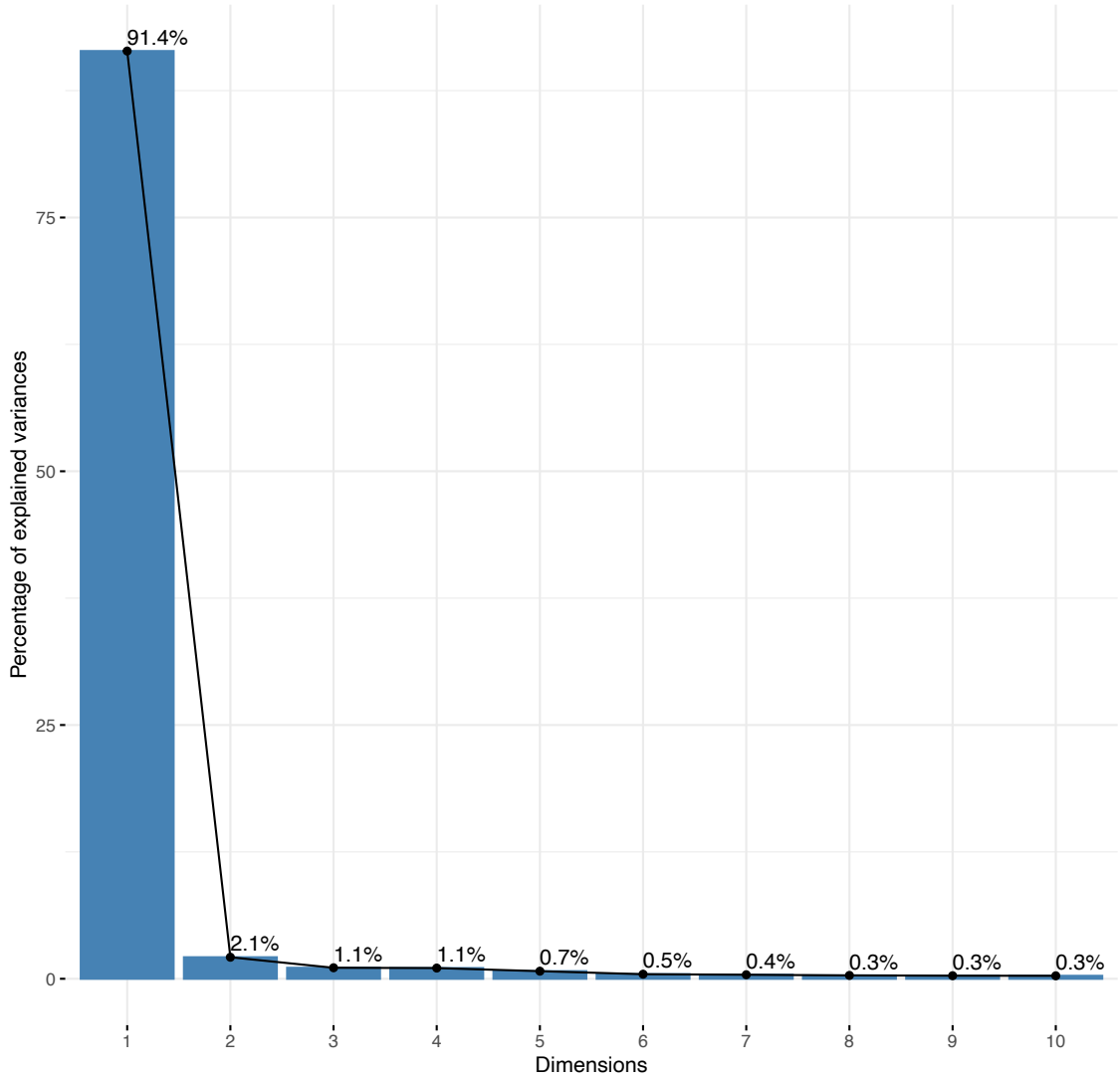

Supplemental Figure 3: Screen plot explaining the variance of the data used for the Next Generation Sequencing analysis (NGS).
Screen plot shows the percentage of variance of the data used for the NGS. The first two principal components explain with ~94 % the majority of the variance.

III. Affidavit/Eidesstattliche Erklärung

I declare under oath that I have produced my thesis independently and without any undue assistance by third parties under consideration of the ‘Principles for the Safeguarding of Good Scientific Practice at Heinrich Heine University Düsseldorf'. The dissertation has not been submitted in its present or similar form to any other faculty. I have not previously undertaken any unsuccessful or successful doctoral attempts.

Ich versichere an Eides Statt, dass die Dissertation von mir selbständig und ohne unzulässige fremde Hilfe unter Beachtung der „Grundsätze zur Sicherung guter wissenschaftlicher Praxis an der Heinrich-Heine-Universität Düsseldorf“ erstellt worden ist. Die Dissertation wurde in der vorgelegten oder in ähnlicher Form noch bei keiner anderen Fakultät eingereicht. Ich habe bisher keine erfolglosen und erfolgreichen Promotionsversuche unternommen.

_____

Date/Datum

_____

Signature/Unterschrift